iScience

CellPress
OPEN ACCESS

Article

Prune-1 drives polarization of tumor-associated macrophages (TAMs) within the lung metastatic niche in triple-negative breast cancer

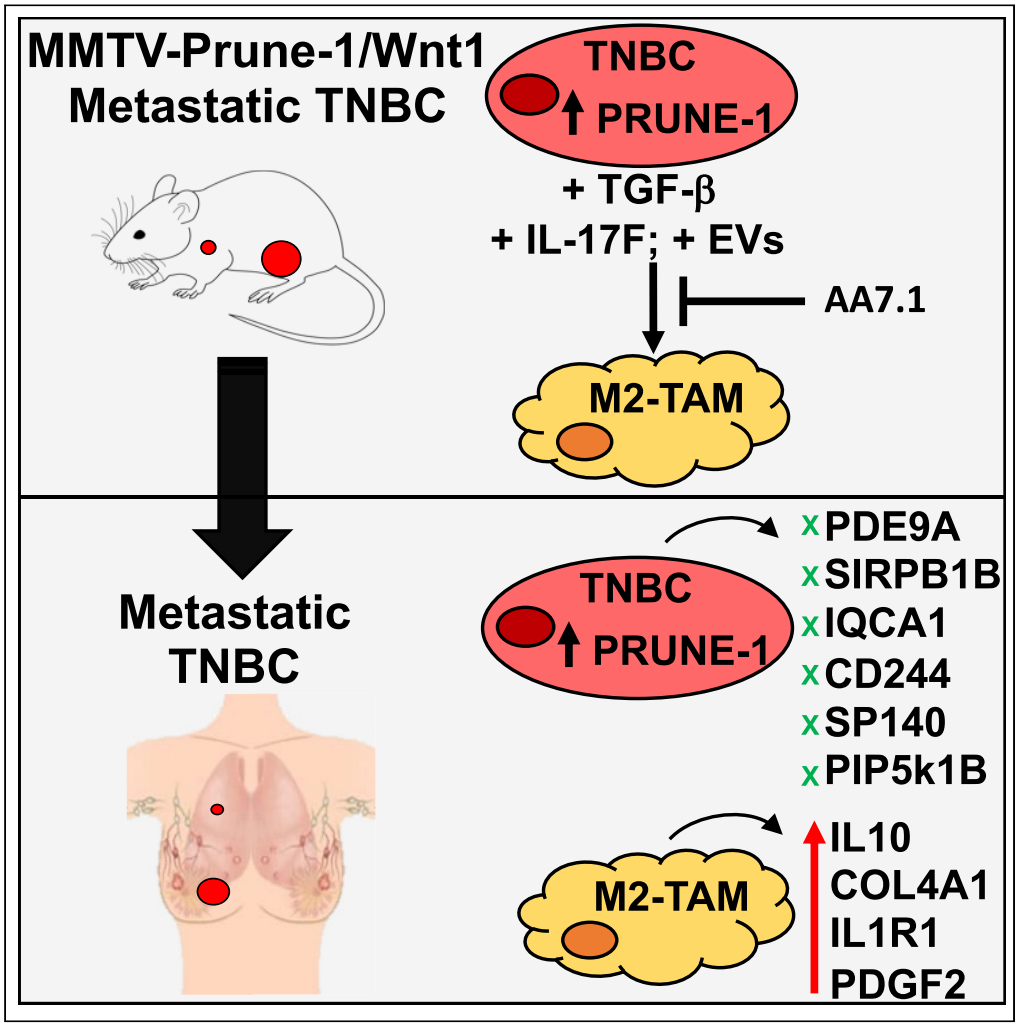

Veronica Ferrucci, Fatemeh Asadzadeh, Francesca Collina, ..., Maurizio di Bonito, Kris Gevaert, Massimo Zollo

massimo.zollo@unina.it

Highlights

Prune-1 correlates to M2-TAMs confirming lung metastatic dissemination in GEMM

Cytokines and EV proteins are responsible of M2-TAMs polarization processes

A small molecule with immunomodulatory properties ameliorates metastatic dissemination

Identification of gene variants within immune response and cell adhesion in TNBC

Ferrucci et al., iScience 24, 101938
January 22, 2021
https://doi.org/10.1016/j.isci.2020.101938

iScience

CellPress
OPEN ACCESS

Article

Prune-1 drives polarization of tumor-associated macrophages (TAMs) within the lung metastatic niche in triple-negative breast cancer

Veronica Ferrucci,[1,2,3] Fatemeh Asadzadeh,[1,2,10] Francesca Collina,[4,10] Roberto Siciliano,[1] Angelo Boccia,[1] Laura Marrone,[1,2] Daniela Spano,[1] Marianeve Carotenuto,[2] Cristina Maria Chiarolla,[1] Daniela De Martino,[2] Gennaro De Vita,[2] Alessandra Macrì,[1] Luisa Dassi,[1] Jonathan Vandenbussche,[5,9] Natascia Marino,[1,6] Monica Cantile,[4] Giovanni Paolella,[1] Francesco D'Andrea,[7] Maurizio di Bonito,[4] Kris Gevaert,[5,9] and Massimo Zollo[1,2,3,8,11,*]

Summary

M2-tumor-associated macrophages (M2-TAMs) in the tumor microenvironment represent a prognostic indicator for poor outcome in triple-negative breast cancer (TNBC).

Here we show that Prune-1 overexpression in human TNBC patients has positive correlation to lung metastasis and infiltrating M2-TAMs. Thus, we demonstrate that Prune-1 promotes lung metastasis in a genetically engineered mouse model of metastatic TNBC augmenting M2-polarization of TAMs within the tumor microenvironment. Thus, this occurs through TGF-β enhancement, IL-17F secretion, and extracellular vesicle protein content modulation.

We also find murine inactivating gene variants in human TNBC patient cohorts that are involved in activation of the innate immune response, cell adhesion, apoptotic pathways, and DNA repair. Altogether, we indicate that the overexpression of Prune-1, IL-10, COL4A1, ILR1, and PDGFB, together with inactivating mutations of PDE9A, CD244, Sirpb1b, SV140, Iqca1, and PIP5K1B genes, might represent a route of metastatic lung dissemination that need future prognostic validations.

Introduction

Triple-negative breast cancer (TNBC) accounts for 20% of breast cancers (BCs) (Neophytou et al., 2018), where the tumorigenic cells are negative for the estrogen receptor (ER), progesterone receptor (PgR), and human epidermal growth factor receptor 2 (HER2; i.e., ER^-, PgR^-, $HER2^-$) (Rakha and Chan, 2011). TNBC is the most aggressive subtype of BCs due to its aggressive clinicopathological features, including young age at onset, large tumor size (Rakha and Chan, 2011), and greater propensity for visceral metastasis to distant sites (Lin et al., 2012). Among the metastatic patients diagnosed with TNBC, 49.3% develop metastasis in the lung (Xiao et al., 2018). Due to the absence of recognized molecular targets for therapy, TNBC patients with lung metastasis have the poorest outcome compared with those diagnosed with other metastatic BC subtypes (Xiao et al., 2018; Cancer Genome Atlas, 2012).

Due to its molecular features, TNBC can be considered one of the most complex tumor disorders in humans. Thus, the application of "*-omics*" technologies is of importance to monitor the genomic evolution of TNBC, which shows dominant TP53, PIK3CA, and PTEN somatic mutations (Shah et al., 2012). Indeed, six distinct molecular TNBC entities have been described: two basal-like-related subgroups (basal-like 1 [BL1] and 2 [BL2]), two mesenchymal-related subgroups (mesenchymal [M], mesenchymal stem-like [MSL]), one luminal androgen receptor (LAR) group, and one immunomodulatory (IM) subgroup, with MSL and IM subtypes that are driven by tumor-associated stromal cells and tumor-infiltrating lymphocytes (TILs), respectively, in the tumor microenvironment (TME) (Lehmann et al., 2011, 2016).

Thus, the immune cells that infiltrate the TME have a dual function in tumor development and metastatic progression. In the early stages of tumorigenesis, they identify and eliminate tumorigenic cells because of

[1]CEINGE, Biotecnologie Avanzate, Naples 80145, Italy

[2]Dipartimento di Medicina Molecolare e Biotecnologie Mediche (DMMBM), 'Federico II' University of Naples, Naples 80134, Italy

[3]European School of Molecular Medicine (SEMM), University of Milan, Milan, Italy

[4]Pathology Unit, Istituto Nazionale Tumori-IRCS-Fondazione G.Pascale, Naples 80131, Italy

[5]VIB-UGent Centre for Medical Biotechnology, Ghent 9052, Belgium

[6]Department of Medicine, Indiana University-Purdue University Indianapolis, Indianapolis 46202, USA

[7]Dipartimento di Sanità pubblica – AOU, Universita; degli Studi di Napoli Federico II, Naples 80131, Italy

[8]DAI Medicina di Laboratorio e Trasfusionale, AOU Federico II, Naples 80131, Italy

[9]Department of Biomolecular Medicine, Ghent University, B9052 Ghent, Belgium

[10]These authors contributed equally

[11]Lead contact

*Correspondence: massimo.zollo@unina.it

https://doi.org/10.1016/j.isci.2020.101938

the expression of tumor-specific antigens (a mechanism known as "tumor immune surveillance"). Later, the tumors undergo immune-editing processes that allow the tumor variants with reduced immunogenicity to escape immunological detection and elimination, thus allowing tumor variants to be clonally selected (Spano and Zollo, 2012).

The greater genomic instability and the mutational burden of TNBC result in higher propensity to generate neoantigens (Spano and Zollo, 2012; Bianchini et al., 2016), thus generating selected tumorigenic clones within the TME that considerably influence the risk of response to chemotherapy and relapse in these patients (Dieci et al., 2014). Recently, new distinct TNBC subtypes were defined based on the types of immune infiltrating cells within the TME: i.e., the pro-tumorigenic M2-polarized tumor-associated macrophages (M2-TAMs) and the immunosuppressive regulatory T cells (Tregs) (Adams et al., 2017). The TNBC subtypes with the poorest prognosis are characterized by higher levels of infiltrating M2-TAMs ($CD163^+$) and Tregs ($FOXP3^+$) in a low TILs environment, with high levels of the immunosuppressive programmed death ligand-1 (PD-L1) and glycolytic monocarboxylate transporter 4 (MCT4) markers (Adams et al., 2017). Thus, clinical evidence indicates that M2-TAMs infiltrating tumor tissues act as a prognostic indicator for poor outcome for patients with TNBC, as they are correlated with higher risk for developing metastasis (Sousa et al., 2015; Yuan et al., 2014), as M2-TAMs exert their immunosuppressive functions through inhibition of the effector functions of TILs (Santoni et al., 2017).

It is worth noting the valuable functions of cytokines withing the TME, which are soluble factors that mediate the communication between tumorigenic and immune cells. Transforming growth factor β (TGF-β) is a master regulator of an immunosuppressive action, and it is produced by both tumorigenic and immune cells and can thus orchestrate the polarization processes of the immune system toward a pro-tumorigenic phenotype and promote cancer progression and metastasis, also in TNBC (Pickup et al., 2013). In addition, extracellular vesicles (EVs; including exosomes) generated by tumor cells can modulate the recruitment of the immune cells and their immunomodulation in the TME (Thery et al., 2002), with a crucial role in promoting organotropic pre-metastatic niche formation in TNBC (Hoshino et al., 2015; Chow et al., 2014).

Here, we focus on Prune-1 protein, which belongs to the phosphodiesterase DHH (Asp-His-His) family (D'Angelo et al., 2004) with exopolyphosphatase activity (Tammenkoski et al., 2008). Via its unfolded C-terminus domain, Prune-1 can interact with intracellular binding partners, including glycogen synthase kinase 3β (GSK-3β (Kobayashi et al., 2006)) and NDPK-A (NM23-H1 or NME1 (D'Angelo et al., 2004)). Through these interactors (i.e., GSK-3β, NDPK-A), Prune-1 modulates intracellular pathways that are in turn translated into extracellular signaling, which includes the canonical Wnt1 (Carotenuto et al., 2014) and TGF-β (Ferrucci et al., 2018) cascades. Prune-1 expression levels and metastatic progression have been described in different solid tumors (Oue et al., 2007; Noguchi et al., 2009; Carotenuto et al., 2014; Nambu et al., 2016; Hashimoto et al., 2016; Ferrucci et al., 2018), including metastatic BC (D'Angelo et al., 2004; Zollo et al., 2005). In this regard, the overexpression of Prune-1 has been correlated with advanced nodal status (*i.e.*, N2-N3 cases) and distant metastasis in BC (Zollo et al., 2005).

Our findings here show that Prune-1 is overexpressed in TNBC patients and positively correlates to lung metastasis, tumor grading, disease progression, and infiltrating M2-TAMs. Through intracellular and extracellular signalings in TNBC cells, Prune-1 takes part in the cross-talk with macrophages, thus enhancing their polarization status toward the M2 phenotype. This action is synergistically mediated by a dual extracellular mode of communication: (i) via enhancement of secretion of soluble cytokines (i.e., interleukin-17F [IL-17F] (Yang et al., 2008; Giles et al., 2016; Starnes et al., 2001), IL-28 (Zhou et al., 2007), IL-20 (Otkjaer et al., 2007)); (ii) using EVs to carry proteins (i.e., Vim (Yamashita et al., 2013), Sdcbp (Yang et al., 2013b; Qian et al., 2013; Koo et al., 2002), Ifitm3 (Yang et al., 2013a)) that are responsible for metastatic process. Furthermore, the overexpression of Prune-1 (together with Wnt1) in the mammary gland of a genetically engineered mouse model (GEMM) of metastatic TNBC (mouse mammary tumor virus-[MMTV]–Prune-1/Wnt1) drives genetic variants involved in activation of the innate immune response (leukocytes and macrophage activation; ANKHD1, FER1L5), cell adhesion (NEXN), apoptotic pathways (BID), and DNA repair (ERCC5). Genetic inactivating mutations in the PDE9A, CD244, Sirpb1b, SV140, Iqca1, and PIP5K1B genes were also found in human BC specimens.

Through this approach we have identified in TNBC a common mutation burden in tumorigenic cells and a related network of action on immunoregulation of the immunosystem, with a focus on macrophages.

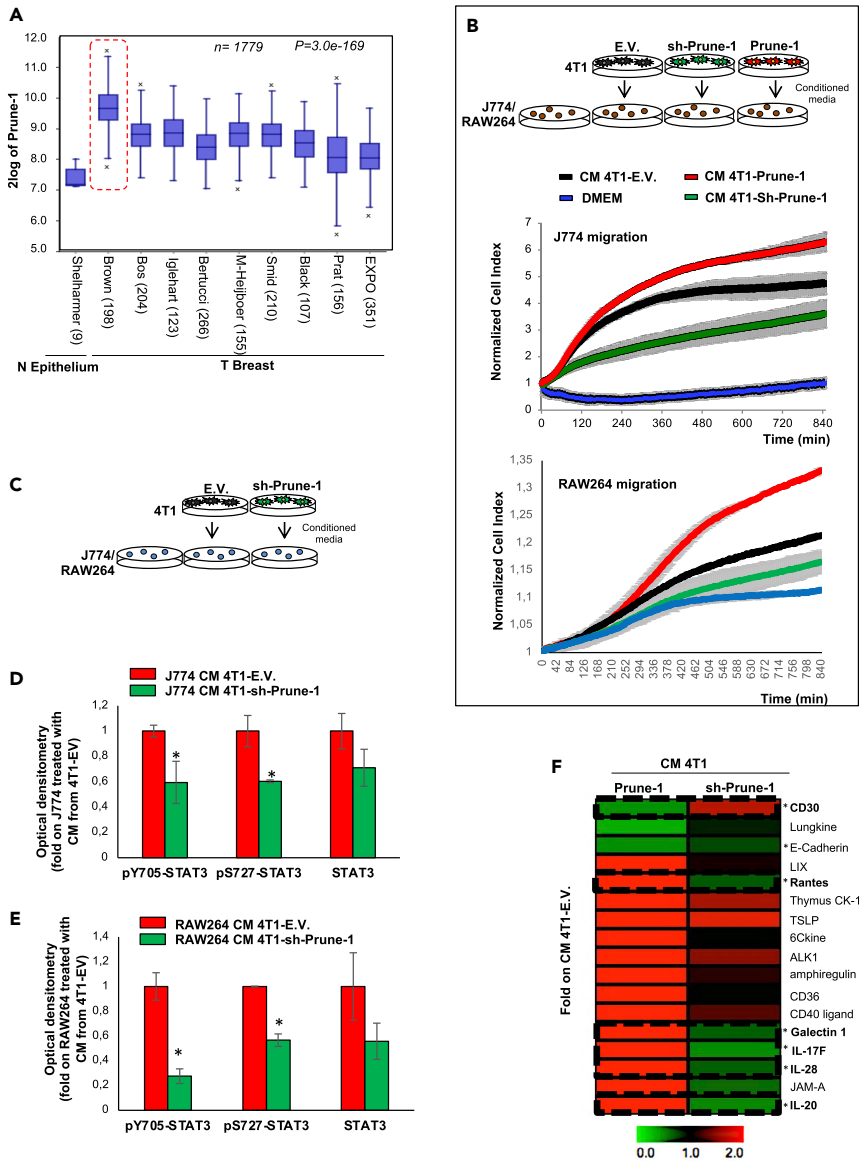

Figure 1. Prune-1 protein is overexpressed in TNBC and promotes macrophage chemotaxis through STAT3 via soluble cytokines

(A) Prune-1 overexpression in TNBC. RNA log2 expression analysis of Prune-1 levels of primary BC samples across different publicly available datasets, compared with normal epithelium (N Epithelium; Shelharmer dataset only). Data from 10 independent public-domain BC gene-expression datasets show the overexpression of Prune-1 in all of the BC samples compared with normal epithelium. Higher Prune-1 expression levels are seen for TNBC samples (i.e., Brown (Burstein et al., 2015); red dashed line) (n = 1779; p = 3.0×10^{-169}).

(B) Overexpression of Prune-1 in TNBC cells enhances macrophage chemotaxis *in vitro*. Normalized Cell Index as a measure of cell migration/chemotaxis of J774A.1 (i.e., J774; **upper panel**) and RAW264.7 (i.e., RAW264; **lower panel**) macrophages as generated by the xCELLigence RTCA software. Migration kinetics were monitored in response to conditioned media from Prune-1-overexpressing (4T1–Prune-1, red), Prune-1-silenced (4T1–Sh-Prune-1, green), and empty vector 4T1 cell clones (black), used as chemoattractants. Dulbecco's modified Eagle's medium was used as the negative control (blue).

(C–E) Conditioned media (CM) from the 4T1 clones were collected after 24 h. J774 or Raw264 macrophages were starved for 6 h in serum-free medium and then grown in the conditioned media for 30 min (C). Densitometer analyses of immunoblotting for the indicated proteins in J774 (D) and Raw264 (E) macrophages grown for 30 min in conditioned media from Prune-1-silenced and control 4T1 clones are shown. Empty vector (EV) 4T1 clones and untreated (UNT) macrophages

Figure 1. *Continued*
were used as the negative controls. β-Actin levels were used as the loading control. *p < 0.05 in Student's t test compared with J774 (D) or Raw264 (E) treated with conditioned media from 4T1 EV control clones.
(F) Prune-1 induces the secretion of soluble proteins by TNBC cells. Densitometer analyses of the cytokines upregulated and downregulated in the conditioned media (CM) derived from Prune-1-overexpressing (4T1–Prune-1) and Prune-1-silenced (4T1–Sh-Prune-1) 4T1 clones (MultiExperiment Viewer, http://www.tm4.org/mev.html). Among the 17 cytokines modulated by Prune-1 in the conditioned media collected from Prune-1-overexpressing (4T1–Prune-1), one was upregulated (CD30) and five were downregulated (Rantes, Galectin-1, IL-17F, IL-28, IL-20) in the conditioned media from 4T1–Sh-Prune-1 cell clones, thus following an opposite trend. *p < 0.05 in Student's t test comparing cytokines levels in conditioned media of 4T1–Sh-Prune-1 cells with those in 4T1 Empty Vector control clones.

Results

Overexpression of Prune-1 in metastatic TNBC cells enhances the canonical TGF-β and Wnt signaling cascades

Through interactions with its protein-binding partners (i.e., NDPK-A (Garzia et al., 2008; D'Angelo et al., 2004), GSK-3β (Kobayashi et al., 2006)), Prune-1 modulates signaling cascades, including the canonical Wnt (Carotenuto et al., 2014) and TGF-β pathways (Ferrucci et al.), which are also involved in BC progression and metastasis (Pohl et al., 2017; Ding et al., 2016).

Here, through applying data mining approaches in public gene expression resources available in BC datasets (R2 Genomics Analysis and Visualisation Platform; http://r2.amc.nl), we found higher Prune-1 expression in all BC samples (n = 1779, $p = 3.0 \times 10^{-169}$; Figure 1A), thus confirming Prune-1 overexpression in BC. Interestingly, we found the highest expression of Prune-1 in the public TNBC dataset (i.e., Brown (Burstein et al., 2015), n = 198; Figures 1A and S1A, within the red dashed line), which thus suggested a role for Prune-1 in this highly metastatic BC subgroup. These data are not surprising, because of the major frequency of chromosome 1q21 gain in basal-like and TNBC (30%–40% (Silva et al., 2015), (Cancer Genome Atlas, 2012)) and also in those with recurrent BC (70% (Goh et al., 2017)).

Triple-negative breast cancer is known to correlate to negative expression of ERs and PgR status (i.e., ER^-/PgR^-/$HER2^-$) (Bianchini et al., 2016). To provide deeper insight into the role of Prune-1 in TNBC, its association with ER, PgR, and HER2 status was also investigated using the public accessible dataset of tumor breast invasive carcinoma, with gene expression data acquired for the BC cohort from The Cancer Genome Atlas (TCGA; n = 1,097). In this dataset, BC samples were stratified according to their ER, PgR, and HER2 scores (as evaluated by immunohistochemistry [IHC]), which ranged from 0 to 3^+, with 0 indicating negativity. Higher expression levels of Prune-1 were identified only in those samples with negative scores for both ER and PgR (i.e., 0), and in those with scores ranging from 0 to 1^+ for HER2 status (Figure S1B, within the red dashed lines). These data prompted us to suggest potential involvement of Prune-1 in the pathogenesis of TNBC.

We have previously defined Prune-1 as an inducer of the SMAD-mediated canonical TGF-β pathway in metastatic medulloblastoma group 3 (MB_{group3}) (Ferrucci et al., 2018). As the TGF-β cascade has a crucial role in tumor metastasis, we investigated the expression levels of its downstream effectors (i.e., SMAD2, SMAD4) in BCs using different public BC datasets. These analyses showed that both SMAD2 and SMAD4 expression levels were higher in the TNBC dataset (i.e., Brown (Burstein et al., 2015); as shown in Figure S1C; SMAD2: $p = 5.6 \times 10^{-230}$; SMAD4: $p = 2.1 \times 10^{-86}$), thus indicating correlation between Prune-1 and canonical TGF-β signaling effectors in TNBC (Drabsch and Ten Dijke, 2012). Further correlation analyses were performed between Prune-1, SMAD2, and SMAD4 in BC samples stratified according to their ERs and PgR status, using additional gene-expression data acquired from the publicly accessible cohort of BC samples in TCGA (n = 1,097; Table S1). This analysis showed that Prune-1 positively correlated with both SMAD2 and SMAD4 levels in the BC samples with PgR, ER, and HER2 negative status (R value, 0.19–0.35; Table S1). Overall, Prune-1 positively correlated with the TGF-β downstream effectors in TNBC. This is of great interest for the immunoregulatory action of TGF-β exerted in the TME.

Using a murine model of metastatic TNBC cells (i.e., 4T1 cells (Yoneda et al., 2000)), independent stable clones were generated: Prune-1-silenced (0.6-fold, p = 0.02; Figure S2A) and h-Prune-1-FLAG-overexpressing (Figure S2B) 4T1 clones. We asked whether any Prune-1-induced perturbation can modulate TGF-β signaling pathways. As shown in Figure S2C, decreased levels of phosphorylated-(Ser467)-SMAD2 (i.e., phospho-SMAD2, the main effector of the canonical TGF-β cascade) were shown in Prune-1-silenced

4T1 clones. In contrast, increased phospho-SMAD2 levels were seen in the Prune-1-overexpressing 4T1 clones (Figure S2D), when compared with the control clones (i.e., empty vector, E.V.). Overall, these data confirmed that Prune-1 enhances the canonical (SMAD2-mediated) TGF-β pathway also in TNBC cells (Ferrucci et al., 2018).

As previous reports had shown that through binding to GSK-3β (Kobayashi et al., 2006), Prune-1 can enhance canonical Wnt signaling (Carotenuto et al., 2014), we also investigated the activated β-catenin protein levels in these 4T1 stable clones using western blotting (Figures S2C and S2D). These data showed reduced protein levels of activated β-catenin (i.e., dephosphorylated on Ser37 and/or Thr41) in Prune-1-silenced 4T1 clones (Figure S2C), whereas increased levels were observed in the Prune-1-overexpressing cells (Figure S2D). Overall, these results also confirm that Prune-1 can positively modulate the canonical Wnt signaling cascade in these TNBC cells, as previously shown for lung cancer (Carotenuto et al., 2014).

In summary, Prune-1 enhances the activation of canonical TGF-β and Wnt signaling pathways *in vitro* in a metastatic model of TNBC (i.e., 4T1 cells).

Prune-1 at the interplay of communication between TNBC cells and macrophages

Tumorigenic and immune cells within the TME communicate through extracellular mediators (e.g., cytokines, EVs, exosomes), which are also sensors in the modulation of immune cells (Spano and Zollo, 2012). We previously reported that Prune-1 has an extracellular role in paracrine communication via Wnt3a cytokine secretion (Carotenuto et al., 2014). As clinical evidence indicates that M2-TAMs positively correlate with metastasis and poor outcome in TNBC (Sousa et al., 2015; Yuan et al., 2014), we here determined the potential involvement of Prune-1 in the intratumoral recruitment of M2-TAMs in TNBC.

In this regard, we evaluated the recruitment/migration of immune cells using murine J774A.1 (#ATCC-TIB-67 (Lam et al., 2009)) and Raw264.7 (ATCC-TIB-71) macrophages, by performing a real-time cell motility assays (Cell Index) in which conditioned media from 4T1-Prune-1 cell clones (as previously described) were used as chemoattractants. As shown in Figure 1B, the conditioned media from Prune-1-overexpressing 4T1 cell clones increased the migration rates of both J774A.1 and Raw264.7 macrophages (Figure 1B, red lines), whereas the media from Prune-1-silenced 4T1 cell clones reduced their migration rate (Figure 1B, green lines). These results were compared with those from EV control clones (Figure 1B, black lines).

Furthermore, the conditioned media from 4T1 cell clones were also used to grow macrophages *in vitro*, to determine the activation status of macrophages by measuring the phosphorylation status of the STAT3 protein (i.e., pY705-STAT3 is required for dimerization and nuclear translocation (Levy and Darnell, 2002), whereas pS727-STAT3 is linked to increased STAT3 transactivation (Decker and Kovarik, 2000)), due to its prominent role in macrophage activation and during M1-M2 switch in the polarization processe (Wang et al., 2014). As shown in Figures 1C–1E, S2E, and S2F, pY705-STAT3 and pS727-STAT3 were significantly decreased in the J774A.1 (pY705-STAT3: 0.6-fold, $p = 0.05$; pS727-STAT3: 0.6-fold, $p = 0.04$; Figures 1D and S2E) and Raw264.7 (pY705-STAT3: 0.27-fold, $p = 0.01$; pS727-STAT3: 0.56-fold, $p = 0.006$; Figures 1E and S2F) macrophages cultured in media from Prune-1-silenced 4T1 clones, compared with those cultured in media from the control clones (EV). In contrast, we did not find any significant downregulation of total STAT3 in both J774A.1 (0.7-fold, $p = 0.17$, Figures 1D and S2E) and Raw264.7 (0.55-fold, $p = 0.18$, Figures 1E and S2F) macrophages. However, the conditioned media collected from the Prune-1-silenced 4T1 cell clone do not completely abolish phosphorylated STAT3 protein levels in the recipient macrophages (Figures 1C–1E, S2E, and S2F). We believe that this is because of the incomplete knockdown of m-Prune-1 in the 4T1 cell clone (0.6-fold downregulation, $p = 0.02$, see Figure S2A). However, it is not possible to exclude the presence of activating factors of STAT3 that are independent of Prune-1 actions.

For the above reasons, we believe that this finding might represent one of the mechanisms in the downregulation of the STAT3 pathway in these macrophages grown in the conditioned media collected from Prune-1-silenced tumorigenic cells.

Secretion of inflammatory cytokines from TNBC cells are modulated by Prune-1

We have here investigated whether Prune-1 can influence the recruitment/activation of macrophages by modulation of the secretion of extracellular mediators (i.e., cytokines, chemokines). For this purpose, we compared the levels of 144 cytokines secreted in the conditioned media collected from three different

independently generated Prune-1-overexpressing 4T1 cell clones (pooled together) and compared them to those secreted by the EV control clones (Figure S3A, upper panel). These analyses showed 17 cytokines that were differentially secreted (14 upregulated >2-fold; three downregulated <0.5-fold; see fold intensity in Figure S3B). In particular, the levels of CD30, lungkine/CXCL15, and E-cadherin were significantly decreased in the pooled conditioned media from Prune-1-overexpressing 4T1 clones, compared with those from the control clones. In contrast, the levels of LIX/CXCL5, thymus CK-1/CXCL7, thymic stromal lymphopoietin (TSLP), 6Ckine, ALK1, amphiregulin (Areg), CD36, CD40 ligand/CD154, galectin 1, IL-17F, IL-28, IL-20, JAM-A/F11R, and "regulated upon activation, normal T cell expressed and secreted" (RANTES or CCL5) were increased in the pooled conditioned media derived from Prune-1-overexpressing 4T1 clones, compared with conditioned media from the control clones (Figure S3B). To further confirm these data, we determined the levels of the selected Prune-1-modulated cytokines (i.e., n = 17) in the conditioned media from Prune-1-silenced 4T1 cell clones (Figure S3A, bottom panel). These data showed that among these 17 cytokines analyzed, E-cadherin, RANTES, galectin 1, IL-17F, IL-20, and IL-28 (also known as type III interferon-λ) levels were significantly decreased (Figures 1F and S3C). In contrast, CD30 levels increased in the conditioned media collected from Prune-1-silenced 4T1 cells, thus following an opposite trend compared with those in conditioned media from Prune-1-overexpressing 4T1 cell clones (Figure 1F). These findings indicated that secretion of the RANTES, galectin 1, IL-17F, IL-20, and IL-28 cytokines might be positively modulated by Prune-1 expression in TNBC cells. Gene Ontology analyses indicated that these cytokines are involved in immune system process (GO:0002376, fdr:0.0046), immune response (GO:0002376, fdr: 0.0138), immune effector processes (GO:0002252, fdr: 0.0302), and innate immune responses (GO:0045087, fdr: 0.0473), thus suggesting involvement in the regulation of immune cells within the TME. Of importance, among these cytokines, IL-20 and IL-28 were reported to take part to JAK-STAT signaling pathway activation (KEGG: mmu04630, fdr: 0.004), which is involved in M1- or M2-macrophage polarization (Wang et al., 2014). Of interest, through its binding to IL-17RA on recipient endothelial cells, the IL17A/IL17F heterodimer was previously reported to activate the STAT3 pathway (mainly via Y705 phosphorylation) and consequently to recruit immune cells (Yuan et al., 2015).

Altogether, we have described here that overexpression of Prune-1 in 4T1 murine TNBC cells might have a role in modulation of macrophage activation through the extracellular secretion of soluble cytokines (i.e., RANTES, galectin1, IL17-F, IL-20, IL-28). We measured the "activation" of macrophages by evaluating their migration rate and STAT3 pathway (Wang et al., 2014), because its activation in TAMs has been shown to induce immunosuppression, angiogenesis, cell growth, and metastasis (Yu et al., 2007; Dang et al., 2015). Furthermore, STAT3 inhibition was also reported to "re-educate" TAMs via reversing their phenotype from M2 to M1 (Fujiwara et al., 2014; Zhang et al., 2013). How Prune-1 influences the expression of these cytokines in tumorigenic cells and the activation of STAT3 in macrophages will be the focus of other studies.

Prune-1 modulates TAMs in the TME in a genetically engineered mouse model of metastatic TNBC

Sequence homology analyses between human (h) and murine (m) Prune-1 protein sequences show a significant similarity (overall aa: 85.43% identity; DHH and DHHA2 enzymatic domains: 88.24% and 82.39% identity, respectively; NME1-binding domain (Carotenuto et al., 2013): 83.33% identity; see Figure S4A). To determine whether the overexpression of h-Prune-1 has similar immune responses (in terms of cytokines expression) to m-Prune1, we transiently transfected h-Prune-1 or m-Prune-1 cDNA plasmid constructs into Raw264 macrophages, because of their lower Prune-1 endogenous expression levels compared with J774 macrophages (Figure S4B). Using real-time PCR analysis, we showed the same levels of upregulation of inflammatory cytokines (i.e., IL-10, Arg1, MMP9, IL-1β) in both h-Prune-1- and m-Prune-1-overexpressing Raw264 macrophages (Figures S4C and S4D). These data show the potential involvement of the Prune-1 protein in the modulation of cytokines expression also in immune cells (i.e., macrophages), and they also show no significant differences between the functional regulation of the human versus murine Prune-1 proteins. For these reasons and to characterize the effects of Prune-1 overexpression in the TME of BC, we generated a GEMM-overexpressing human Prune-1 in the mammary gland.

This GEMM was generated using a vector construct that contained h-Prune-1 cDNAs under the control of the MMTV promoter (Callahan and Smith, 2000) (Figure S4E). Female mice harboring h-PRUNE-1 cDNA overexpressed in mammary glands (i.e., MMTV–Prune-1) developed mammary hyperplasia early in life (by 80 days of age), compared with the control FVB mice, as shown in Figure S4F. These MMTV–Prune-1 mice were monitored for 12 months. Although benign mammary lesions that were usually hyperplasia

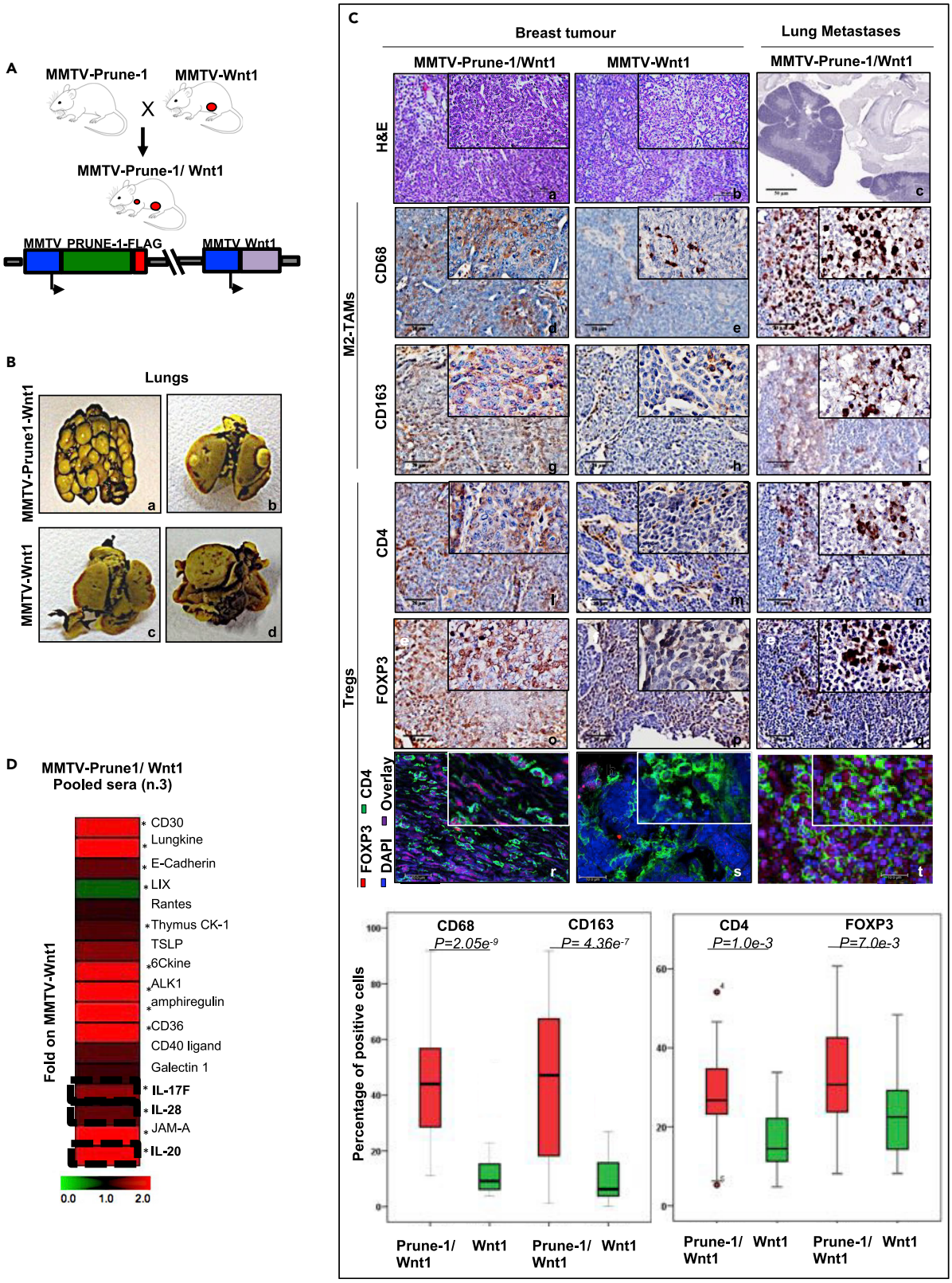
A
MMTV-Prune-1
MMTV-Wnt1
X
MMTV-Prune-1/ Wnt1
MMTV_PRUNE-1-FLAG
MMTV_Wnt1
B
Lungs
MMTV-Prune1-Wnt1
MMTV-Wnt1
a
b
c
d
C
Breast tumour
Lung Metastases
MMTV-Prune-1/Wnt1
MMTV-Wnt1
MMTV-Prune-1/Wnt1
H&E
M2-TAMs
CD68
CD163
Tregs
CD4
FOXP3
FOXP3 CD4 Overlay DAPI
Percentage of positive cells
CD68
P=2.05e-9
CD163
P= 4.36e-7
CD4
P=1.0e-3
FOXP3
P=7.0e-3
Prune-1/ Wnt1
Wnt1
D
MMTV-Prune1/ Wnt1
Pooled sera (n.3)
Fold on MMTV-Wnt1
CD30
Lungkine
E-Cadherin
LIX
Rantes
Thymus CK-1
TSLP
6Ckine
ALK1
amphiregulin
CD36
CD40 ligand
Galectin 1
IL-17F
IL-28
JAM-A
IL-20
0.0
1.0
2.0

Figure 2. Prune-1 protein overexpressed in metastatic TNBC mouse model (MMTV–Prune-1/Wnt1) promotes M2-TAMs recruitment in both primary tumor and metastatic niche via soluble cytokines

(A) Schematic diagram showing the cross between MMTV–Prune-1 and MMTV–Wnt1 mice to obtain the double transgenic MMTV–Prune-1/Wnt1 model.

(B) Representative photographs of the lungs from MMTV–Prune-1/Wnt1 **(a–b)** and MMTV–Wnt1 **(c–d)** mice fixed in Bouin's solution. Metastatic foci (i.e., macrometastasis) are visible in the lungs from MMTV–Prune-1/Wnt1 **(a–b)**.

(C) Representative hematoxylin-eosin staining **(a–c)**, immunohistochemistry (IHC; **d–q)**, and immunofluorescence (IF; **r–t**) performed on sections of mammary tumors developed from MMTV–Prune-1/Wnt1 and MMTV–Wnt1 mice, and metastatic lungs from MMTV–Prune-1/Wnt1 mice, using antibodies against the following: CD68 **(d–f)** and CD163 **(g–i)**, as markers for M2-TAMs; CD4 **(l–n)**, as a marker for T cells; and FOXP3 **(o–q)**, as a marker for Tregs. Double indirect IF was performed to detect Tregs (i.e., CD4+ FOXP3+, **r–t**). CD4: green; FOXP3: red; DAPI: blue. Quantification was performed using a quantitative pathology workstation (Mantra) with image analysis software (inform). Data were calculated from three independent tumors. Graphs were constructed using the IBM SPSS statistics software. Magnification, 5×, 20×, 40×. Scale bar: 50 μm, hematoxylin-eosin; 20 μm, IHC; 10 μm, IF.

(D) Prune-1 induces secretion of soluble cytokines *in vivo*. Densitometer analyses of the cytokines upregulated and downregulated in the sera collected and pooled from three MMTV–Prune-1/Wnt1 mice and MMTV–Wnt1 mice. Among the cytokines modulated by Prune-1, significant upregulation of IL-17F, IL-28, and IL-20 was seen, with an opposite trend compared with the cytokines in the conditioned media from Prune-1-silenced 4T1 cells. Data are means ± standard deviation. Data were represented using MultiExperiment Viewer (http://www.tm4.org/mev.html). *, $p < 0.05$ in Student's t test comparing cytokines levels of pooled sera from n.3 MMTV-Prune-1/Wnt1 mice with those from n.3 MMTV-Wnt1 mice.

were seen in 100% of the female mice, none developed tumors in the mammary glands over 1 year of observation.

For these reasons, female MMTV–Prune-1 mice were then crossed with MMTV–Wnt1 mice (Figures 2A and S4G), a GEMM resembling "basal-like" TNBC (Li et al., 2000; Yu et al., 2016; Herschkowitz et al., 2007), which rarely develops spontaneous metastasis to the lungs (Huang et al., 2008). The resulting double transgenic MMTV–Prune-1/Wnt1 mouse model (n = 31) developed mammary tumors (with 100% penetrance), as did the MMTV–Wnt1 mice (n = 44). Interestingly, the overexpression of both Prune-1 and Wnt1 in the mammary glands did not alter mammary tumor onset, compared with the MMTV–Wnt1 mice (Figure S4H). Furthermore, through IHC analysis, we confirmed that the mammary tumors that were generated in the double transgenic MMTV–Prune-1/Wnt1 mice resemble the TNBC subgroup with undetectable levels of both ERs and PgRs (Figure S5A), thus confirming these models as GEMM of TNBC. Nevertheless, although MMTV–Wnt1 mice did not develop lung metastasis at 2 months from tumor onset, MMTV–Prune-1/Wnt1 mice showed macro-metastasis in the lungs at 97% penetrance (Figure 2B, Table S2).

In addition, we investigated the presence of immune infiltrating cells in the mammary TME. Among the immune infiltrating cells, we focused on M2-TAMs ($CD163^+$) and Tregs ($FOXP3^+$), which have been reported as markers for the subtype of TNBC with poorest prognosis (Adams et al., 2017). As shown in Figure 2C, our quantitative IHC and immunofluorescence (IF) analyses (using a quantitative pathology approach; see Methods) revealed increased levels of both M2-TAMs (i.e., $CD68^+$ $CD163^+$ cells) and Tregs (i.e., $FOXP3^+$ $CD4^+$ cells) in the TME of MMTV–Prune-1/Wnt1 mice compared with MMTV–Wnt1 (CD68: $p = 2.05 \times 10^{-9}$; CD162: $p = 4.36 \times 10^{-7}$; CD4: $p = 1.0 \times 10^{-3}$; FOXP3: $p = 7.0 \times 10^{-3}$). Of note, M2-TAMs and Tregs were also found in the metastatic niche into the lungs of the MMTV–Prune-1/Wnt1 mice (Figure 2C). Of interest, we performed the same IHC and IF analyses on the contralateral nontumoral mammary glands of MMTV–Prune-1/Wnt1 and MMTV–Wnt1 mice, and on the lungs from MMTV–Wnt1 mice (Figure S5B), where immune infiltrating cells were not found. Altogether these data indicate a role for Prune-1 in combination with other factors in the recruitment/activation of immunosuppressive cells in the TME of both the primary tumor and lung metastatic microenvironments in TNBC.

To better underpin the role of Prune-1 in metastatic TNBC, we also investigated the function of Prune-1 in the activation of TGF-β signaling and induction of epithelial-mesenchymal transition (EMT) (Ferrucci et al., 2018). Here, higher SMAD2/3 levels were detected in primary mammary tumors derived from the double transgenic mice (i.e., MMTV–Prune-1/Wnt1), compared with those from MMTV–Wnt1 models (Figures S6A and S6B). Furthermore, undetectable E-cadherin and higher N-cadherin levels were found in the tumors from MMTV–Prune-1/Wnt1 mice compared with those from MMTV–Wnt1 mice, which in contrast showed higher E-cadherin and lower N-cadherin levels (Figures S6A and S6B). Of interest, the microenvironment of the nontumoral contralateral mammary gland also shows higher SMAD2/3 and N-cadherin and lower E-cadherin levels in MMTV–Prune-1/Wnt1 compared with those from MMTV–Wnt1 models (Figures S6C and S6D). These data thus confirm that Prune-1 enhances TGF-β and EMT also in this GEMM of metastatic TNBC.

Furthermore, of interest, there were increased levels of IL-17F, IL-20, and IL-28 in the sera from MMTV–Prune-1/Wnt1 mice (as pooled sera from three mice) compared with those from MMTV–Wnt1, as shown

in Figures 2D, S7A, and S7B. These cytokines were previously shown to be overexpressed in conditioned media collected from Prune-1-overexpressing 4T1 cells and downregulated in those derived from Prune-1-silenced 4T1 clones (Figure 1F), thus translating the *in-vitro* findings into the *in-vivo* results.

Thus, as overexpressed in this GEMM of metastatic TNBC, Prune-1 can modulate immunosuppressive cells (including M2-TAMs) in the TME also through the secretion of these extracellular soluble mediators (i.e., IL-17F, IL-20, IL-28).

Prune-1 activates metastatic pathways and enhances the migratory phenotype in murine TNBC primary cells

To dissect out the function of Prune-1 in TNBC, primary murine tumorigenic cells were obtained from the tumors generated from MMTV–Prune-1/Wnt1 and MMTV–Wnt1 mice (at 2 months from the tumor onset; Figures S8A and S8B). Here we show the activation of both canonical TGF-β and Wnt signaling in MMTV–Prune-1/Wnt1 cells compared with MMTV–Wnt1 cells, as shown by increased levels of phospho-Ser467-SMAD2, phospho-Ser9/21-GSK-3β, and Wnt3a (Figure S8C). Importantly, the same analysis also showed increased levels of EMT markers in MMTV–Prune-1/Wnt1 cells (i.e., undetectable E-cadherin, higher N-cadherin levels), increased phosphorylation levels of phospho-(Ser-473)-AKT, and decreased expression of its repressor PTEN, compared with MMTV-Wnt1 cells (Figure S8C). These data also showed increased levels of phosphorylated Ser120-122-125-NME1 (or NDPK-A; sign of complex formation with the Prune-1 protein) in these primary cells (Garzia et al., 2008) (Figure S8C). Altogether, these results indicate the activation of Prune-1–metastatic pathway (as Prune-1 in complex formation with NME1; as previously described for medulloblastoma (Ferrucci et al., 2018)) also in these murine TNBC primary cells (i.e., MMTV–Prune-1/Wnt1 cells), thus overall suggesting increased migratory properties of these primary Prune-1-overexpressing TNBC cells.

These findings were further supported *in vitro* by assays performed using real-time proliferation and migration assays. These data showed that the primary MMTV–Prune-1/Wnt1 cells have higher proliferative index (Figure S8D), shorter doubling time (i.e., MMTV–Prune-1/Wnt1: 28.4 h; MMTV–Wnt1: 35.8 h; $p = 4.1 \times 10^{-5}$; Figure S8E) and greater migration rate (using 10% FBS as chemoattractant, Figure S8F) when compared with MMTV–Wnt1 cells.

Overall these data indicate that Prune-1 can enhance the proliferative and migratory properties also in these primary tumorigenic cells derived from mammary tumors generated from our GEMM.

Macrophage polarization is enhanced by Prune-1 overexpression in TNBC

Whether Prune-1 has a role in the polarization process of macrophages in these primary murine TNBC cells was also investigated. For this purpose, conditioned media from MMTV–Prune-1/Wnt1 and MMTV–Wnt1 primary cells (collected over 24 h) were used to grow J774A.1 and Raw264 macrophages *in vitro* (Figure 3A), to evaluate their "polarization status" by measuring the expression levels of "M2-associated genes" (Orecchioni et al., 2019) through whole-genome RNA sequencing approaches (i.e., RNAseq; Figures 3B and 3C; see Additional Data). Untreated macrophages were used as the negative control. These data showed up-regulation (i.e., fold change on untreated macrophages >2, $p < 0.01$) of 24 genes (Figure 3B, Table S3) and 27 genes (Figure 3C, Table S3) belonging to "M2-associated genes" in the J774A.1 and Raw264 macrophages, respectively, grown in the conditioned media collected from MMTV–Prune-1/Wnt1 cells, as compared with those grown in MMTV–Wnt1-derived media. In contrast, only one gene (i.e., Emp1) was up-regulated (i.e., fold change over untreated macrophages >2; $p < 0.01$) in J774A.1 cells treated with conditioned media from MMTV–Wnt1 cells (Figure 3B). This thus indicated that Prune-1 takes part in the polarization processes. Of interest, among those upregulated genes in the macrophages grown in the conditioned media from MMTV–Prune-1/Wnt1 cells, 11 were common between J774A.1 and Raw264 macrophages (Figures 3B and 3C, black boxes). These included the most representative M2-associated genes (i.e., MMP-9, arginase-1 [Arg1], IL-10 (Mantovani et al., 2002)) and IL-1β, the intracellular accumulation of which was reported during the switch from M1-status toward M2-status of macrophages (Martinez et al., 2006; Pelegrin and Surprenant, 2009). Moreover, our data also showed higher phospho-STAT3 levels in J774A.1 macrophages grown in the conditioned media from the MMTV–Prune-1/Wnt1 cells, compared with those treated with the conditioned media from the MMTV–Wnt1 cells (Figure S9A). These data suggest that in a "Prune-1–overexpression status" in tumorigenic cells, modulation of the M1-M2 switch of macrophages occurs.

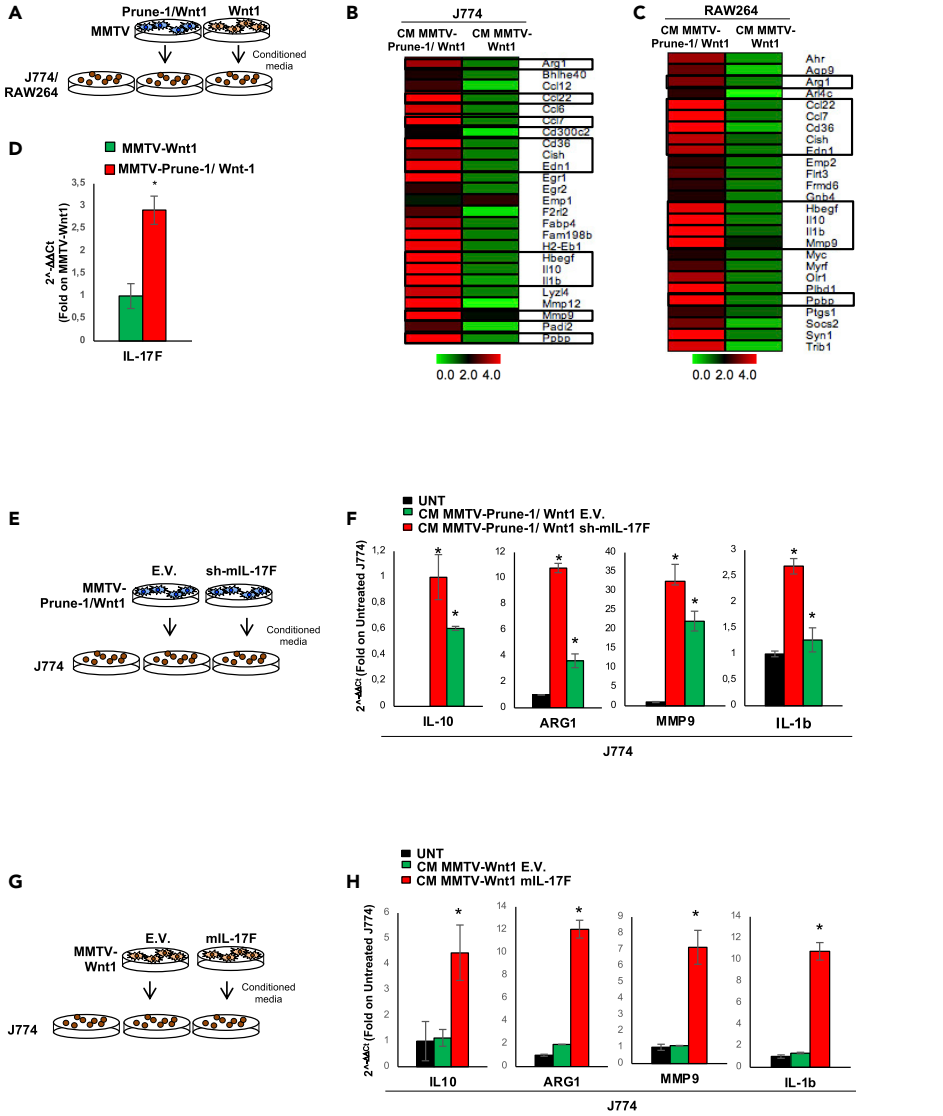

Figure 3. Prune-1 overexpressed in TNBC cells promotes M2-polarization of macrophages *in vitro* through IL-17F

(A–C) J774A.1 and Raw264 macrophages were grown for 48 h in conditioned media collected (after 24 h) from MMTV–Prune-1/Wnt1 or MMTV–Wnt1 cells (A). Fold-change heatmap (http://www.tm4.org/mev.html) for upregulated M2-associated genes (fold change on untreated macrophages >2, $p < 0.01$) in J774A.1 (B) and Raw264 (C) macrophages grown in conditioned media from MMTV–Prune-1/Wnt1 versus MMTV–Wnt1 cells. The black boxes indicate the common genes upregulated in both J774A.1 and Raw264 macrophages. The color scale under the heatmap illustrates the fold-change values shown in the heatmap.

(D) Real-time PCR analysis of IL-17F in MMTV–Prune-1/Wnt1 (red) and MMTV–Wnt1 (green) cells. *$p < 0.05$ in Student's t test comparing IL-17F levels of MMTV-Prune-1/Wnt1 with MMTV-Wnt1 cells.

(E and F) J774A.1 macrophages were grown for 48 h in conditioned media collected (after 24 h) from MMTV–Prune-1/Wnt1 previously transfected with murine sh-IL17F plasmid or empty vector (EV) as negative control (E). Real-time PCR analysis of some M2-associated genes, including IL-10, Arg-1, MMP-9, and IL-1β, in J774A.1 macrophages grown for 48 h in conditioned media from MMTV–Wnt1 cells transfected with sh-IL-17F (red) or EV control (green) (F). Untreated J774A.1 macrophages were used as the negative controls (UNT, black). *$p < 0.05$ in Student's t test compared with untreated macrophages.

(G and H) J774A.1 macrophages were grown for 48 h in conditioned media collected (after 24 h) from MMTV–Wnt1 previously transfected with murine IL-17F or EV as negative control (G). Real-time PCR analysis of some M2-associated genes, including Arg-1, MMP-9, and IL-1β, in J774A.1 macrophages grown for 48 h in conditioned media from MMTV–Wnt1 cells transfected with IL-17F (red) or EV control (green). Untreated J774A.1 macrophages were used as the negative controls (UNT, black) (H). *$p < 0.05$ in Student's t test compared with untreated macrophages.

Then, to better dissect out how Prune-1 can take part in extracellular communication between TNBC cells and macrophages, we investigated whether Prune-1 can act in the modulation of M2-polarization through the release of soluble mediators. We focused on IL17-F due to its role in leukocyte infiltration and recruitment (i.e., macrophages, lymphocytes) (Yang et al., 2008; Giles et al., 2016; Starnes et al., 2001) (Shahrara et al., 2009; Nonaka et al., 2009). In this regard, the expression level of IL-17F was higher in MMTV–Prune-1/Wnt1, as compared with MMTV–Wnt1 cells (Figure 3D). Then, J774A.1 macrophages were grown in conditioned media derived from MMTV–Prune-1/Wnt1 cells or sh-IL17F-MMTV–Prune-1/Wnt1 (0.2-fold, Figures 3E and S9B). These data showed that J774A.1 macrophages treated with media from MMTV–Prune-1/Wnt1 cells expressed higher levels of Arg1, MMP9, IL-10, and IL-1β (Figure 3F), compared with untreated macrophages, thus confirming the RNAseq data. In contrast, lower levels of these M2-genes (i.e., Arg1, MMP9, IL-10, IL-1β) were found in the J774A.1 macrophages grown in the conditioned media from sh-IL17F-MMTV–Prune-1/Wnt1 cells (Figure 3F).

In contrast, J774A.1 macrophages were grown in the conditioned media derived from MMTV–Wnt1 cells or MMTV–Wnt1 cells overexpressing IL-17F (Figures 3G and S9C). These data showed that J774A.1 macrophages expressed higher levels of M2-associated genes (i.e., Arg1, MMP9, IL-10, IL-1β) only when they were grown in conditioned media from MMTV–Wnt1 cells overexpressing IL17F, as compared with those grown in conditioned media from MMTV–Wnt1 cells or untreated macrophages (Figure 3H). These data indicated a potential role for this inflammatory cytokine (i.e., IL17F) in the polarization process of immune cells.

Altogether, these data suggested that M2-polarization of TAMs (i.e., IL-10^{High}, Arg1^{High}, MMP9^{High}, IL-1β^{High}) in metastatic TNBC is evident in a Prune-1-overexpression status. Indeed, as shown here, Prune-1 takes part in the extracellular communication between tumorigenic and immune cells through secretion of IL-17F. Details on how this occurs will be the focus of future studies.

Prune-1 induces macrophage polarization via extracellular vesicles

Tumor-derived EVs (including exosomes) have begun to emerge as new factors in tumor progression and organotropic metastatic dissemination. These have been reported to act via several mechanisms, including modulation of the antitumor immune response in the TME (Thery et al., 2009).

As Prune-1 induces M2-macrophage recruitment in the TME and promotes lung metastasis in the present GEMM of metastatic TNBC, we investigated whether EVs derived from MMTV–Prune-1/Wnt1 cells also contribute to these processes. To define a global picture of Prune-1–driven EV-proteins, a proteomic analysis was performed for those EVs secreted by both MMTV–Prune-1/Wnt1 and MMTV–Wnt1 cells. For this purpose, EVs were isolated (as previously described (Thery et al., 2006)) from media derived from both MMTV–Prune-1/Wnt1 and MMTV–Wnt1 cells. Subsequently, to define potential changes in EV-protein content in Prune-1-overexpressing cells, the extracellular proteins were analyzed using label-free quantitative mass spectrometry technology (as described in Supplemental Information (Cox et al., 2014)). These analyses showed that the EVs isolated from the media from both of these murine primary TNBC cells shared 31 proteins in common, whereas those derived from the MMTV–Prune-1/Wnt1 cells and the MMTV–Wnt1 cells had 21 and 10 mutually exclusive proteins, respectively (as summarized in Figures 4A and S9D). Among the extracellular proteins secreted by the MMTV–Prune-1/Wnt1 cells, we identified some extracellular proteins linked to EMT, motility, and metastasis in BC, including vimentin (Vim; (Yamashita et al., 2013)), interferon-induced transmembrane protein 3 (Ifitm3; (Yang et al., 2013a)), and syndecan-binding protein (syntenin-1/Sdcbp (Yang et al., 2013b; Qian et al., 2013; Koo et al., 2002)) (Table 1). These data suggested that Prune-1 promotes distant metastasis in TNBC also by modulation of EV-protein content.

Then, to investigate the potential role for these extracellular proteins secreted via EVs from MMTV–Prune-1/Wnt1 cells in the modulation of M2-associated genes (i.e., IL-10, MMP9, Arg1, IL-1β), J774A.1 macrophages were grown in conditioned media from MMTV–Prune-1/Wnt1 cells depleted of EVs (Figures 4B and S9E). These data showed reduction of IL-10, IL-1β, and Arg1 expression levels in the macrophages grown in the conditioned media without EVs, compared with those treated with complete supernatant (Figure 4C), whereas the expression levels of MMP9 were increased. This thus suggested different mechanisms of extracellular regulation of MMP9 in our model system. In contrast, the depletion of EVs from the media from MMTV–Wnt1 cells did not change the expression levels of M2-associated genes (i.e., MMP9, Arg1, IL-1β) in J774A.1 macrophages, with the exception of IL-10 (Figures 4D and 4E). The *in-vitro* data further

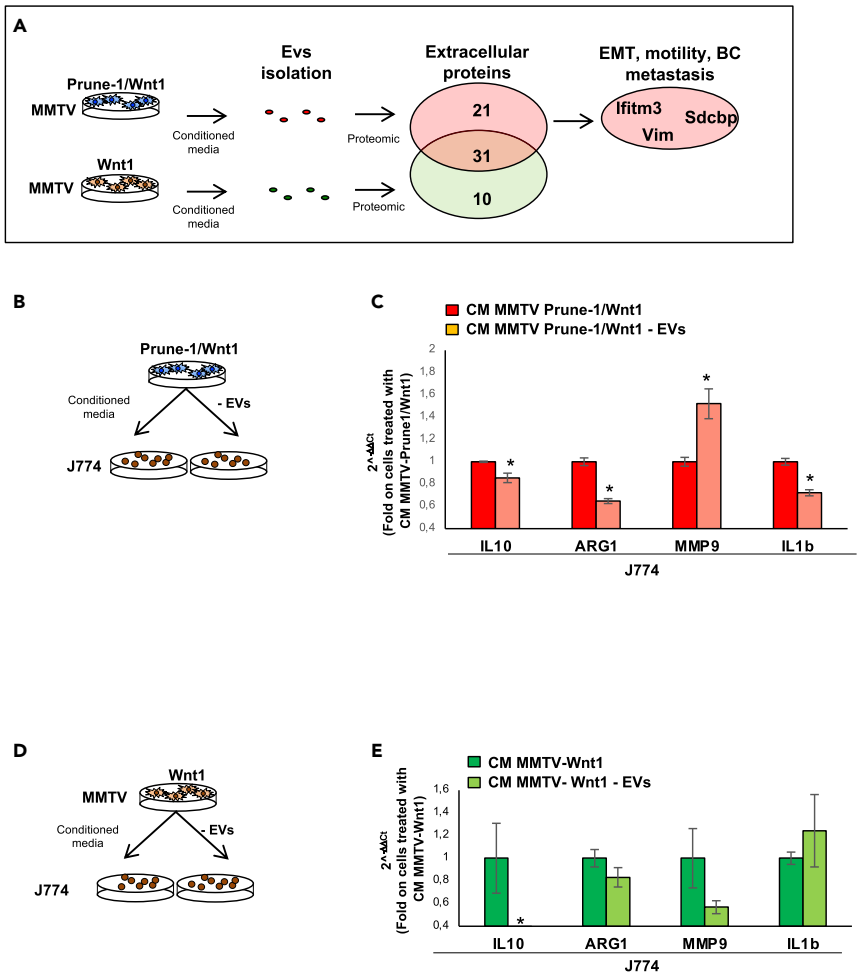

Figure 4. Prune-1 overexpressed in TNBC cells promotes M2-polarization of macrophages *in vitro* through modulation of EV-protein content

(A) Representative scheme for proteomic analyses performed on extracellular vesicles (EVs). EVs were isolated from media from murine primary MMTV–Prune-1/Wnt1 and MMTV–Wnt1 cells. Proteomic analyses were performed on isolated EVs using label-free quantitative mass spectrometry. Data show 31 extracellular proteins in common between EVs from media of MMTV–Prune-1/Wnt1 and MMTV–Wnt cells, and 21 and 10 mutually exclusive extracellular proteins from MMTV–Prune-1-Wnt cells (red) and MMTV–Wnt1 cells (green). Data are representative of two independent experiments.

(B and C) J774 macrophages were grown for 48 h in conditioned media collected (after 24 h) from MMTV–Prune-1/Wnt1 cells depleted or not in EVs from the culture supernatant (B). Real-time PCR analysis of some M2-associated genes, including IL-10, Arg-1, MMP-9, and IL-1β, in J774 macrophages grown for 48 h in conditioned media from MMTV–Prune-1/Wnt1 depleted (red) or not (light red) in EVs (C). *$p < 0.05$ in Student's t test compared with macrophages treated with conditioned media from MMTV-Prune-1/Wnt1 cells not depleted in EVs.

(D and E) J774 macrophages were grown for 48 h in conditioned media collected (after 24 h) from MMTV–Wnt1 cells depleted or not in EVs from the culture supernatant (D). Real-time PCR analysis of some M2-associated genes, including IL-10, Arg-1, MMP-9, and IL-1β, in J774 macrophages grown for 48 h in conditioned media from MMTV–Wnt1 depleted (light green) or not (dark green) in EVs (E). *$p < 0.05$ in Student's t test compared with macrophages treated with conditioned media from MMTV-Wnt1 cells not depleted in EVs.

indicated specific actions of those extracellular proteins secreted from Prune-1-overexpressing cells (i.e., MMTV–Prune-1/Wnt1 cells) in the modulation of M2-macrophage polarization.

To confirm these findings, we evaluated the polarization genes in J774A.1 macrophages grown in conditioned media derived from MMTV–Wnt1 cells that had been previously pre-treated with the supernatant of MMTV–Prune-1/Wnt1 cells containing or depleted in EVs (Figure S9F). These data showed increased

Table 1. Mutually exclusive proteins found into extracellular vesicles (EVs) derived from MMTV-Prune-1/Wnt1 cells

Gene symbol	Gene name	Accession	Number of distinct peptides	% of total peptides	Protein function (GO)
Htra1	Serine protease HTRA1	Q9R118	3	0.42%	Serine protease HTRA1; serine protease with a variety of targets, including extracellular matrix proteins such as fibronectin. HTRA1-generated fibronectin fragments further induce synovial cells to upregulate MMP1 and MMP3 production. May also degrade proteoglycans, such as aggrecan, decorin, and fibromodulin. Through cleavage of proteoglycans, may release soluble FGF-glycosaminoglycan complexes that promote the range and intensity of FGF signals in the extracellular space. Regulates the availability of insulin-like growth factors (IGFs) by cleaving IGF-binding proteins.
Cd81	CD81 antigen	P35762	2	0.31%	CD81 antigen; may play an important role in the regulation of lymphoma cell growth. May be involved in the acrosome reaction.
Anxa11	Annexin A11	P97384	8	0.86%	Required for midbody formation and completion of the terminal phase of cytokinesis (by similarity). Binds specifically to calcyclin in a calcium-dependent manner.
Emilin2	Elastin microfibril interfacer 2	Q8K482	5	0.87%	May be responsible for anchoring smooth muscle cells to elastic fibers and may be involved not only in the formation of the elastic fiber but also in the processes that regulate vessel assembly.
Ifitm3	Interferon-induced transmembrane protein 3	Q9CQW9	3	0.47%	IFN-induced antiviral protein that inhibits the entry of viruses to the host cell cytoplasm, permitting endocytosis, but preventing subsequent viral fusion and release of viral contents into the cytosol. Active against multiple viruses, including influenza A virus, SARS coronavirus (SARS-CoV), Marburg virus (MARV) and Ebola virus (EBOV), Dengue virus (DNV), West Nile virus (WNV) and human immunodeficiency virus type 1.
Vim	Vimentin	P20152	6	0.73%	Vimentins are class-III intermediate filaments found in various non-epithelial cells, especially mesenchymal cells. Vimentin is attached to the nucleus, endoplasmic reticulum (ER), and mitochondria, either laterally or terminally.
Stom	Stomatin	P54116	6	0.80%	Erythrocyte band 7 integral membrane protein; regulates ion channel activity and transmembrane ion transport. Regulates ASIC2 and ASIC3 channel activity.
Mme	Membrane metalloendopeptidase	Q61391	5	0.57%	Thermolysin-like specificity but is almost confined on acting on polypeptides of up to 30 amino acids. Biologically important in the destruction of opioid peptides such as Met- and Leu-enkephalins by cleavage of a Gly-Phe bond. Able to cleave angiotensin-1, angiotensin-2, and angiotensin 1–9.
Sdcbp	Syndecan-binding protein	O08992	5	0.71%	Multifunctional adapter protein involved in diverse array of functions including trafficking of transmembrane proteins, neuro and immunomodulation, exosome biogenesis, and tumorigenesis. Positively regulates TGFB1-mediated SMAD2/3 activation and TGFB1-induced epithelial-to-mesenchymal transition (EMT) and cell migration in various cell types. May increase TGFB1 signaling by enhancing cell-surface expression of TGFR1 by preventing the interaction between TGFR1 and CAV1 and subsequent CAV1-dependent internalization and degradation of TGFR1.

(*Continued on next page*)

Table 1. *Continued*

Gene symbol	Gene name	Accession	Number of distinct peptides	% of total peptides	Protein function (GO)
Vcp	Valosin-containing protein	Q01853	12	2.10%	Necessary for the fragmentation of Golgi stacks during mitosis and for their reassembly after mitosis. Involved in the formation of the transitional ER(tER). The transfer of membranes from the ER to the Golgi apparatus occurs via 50–70 nm transition vesicles that derive from part-rough, part-smooth transitional elements of the ER(tER). Vesicle budding from the tER is an ATP-dependent process.
Gnai2	Guanine nucleotide-binding protein alpha inhibiting 2	P08752	4	0.53%	Guanine nucleotide-binding proteins (G proteins) are involved as modulators or transducers in various transmembrane signaling systems. The G(i) proteins are involved in hormonal regulation of adenylate cyclase—they inhibit the cyclase in response to beta-adrenergic stimuli.
Chmp4b	Charged multivesicular body 4B	Q9D8B3	3	0.35%	Probable core component of the endosomal sorting required for transport complex III (ESCRT-III), which is involved in multivesicular bodies (MVBs) formation and sorting of endosomal cargo proteins into MVBs. MVBs contain intraluminal vesicles (ILVs) that are generated by invagination and scission from the limiting membrane of the endosome and mostly are delivered to lysosomes enabling degradation of membrane proteins, such as stimulated growth factor receptors, lysosomal enzymes, and lipids.
Igsf8	Immunoglobulin superfamily, member 8	Q8R366	6	0.87%	May play a key role in diverse functions ascribed to CD81 and CD9 such as oocytes fertilization or hepatitis C virus function. May regulate proliferation and differentiation of keratinocytes. May be a negative regulator of cell motility—suppresses T cell mobility coordinately with CD81, associates with CD82 to suppress prostate cancer cell migration, regulates epidermoid cell reaggregation and motility on laminin-5 with CD9 and CD81 as key linkers. May also play a role on integrin-dependent morphology and motility functions.
Anxa7	Annexin A7	Q07076	5	0.57%	Calcium-/phospholipid-binding protein that promotes membrane fusion and is involved in exocytosis
Ifitm2	Interferon-induced transmembrane 2	Q99J93	2	0.31%	IFN-induced antiviral protein that inhibits the entry of viruses to the host cell cytoplasm, permitting endocytosis, but preventing subsequent viral fusion and release of viral contents into the cytosol. Active against multiple viruses, including influenza A virus, SARS coronavirus (SARS-CoV), Marburg virus (MARV) and Ebola virus (EBOV), Dengue virus (DNV), and West Nile virus (WNV). Can inhibit influenza-virus-hemagglutinin protein-mediated viral entry, MARV and EBOV GP1,2-mediated viral entry, and SARS-CoV S-protein-mediated viral entry.
Ehd2	EH-domain containing 2	Q8BH64	3	0.40%	ATP- and membrane-binding protein that controls membrane reorganization/tubulation upon ATP hydrolysis. Plays a role in membrane trafficking between the plasma membrane and endosomes. Important for the internalization of GLUT4. Required for fusion of myoblasts to skeletal muscle myotubes. Required for normal translocation of FER1L5 to the plasma membrane.
Hist1h2bf	Histone cluster 1, H2bf	P10853	2	0.31%	Core component of nucleosome.
Ldha	lactate dehydrogenase A	P06151	6	0.80%	Ldha catalyzes the conversion of L-lactate and NAD to pyruvate and NADH in the final step of anaerobic glycolysis. The protein is found predominantly in muscle tissue and belongs to the lactate dehydrogenase family.

(*Continued on next page*)

Table 1. *Continued*

Gene symbol	Gene name	Accession	Number of distinct peptides	% of total peptides	Protein function (GO)
Rab11	Ras-related protein Rab-11B	P46638	5	0.53%	The small GTPases Rab are key regulators of intracellular membrane trafficking, from the formation of transport vesicles to their fusion with membranes. Rabs cycle between an inactive GDP-bound form and an active GTP-bound form that is able to recruit to membranes different set of downstream effectors directly responsible for vesicle formation, movement, tethering, and fusion. That Rab regulates endocytic recycling. Acts as a major regulator of membrane delivery during cytokinesis. Together with MYO5B and RAB8A participates in epithelial cell polarization.
Anxa4	Annexin A4	P97429	9	1.29%	Calcium-/phospholipid-binding protein that promotes membrane fusion and is involved in exocytosis.
Actbl2	Actin, beta-like 2	Q8BFZ3	6	0.62%	Actins are highly conserved proteins that are involved in various types of cell motility and are ubiquitously expressed in all eukaryotic cells.

The mutually exclusive extracellular proteins (analyzed using label-free quantitative mass spectrometry technology) secreted within EVs isolated from the media culture supernatant of MMTV–Prune-1/Wnt1 cells are listed.

levels of IL-10, Arg1, and IL-1β in J774A.1 macrophages when the MMTV–Wnt1 cells were grown in EV-containing media derived from MMTV–Prune-1/Wnt1 cells (Figure S9G).

In summary, Prune-1 is involved in extracellular mechanisms of communication between TNBC cells and immune cells (i.e., macrophages) not only through modulation of soluble mediators (e.g., IL-17F) but also through modulation of the EV-protein content.

Genetics, RNA expression, and mutational rate in the TNBC microenvironment

To define a more global picture of the mechanism of communication between Prune-1-overexpressing TNBC cells and macrophages, we analyzed the mutational rates (through whole-exome sequencing [WES] analyses) in MMTV–Prune-1/Wnt1 cells and the global trascriptome (via RNAseq) of macrophages that received conditioned media from these tumorigenic cells (Figure 5A).

For this purpose, we took into account all of the common genes there were overexpressed in both J774A.1 and Raw264.7 macrophages that had been grown in the media obtained from MMTV–Prune-1/Wnt1 cells (as compared with MMTV–Wnt1 cells). Then, to identify a subset of "core genes" upregulated in macrophages in response to Prune-1 overexpression in TNBC cells, we compared the lists of genes from the leading edge of enriched gene-sets from each canonical pathway sub-collection (i.e., Biocarta, Kegg, Pid, Reactome, Naba) and selected those shared by at least four out of five of them (Table 2). A protein interaction network was generated using the Search Tool for the Retrieval of Interacting Genes/Proteins (STRING) database (confidence: 0.4; https://string-db.org/cgi/network.pl?taskId=41jaTsLzWNqT). This network identified proteins involved in immune system processes (GO:0002376), cytokine-mediated signaling pathways (GO:0019221), positive regulation of MAPK cascade (GO:0043410), positive regulation of cell migration (GO:0030335), regulation of inflammatory responses (GO:0050727), positive regulation of ERK1 and ERK2 cascade (GO:0070374), positive regulation of chemotaxis (GO:0050921), and positive regulation of tyrosine phosphorylation of STAT protein (GO:0042531) and macrophage chemotaxis (GO:0048246) (Figure 5B). Of interest, among these protein interaction networks derived from the "core genes" identified here, the expression levels of COL4A1, IL-10, IL1R1, and PDGFB were positively correlated with poor prognosis in BC patients in terms of 5-year survival data analyzed from the publicity available dataset of Breast Invasive Carcinoma (n = 1,075) from The Cancer Genome Atlas (TCGA) (Figure S10).

Then, we profiled the mutation spectra in our primary murine TNBC cells that overexpressed Prune-1. WES analyses were applied to both MMTV–Prune-1/Wnt1 cells and MMTV–Wnt1 cells. We found mutually exclusive coding variants with predicted higher/moderate impact on MMTV–Prune-1-Wnt1 cells (177 variants in

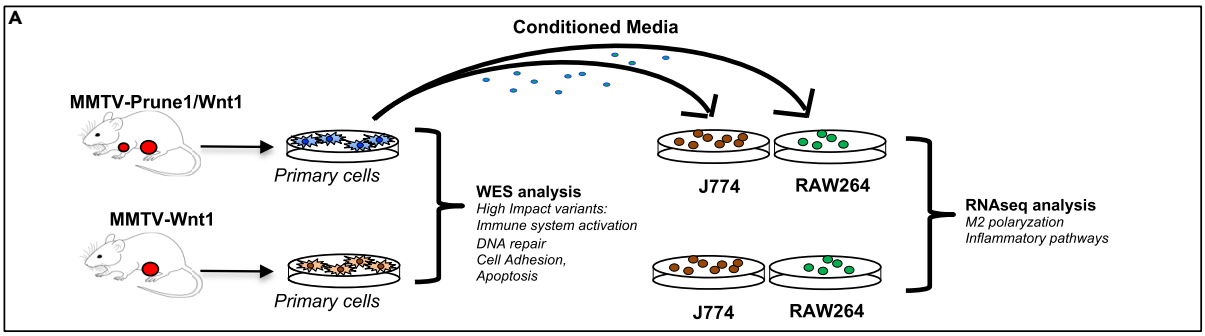
A
Conditioned Media
MMTV-Prune1/Wnt1
Primary cells
MMTV-Wnt1
Primary cells
WES analysis
High Impact variants:
Immune system activation
DNA repair
Cell Adhesion,
Apoptosis
J774
RAW264
J774
RAW264
RNAseq analysis
M2 polaryzation
Inflammatory pathways

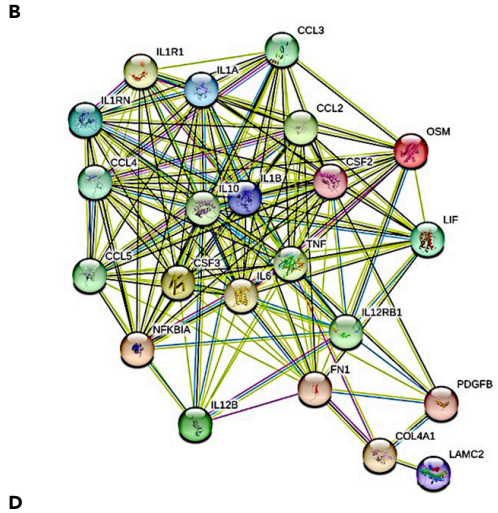
B
CCL3
IL1R1
IL1A
IL1RN
CCL2
OSM
CCL4
CSF2
IL1B
IL10
LIF
TNF
CCL5
CSF3
IL6
IL12RB1
NFKBIA
FN1
PDGFB
IL12B
COL4A1
LAMC2

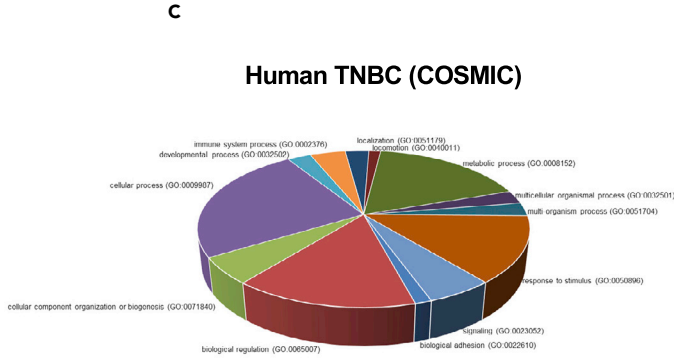
C
Human TNBC (COSMIC)
immune system process (GO:0002376)
developmental process (GO:0032502)
localization (GO:0051179)
locomotion (GO:0040011)
metabolic process (GO:0008152)
cellular process (GO:0009987)
multicellular organismal process (GO:0032501)
multi organism process (GO:0051704)
response to stimulus (GO:0050896)
cellular component organization or biogenesis (GO:0071840)
Signaling (GO:0023052)
biological regulation (GO:0065007)
biological adhesion (GO:0022610)

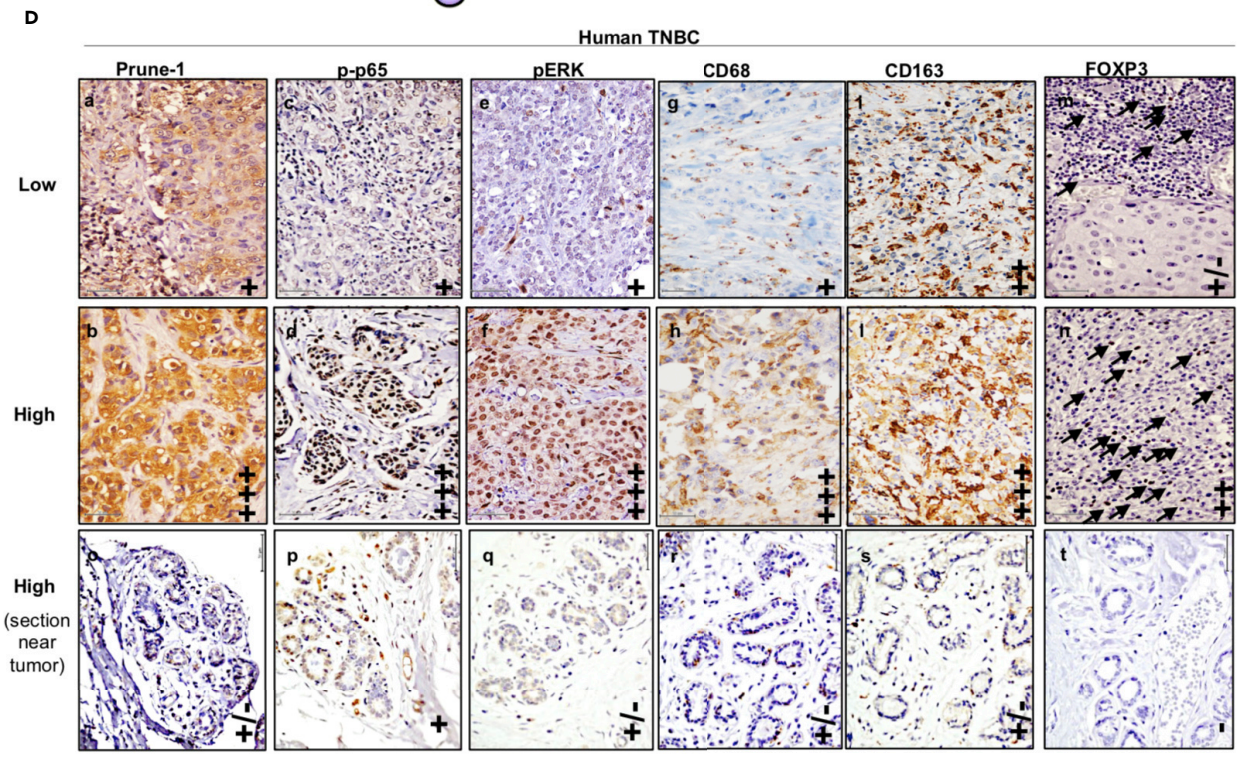
D
Human TNBC
Prune-1
p-p65
pERK
CD68
CD163
FOXP3
Low
High
High
(section
near
tumor)

Figure 5. Mutational spectrum in TNBC cells overexpressing Prune-1 regulating M2-macrophages polarization

(A) Representative scheme for the experimental design. DNA from MMTV–Prune-1/Wnt1 and MMTV–Wnt1 cells was used for next-generation sequencing analyses through a whole-exome sequencing approach. J774A.1 and Raw264.7 macrophages were grown in conditioned media collected from MMTV–Prune-1/Wnt1 and MMTV–Wnt1 cells for 48 h. Total RNA was extracted from these macrophages, and RNAseq analyses were performed.

(B) The inflammatory protein network generated via Search Tool for Retrieval of Interacting Genes/Proteins (STRING) database using the "core genes" defined as the common genes that are overexpressed in both the J774A.1 and RAW264.7 macrophages grown in media obtained from MMTV–Prune-1/Wnt1 cells (as compared with MMTV–Wnt1 cells) shared by at least four of five enriched gene sets from each canonical pathway sub-collection (i.e., Biocarta, Kegg, Pid, Reactome, Naba). The protein interaction network was generated using the STRING database (confidence: 0.4; https://string-db.org/cgi/network.pl?taskId=41jaTsLzWNqT).

(C) Pie chart illustrating the Gene Ontology (GO) term analysis of deleterious variants of the 39 genes in MMTV–Prune-1/Wnt1 cells (compared with MMTV–Wnt1 cells) and in the public database of human basal TNBC (COSMIC, v91).

(D) Representative immunostaining (IHC) from "tumor" **(a–n)** and "near tumor" **(o–t)** sections of our TNBC tissue cohort (n = 138) derived from patients who underwent mastectomy, quadrantectomy, or metastectomy at the "Giovanni Pascale" National Cancer Institute of Naples (Italy) from 2003 to 2010, with antibodies against the following: Prune-1 **(a-b-o)**, phosphorylated-(Ser311)-p65 **(c-d-p)**, phosphorylated-ERK1/2 (i.e., phospho-[Thr202/Tyr204]-ERK1 and phospho-[Thr185/Tyr187]-ERK2) **(e-f-q)**, CD68 **(g-h-r)** and CD163 **(i-l-s)** (as markers for M2-TAMs), and FOXP3 **(m-n-t)** (as marker for Tregs). Magnification 40×. Scale bar: 50 μm; (−): negativity; (+): low immunopositivity; (++) medium immunopositivity; (+++): high immunopositivity.

126 genes; see Methods; Table 3; Figure S11A). Among these, 39 gene variants were also found in the public data in the Catalog Of Somatic Mutations In Cancer (COSMIC, v91; released April 7, 2020) of human basal TNBC (426 samples collected) (see Table 3). Gene Ontology analyses performed on these human genes showed some deleterious variants involved in the activation of innate immune responses (leukocyte and macrophage activation; ANKHD1, FER1L5), cell adhesion (NEXN), apoptotic pathways (BID), and DNA repair (ERCC5) (Figure 5C). Then, among these 39 genes that were mutated in the human basal TNBC dataset available in COSMIC, we focused on those with unfavorable prognosis in BC patients in terms of their expression levels and 5-year survival. For this purpose, we took into account the analyses of survival data obtained from the publicly available dataset of breast invasive carcinoma (n = 1,075) from TCGA. Of interest, low expression levels of the PDE9A, ERCC5, Iqca, Sirpb1b, CD244, SP140, and PIP5k1b genes were associated with decreased 5-year survival rate in BC patients, thus suggesting their potential association with unfavorable prognosis (Figure S11B). The Rrs1 and A2M genes were excluded from this analysis because only one patient out of 426 had mutations in this gene in the public data of human basal TNBC in COSMIC (v91).

Of interest, all of the genes listed earlier (with the exception for ERCC5) were also mutated in the publicly available dataset of metastatic BC (n = 216 (Lefebvre et al., 2016)), with a total frequency of 3.7% (Cbioportal for cancer genomics; https://www.cbioportal.org) (Figure S11C), thus indicating a potential role in metastatic processes in BC.

Dataset validation in a human cohort of TNBC patients positively correlated with M2-TAMs and distant metastasis

To further underpin these data, Prune-1 protein expression was analyzed in human TNBC by IHC on tissue micro-arrays using a collection cohort of primary TNBC specimens. In this cohort analysis, 138 TNBC samples were included (113 ductal, 25 not ductal). The patients age ranged from 24 to 93 years, with mean age 57 years. At surgery, tumors >2 cm were seen for 53% of these patients (72/136; for two patients this information was not available), and metastatic lymph nodes were seen for 40.2% of patients (55/137; for one patient this information was not available). The tumor gradings were as follows: grade 3, 87.7% (121/138) and grade 1 or 2, 12.3% (17/138). The expression of the proliferation marker Ki67 was high (>20%) in 80.6% of patients (108/134) and low (≤20%) in 19.4% of patients (26/134; for four patients this information was not available; see Table 4).

Prune-1 protein expression was detected in 89.9% (124/138) of the samples from this tissue cohort. In 50.7% of the samples (68/138) there was low Prune-1 expression, and in 49.3% of the samples (70/138) there was high Prune-1 expression (Figure 5D, a, b). These findings indicated that about 50% (i.e., 49.3%) of the TNBC samples in this tissue cohort showed overexpression of Prune-1 protein.

Statistical analysis of Prune-1 protein expression (i.e., based on intensity, percent expression) in terms of the other clinicopathological parameters in this TNBC tissue cohort indicated that Prune-1 was positively correlated with Ki67 proliferative index ($p = 0.011$; $R = 0.219$), high-grade ($p = 0.005$; $R = 0.237$), disease progression ($p = 0.031$; $R = 0.212$) and presence of lung metastasis ($p = 0.027$; $R = 0.254$), as shown in Table

Table 2. The "core genes" upregulated in macrophages in response to Prune-1 overexpression in TNBC cells

Gene	Description	Annotation
CCL2	Chemokine (C-C motif) ligand 2	C-C motif chemokine 2; chemotactic factor that attracts monocytes and basophils but not neutrophils or eosinophils. Augments monocyte anti-tumor activity. Has been implicated in the pathogenesis of diseases characterized by monocytic infiltrates, such as psoriasis, rheumatoid arthritis, or atherosclerosis. May be involved in the recruitment of monocytes into the arterial wall during the disease process of atherosclerosis; belongs to the intracrine beta (chemokine CC) family
CCL3	Chemokine (C-C motif) ligand 3	C-C motif chemokine 3; monokine with inflammatory and chemokinetic properties. Binds to CCR1, CCR4, and CCR5. One of the major HIV-suppressive factors produced by CD8+ T cells. Recombinant MIP-1-alpha induces a dose-dependent inhibition of different strains of HIV-1, HIV-2, and simian immunodeficiency virus (SIV); belongs to the intercrine beta (chemokine CC) family
CCL4	Chemokine (C-C motif) ligand 4	C-C motif chemokine 4; monokine with inflammatory and chemokinetic properties. Binds to CCR5. One of the major HIV-suppressive factors produced by CD8+ T cells. Recombinant MIP-1-beta induces a dose-dependent inhibition of different strains of HIV-1, HIV-2, and simian immunodeficiency virus (SIV). The processed form MIP-1-beta(3-69) retains the abilities to induce down-modulation of surface expression of the chemokine receptor CCR5 and inhibit the CCR5-mediated entry of HIV-1 in T cells. MIP-1-beta(3-69) is also a ligand for CCR1 and CCR2 isoform B;
CCL5	Chemokine (C-C motif) ligand 5	C-C motif chemokine 5; chemoattractant for blood monocytes, memory T-helper cells, and eosinophils. Causes the release of histamine from basophils and activates eosinophils. May activate several chemokine receptors including CCR1, CCR3, CCR4, and CCR5. One of the major HIV-suppressive factors produced by CD8+ T-cells. Recombinant RANTES protein induces a dose-dependent inhibition of different strains of HIV-1, HIV-2, and simian immunodeficiency virus (SIV). The processed form RANTES(3-68) acts as a natural chemotaxis inhibitor and is a more potent inhibitor of HIV-1 infection.
COL4A1	Collagen, type IV, alpha 1	Collagen alpha 1(IV) chain; type IV collagen is the major structural component of glomerular basement membranes (GBM), forming a "chicken-wire" meshwork together with laminins, proteoglycans, and entactin/nidogen.
CSF2	Colony-stimulating factor 2 (granulocyte-macrophage)	Granulocyte-macrophage colony-stimulating factor; cytokine that stimulates the growth and differentiation of hematopoietic precursor cells from various lineages, including granulocytes, macrophages, eosinophils, and erythrocytes; belongs to the GM-CSF family.
CSF3	Colony-stimulating factor 3 (granulocyte)	Granulocyte colony-stimulating factor; granulocyte/macrophage colony-stimulating factors are cytokines that act in hematopoiesis by controlling the production, differentiation, and function of 2 related white cell populations of the blood: the granulocytes and the monocytes-macrophages. This CSF induces granulocytes; belongs to the IL-6 superfamily.
FN1	Fibronectin 1	Fibronectin type III domain containing; endogenous ligands
IL-10	Interleukin-10	Interleukin-10; inhibits the synthesis of a number of cytokines, including IFN-gamma, IL-2, IL-3, TNF, and GM-CSF produced by activated macrophages and by helper T cells; belongs to the IL-10 family
IL12B	Interleukin-12b	Interleukin-12 subunit beta; cytokine that can act as a growth factor for activated T and NK cells, enhance the lytic activity of NK/lymphokine-activated killer cells, and stimulate the production of IFN-gamma by resting PBMC; belongs to the type I cytokine receptor family. Type 3 subfamily.
IL12RB1	Interleukin-12 receptor, beta 1	Interleukin-12 receptor subunit beta-1; functions as an interleukin receptor that binds interleukin-12 with low affinity and is involved in IL-12 transduction. Associated with IL12RB2 it forms a functional, high-affinity receptor for IL-12. Associates also with IL23R to form the interleukin-23 receptor, which functions in IL-23 signal transduction probably through activation of the Jak-Stat signaling cascade; CD molecules
IL1A	Interleukin-1 alpha	Interleukin-1 alpha; produced by activated macrophages, IL-1 stimulates thymocyte proliferation by inducing IL-2 release, B-cell maturation and proliferation, and fibroblast growth factor activity. IL-1 proteins are involved in the inflammatory response, being identified as endogenous pyrogens, and are reported to stimulate the release of prostaglandin and collagenase from synovial cells.
IL1B	Interleukin-1 beta	Interleukin-1 beta; potent proinflammatory cytokine. Initially discovered as the major endogenous pyrogen, induces prostaglandin synthesis, neutrophil influx and activation, T cell activation and cytokine production, B-cell activation and antibody production, and fibroblast proliferation and collagen production. Promotes Th17 differentiation of T cells.

(*Continued on next page*)

Table 2. *Continued*

Gene	Description	Annotation
IL1R1	Interleukin-1 receptor, type I	Interleukin-1 receptor type 1; receptor for IL1A, IL1B, and IL1RN. After binding to interleukin-1 associates with the coreceptor IL1RAP to form the high-affinity interleukin-1 receptor complex that mediates interleukin-1-dependent activation of NF-κB, MAPK, and other pathways. Signaling involves the recruitment of adapter molecules such as TOLLIP, MYD88, and IRAK1 or IRAK2 via the respective TIR domains of the receptor/coreceptor subunits. Binds ligands with comparable affinity, and binding of antagonist IL1RN prevents association with IL1RAP to form a signaling complex.
IL1RN	Interleukin-1 receptor antagonist	Interleukin-1 receptor antagonist protein; inhibits the activity of interleukin-1 by binding to receptor IL1R1 and preventing its association with the coreceptor IL1RAP for signaling. Has no interleukin-1-like activity. Binds functional interleukin-1 receptor IL1R1 with greater affinity than decoy receptor IL1R2; however, the physiological relevance of the latter association is unsure; endogenous ligands.
IL6	Interleukin-6	Interleukin-6; cytokine with a wide variety of biological functions. It is a potent inducer of the acute phase response. Plays an essential role in the final differentiation of B-cells into Ig-secreting cells involved in lymphocyte and monocyte differentiation. Acts on B cells, T cells, hepatocytes, hematopoietic progenitor cells, and cells of the CNS. Required for the generation of T(H)17 cells. Also acts as a myokine. It is discharged into the bloodstream after muscle contraction and acts to increase the breakdown of fats and to improve insulin resistance. It induces myeloma and plas […]
LAMC2	Laminin, gamma-2	Laminin subunit gamma-2; binding to cells via a high-affinity receptor, laminin is thought to mediate the attachment, migration, and organization of cells into tissues during embryonic development by interacting with other extracellular matrix components. Ladsin exerts cell- scattering activity toward a wide variety of cells, including epithelial, endothelial, and fibroblastic cells.
LIF	Leukemia inhibitory factor	Leukemia inhibitory factor; LIF has the capacity to induce terminal differentiation in leukemic cells. Its activities include the induction of hematopoietic differentiation in normal and myeloid leukemia cells, the induction of neuronal cell differentiation, and the stimulation of acute-phase protein synthesis in hepatocytes; endogenous ligands.
NFKBIA	Nuclear factor of kappa light polypeptide gene enhancer in B cells inhibitor, alpha	NF-κB inhibitor alpha; inhibits the activity of dimeric NF-κB/REL complexes by trapping REL dimers in the cytoplasm through masking of their nuclear localization signals. On cellular stimulation by immune and proinflammatory responses, becomes phosphorylated promoting ubiquitination and degradation, enabling the dimeric RELA to translocate to the nucleus and activate transcription.
OSM	Oncostatin M	Oncostatin-M; growth regulator. Inhibits the proliferation of a number of tumor cell lines. Stimulates proliferation of AIDS-KS cells. It regulates cytokine production, including IL-6, G-CSF, and GM-CSF from endothelial cells. Uses both type I OSM receptor (heterodimers composed of LIPR and IL6ST) and type II OSM receptor (heterodimers composed of OSMR and IL6ST). Involved in the maturation of fetal hepatocytes, thereby promoting liver development and regeneration.
PDGFB	Platelet-derived growth factor, B polypeptide	Platelet-derived growth factor subunit B; growth factor that plays an essential role in the regulation of embryonic development, cell proliferation, cell migration, survival, and chemotaxis. Potent mitogen for cells of mesenchymal origin. Required for normal proliferation and recruitment of pericytes and vascular smooth muscle cells in the central nervous system, skin, lung, heart, and placenta. Required for normal blood vessel development and for normal development of kidney glomeruli.
TNF	Tumor necrosis factor	Tumor necrosis factor; cytokine that binds to TNFRSF1A/TNFR1 and TNFRSF1B/TNFBR. It is mainly secreted by macrophages and can induce cell death of certain tumor cell lines. It is potent pyrogen causing fever by direct action or by stimulation of interleukin-1 secretion and is implicated in the induction of cachexia. Under certain conditions it can stimulate cell proliferation and induce cell differentiation. Impairs regulatory T cells (Treg) function in individuals with rheumatoid arthritis via FOXP3 dephosphorylation. Upregulates the expression of protein phosphatase 1 (PP1).

The common genes there are found overexpressed in both J774A.1 and RAW264.7 macrophages grown in the media supernatant from MMTV-Prune-1/Wnt1 cells (as compared with those from MMTV-Wnt-1 cells) shared by at least 4 out of 5 enriched gene-sets coming from canonical pathway sub-collection (i.e., Biocarta, Kegg, Pid, Reactome and Naba) are listed. Gene, common gene name (HGNC); Description, gene description; Annotation, annotated using Sequence Ontology terms.

4. No significant correlations were found between Prune-1 levels and patients age, lymph node metastases, and tumor histotype and size (Table 4). Altogether, these data further supported the concept that overexpression of Prune-1 can be used to predict lung metastases in TNBC.

Table 3. Mutually exclusive coding variants with predicted higher/moderate impact in MMTV-Prune-1/Wnt1 cells

Chrom	#Pos	ALT	REF	Zygosity	Annotation	Gene Name	Feature_ID	HGVS.c	HGVS.p	dbSNP142_ ID	Number of variants in human TNBC samples (COSMIC)
11	69588736	G	T	HET	stop_gained&splice_ region_variant	Trp53	NM_011640.3	c.661G > T	p.Glu221*	.	>200
11	69588393	C	G	HET	missense_variant	Trp53	NM_011640.3	c.396C > G	p.Cys132Trp	.	>200
17	31443854	GAGCTGAAAGCCGA	G	HET	frameshift_variant	Pde9a	NM_001163748.1	c.337_349delCTGA AAGCCGAAG	p.Leu113fs	.	38
1	82729275	T	C	HET	missense_variant	Mff	NM_029409.2	c.20T > C	p.Ile7Thr	.	18
1	82751668	C	G	HET	missense_variant	Mff	NM_029409.2	c.828C > G	p.Ile276Met	rs580786331	18
1	44167090	T	C	HET	missense_variant	Ercc5	NM_011729.2	c.1162T > C	p.Cys388Arg	rs8253429	16
2	71820255	G	GGA	HET	splice_donor_variant& intron_variant	Itga6	NM_001277970.1	c.643 + 1_643+ 2insGA	.	.	10
2	71833793	TGGTGAGTCCCTTTT CTGGGCGCTGG CTCAGTTCTCAGCT TGGCGATGAGCTC CTTGACATGATGA GCCACTGAGAAGGG GAAGGGTGCACTG GACAAAGGGACAAGT CGAGACACTGTC CAGCAGCCAGTGG GGACACTGGAG GGCTGGGGACA AGGTGGGGTCT TCCACTGCTACAG TGCATCTTTTAAG AAATATGTGTT TGATTTTATGCA	T	HET	frameshift_variant& splice_acceptor_ variant& splice_donor_variant& splice_region_variant& splice_region_variant& splice_region_variant& intron_variant	Itga6	NM_001277970.1	c.1487_1488-2del	p.Cys496fs	.	10
6	118525854	G	A	HET	missense_variant	Ankrd26	NM_001081112.1	c.2354C > T	p.Ser785Leu	rs30264502	10
6	118525855	A	T	HET	missense_variant	Ankrd26	NM_001081112.1	c.2353T > A	p.Ser785Thr	rs30363420	10
6	118535096	C	G	HET	missense_variant	Ankrd26	NM_001081112.1	c.1564G > C	p.Glu522Gln	rs261478249	10
6	120895769	C	T	HET	missense_variant	Bid	NM_007544.3	c.426G > A	p.Met142Ile	.	10
1	90047844	G	T	HET	stop_gained	Iqca	NM_029122.2	c.2079C > A	p.Cys693*	.	9
3	15548792	G	A	HET	stop_gained	Sirpb1b	NM_001173460.1	c.229C > T	p.Gln77*	.	9
3	15548740	G	T	HET	missense_variant	Sirpb1b	NM_001173460.1	c.281C > A	p.Thr94Lys	.	9
3	15548774	G	A	HET	missense_variant	Sirpb1b	NM_001173460.1	c.247C > T	p.His83Tyr	.	9
3	15548789	A	G	HET	missense_variant	Sirpb1b	NM_001173460.1	c.232T > C	p.Ser78Pro	.	9

(*Continued on next page*)

Table 3. *Continued*

Chrom	#Pos	ALT	REF	Zygosity	Annotation	Gene Name	Feature_ID	HGVS.c	HGVS.p	dbSNP142_ ID	Number of variants in human TNBC samples (COSMIC)
3	15548790	C	G	HET	missense_variant	Sirpb1b	NM_001173460.1	c.231G > C	p.Gln77His	.	9
3	15548854	G	T	HET	missense_variant	Sirpb1b	NM_001173460.1	c.167C > A	p.Ser56Tyr	.	9
12	98213021	T	TATACACTGAGG GCATCTCTC ACACACCAGTGG TGATCGCCT ATAACACTGATTG TGCTGGAA GCGTATACA	HET	frameshift_ variant&stop_ gained	Galc	NM_008079.4	c.1627_1628insTG TATACGCTT CCAGCACAATCA GTGTTATAG GCGATCACCACT GGTGTGTGA GAGATGCCCTC AGTGTAT	p.Asp543fs	.	9
1	36412593	C	T	HET	missense_variant	Fer1l5	NM_001277076.1	c.3781C > T	p.Arg1261Cys	rs32520256	8
2	73819145	G	GCAGTATGATAGC CAGACTTC TTCTGCATGGCA GTTACAGGG CAATCTTTATGA GCCAGAAGA AGCTGTTT	HET	frameshift_variant&stop_ gained&splice_region_ variant	Atf2	NM_001025093.2	c.1240_1241insAA ACAGCTTCTT CTGGCTCATAAA GATTGCCCTG TAACTGCCATGCA GAAGAAGTC TGGCTATCATACTG	p.Ala414fs	.	8
2	73829942	C	CATTTTTGCTTCT GACTGGACT GGTTGAGGAGAG GAAGGGCCT GGGATTCCTGGAA CACTAGGC ACCATGG	HET	splice_acceptor_ variant&intron_variant	Atf2	NM_001025093.2	c.775-2_775-1ins CCATGGTGC CTAGTGTTCCA GGAATCCCAG GCCCTTCCTCTC CTCAACCAG TCCAGTCAGAA GCAAAAAT	.	.	8
5	3344393	C	CT	HET	frameshift_variant&stop_ gained	Cdk6	NM_009873.2	c.27_28insT	p.Asp10fs	.	8
17	49488248	T	C	HET	missense_variant	Daam2	NM_001008231.2	c.916A > G	p.Met306Val	.	7
1	171573958	C	CAGAA	HET	frameshift_variant	Cd244	NM_018729.2	c.340_341insGAAA	p.Thr114fs	.	6
1	171573961	AGGCG	A	HET	frameshift_variant	Cd244	NM_018729.2	c.344_347delGCGG	p.Gly115fs	.	6
18	36648429	C	A	HET	missense_variant	Ankhd1	NM_175375.3	c.6533C > A	p.Ser2178Tyr	.	6
1	85635605	A	G	HET	missense_variant&splice_ region_variant	Sp140	NM_001013817.2	c.1019A > G	p.Glu340Gly	.	5
11	3146254	TCG	T	HET	frameshift_variant	Sfi1	NM_030207.2	c.1378_1379delCG	p.Arg460fs	rs386949583	5

(*Continued on next page*)

Table 3. *Continued*

Chrom	#Pos	ALT	REF	Zygosity	Annotation	Gene Name	Feature_ID	HGVS.c	HGVS.p	dbSNP142_ ID	Number of variants in human TNBC samples (COSMIC)
13	119450010	G	GAGAT	HET	splice_donor_variant &intron_variant	Paip1	NM_145457.4	c.842_842+1insAGAT	.	.	4
17	45568364	C	CCT	HET	frameshift_variant	Hsp90ab1	NM_008302.3	c.1928_1929dupAG	p.Ala644fs	.	4
17	45568460	G	A	HET	stop_gained	Hsp90ab1	NM_008302.3	c.1834C > T	p.Arg612*	.	4
17	45568347	T	G	HET	missense_variant	Hsp90ab1	NM_008302.3	c.1947A > C	p.Lys649Asn	.	4
17	45568405	G	A	HET	missense_variant	Hsp90ab1	NM_008302.3	c.1889C > T	p.Pro630Leu	.	4
17	45568409	T	A	HET	missense_variant	Hsp90ab1	NM_008302.3	c.1885A > T	p.Asn629Tyr	.	4
17	45568434	C	T	HET	missense_variant	Hsp90ab1	NM_008302.3	c.1860G > A	p.Met620Ile	.	4
17	45568435	A	G	HET	missense_variant	Hsp90ab1	NM_008302.3	c.1859T > C	p.Met620Thr	.	4
19	24350205	C	A	HET	missense_variant	Pip5k1b	NM_008846.2	c.1286G > T	p.Ser429Ile	.	4
4	119422160	C	T	HET	missense_variant	Ppcs	NM_026494.3	c.194G > A	p.Arg65His	.	3
18	49755396	TC	T	HET	frameshift_variant	Dtwd2	NM_026854.3	c.142delG	p.Asp48fs	.	3
3	152247927	ACTTGCCATGT GCCTTCTCGC CTCCTCAAAGG AACGTCTCTC TTCTTCTAAGCG TCGTCTCGC TTCCTCTTCCG CTTGCTTCTTG	A	HET	frameshift_variant&splice_ donor_variant&splice_ region_variant&splice_ region_variant&intron_ variant	Nexn	NM_199465.2	c.579_657+5delCAA GAAGCAAGCGG AAGA GGAAGCGAGAC GACGCTTAGA AGAAGAGAGAC GTTCCTTTGAG GAGGCGAGAAG GCACATGGCAAG	p.Arg193fs	.	2
4	106585909	G	T	HET	missense_variant	Dhcr24	NM_053272.2	c.1140G > T	p.Gln380His	.	2
6	120958949	G	C	HET	missense_variant	Mical3	NM_001270475.1	c.4615C > G	p.Leu1539Val	.	2
6	121024818	T	A	HET	missense_variant	Mical3	NM_001270475.1	c.1712A > T	p.Asp571Val	.	2
11	98224575	C	CA	HET	frameshift_variant	Cdk12	NM_001109626.1	c.2546dupA	p.Asn850fs	.	2
13	70603400	C	CTATGGTTCCAGA TTTCTTTC CTAGGGTTTCTAT CTCTAGTGT TGCCTCGT	HET	frameshift_variant	Ice1	NM_144837.3	c.4565_4566insAC GAGGCAACA CTAGAGATAGAA ACCCTAGGA AAGAAATCTG GAACCATA	p.Ile1523fs	.	2
17	78985311	G	T	HET	missense_variant	Prkd3	NM_001171004.1	c.331C > A	p.Leu111Ile	.	2

(*Continued on next page*)

Table 3. *Continued*

Chrom	#Pos	ALT	REF	Zygosity	Annotation	Gene Name	Feature_ID	HGVS.c	HGVS.p	dbSNP142_ ID	Number of variants in human TNBC samples (COSMIC)
19	15907067	T	TACATAAAATCC TTGAGAATTA TCAATGATCTCAT AAATCATTT GGGATTTGATGGAG	HET	splice_acceptor_ variant&intron_variant	Psat1	NM_177420.2	c.870-1_870insC TCCATCAAAT CCCAAATGATTT ATGAGATCA TTGATAATTCTCA AGGATTTTATGT	.	.	2
1	9546377	C	T	HET	missense_variant	Rrs1	NM_021511.2	c.854C > T	p.Thr285Met	.	1
2	156267542	G	GCT	HET	splice_donor_variant &intron_variant	Phf20	NM_172674.2	c.808_808+1insCT	.	.	1
6	121671068	A	C	HET	missense_variant	A2m	NM_175628.3	c.3518A > C	p.Glu1173Ala	rs50350755	1
8	24962858	ACTGGCGGTCT GGAGACAC CTGGGCCCC	A	HOM	exon_loss_variant& splice_acceptor_variant& splice_donor_variant& splice_region_variant& splice_region_variant& intron_variant&intron_ variant	Adam9	NM_007404.2	c.2360-9_2376+ 1delGGGGCCC AGGTGTC TCCAGACCG CCAG	.	.	1
8	70065135	G	A	HET	missense_variant	Sugp1	NM_027481.2	c.1174G > A	p.Val392Met	.	1
12	76837652	G	GCCAAAGTAGAA GAGAAGATC CAGGAGGTCTTC AGTTCTTAC AAGTTTAACCACC TTGTACCA AGGCTCATTT	HET	splice_donor_variant& intron_variant	Fntb	NM_145927.2	c.144 + 1_144+2insCCA AAGTAGAAGAGAAG ATCCAGGAGGT CTTCAGTTC TTACAAGTTTA ACCACCTTGT ACCAAGGCTCATTT	.	.	1
15	77785100	G	T	HET	missense_variant	Myh9	NM_022410.3	c.1721C > A	p.Ala574Asp	.	1
19	60537503	G	GGCATTAGGCTGT AAATGTG CTTCTCTGCAAC ATGTTCCCA AAGGGTTATTATA TTCCACAG TCAGGGATTTGC AACTGTTTG CTAGTGC	HET	splice_acceptor_ variant&intron_ variant	Cacul1	NM_030197.2	c.821-1_821insGC ACTAGCAA ACAGTTGCAAA TCCCTGACTG TGGAATATAAT AACCCTTTGG GAACATGTTGC AGAGAAGCAC ATTTACAGCC TAATGC	.	.	1
X	74303948	C	T	HET	missense_variant	Atp6ap1	NM_018794.4	c.1334C > T	p.Thr445Ile	.	1

(*Continued on next page*)

Table 3. *Continued*

Chrom	#Pos	ALT	REF	Zygosity	Annotation	Gene Name	Feature_ID	HGVS.c	HGVS.p	dbSNP142_ ID	Number of variants in human TNBC samples (COSMIC)
X	74303956	C	T	HET	missense_variant	Atp6ap1	NM_018794.4	c.1342C > T	p.Arg448Cys	.	1
X	74303965	G	A	HET	missense_variant	Atp6ap1	NM_018794.4	c.1351G > A	p.Asp451Asn	.	1
X	74303977	C	T	HET	missense_variant	Atp6ap1	NM_018794.4	c.1363C > T	p.Pro455Ser	.	1
1	161150967	AT	A	HOM	frameshift_variant	Ankrd45	NM_028664.1	c.95delT	p.Leu32fs	.	
1	34536493	C	A	HET	missense_variant	Cfc1	NM_007685.2	c.247C > A	p.Pro83Thr	rs31623365	
1	46066957	C	T	HET	missense_variant	Dnah7b	NM_001160386.1	c.100C > T	p.Pro34Ser	rs32596568	
1	46066960	A	G	HET	missense_variant	Dnah7b	NM_001160386.1	c.103A > G	p.Ile35Val	rs31532497	
1	174027191	A	ACCTGGGCTGT AGAAGTCCCC GCCTGAGCTGT GGAAGTCCCCG	HET	splice_donor_variant& intron_variant	Ifi205	NM_172648.3	c.399 + 1_399+ 2insCGGG GACTTCCACAG CTCAGGCGGGG ACTTCTACAG CCCAGG	.	.	
1	37897787	C	T	HET	missense_variant	Mrpl30	NM_027098.2	c.232C > T	p.Arg78Cys	rs30993281	
1	34560871	C	T	HET	missense_variant	Prss40	NM_009356.2	c.34G > A	p.Gly12Ser	rs48246656	
1	34560895	T	C	HET	missense_variant	Prss40	NM_009356.2	c.10A > G	p.Ile4Val	rs46691245	
2	90917709	G	GA	HOM	frameshift_variant	Ptpmt1	NM_025576.2	c.277dupT	p.Ser93fs	rs231270167	
2	156142243	C	CAGAGGAGTG GTGGCCTGTAC GTCCATGTAG AGAGGTCGCAG CACTGCCTCT GCCTCTGAG	HET	splice_acceptor_variant& intron_variant	Nfs1	NM_010911.2	c.214-2_214-1ins CTCAGAGGCAG AGGCAGTGCTG CGACCTCTCTA CATGGACGTACA GGCCACCAC TCCTCT	.	.	
2	86085529	C	A	HET	stop_gained	Olfr1037	NM_001011532.2	c.247G > T	p.Glu83*	.	
2	86785928	G	T	HET	missense_variant	Olfr1093	NM_146366.1	c.197G > T	p.Arg66Leu	.	
2	90149325	G	T	HET	missense_variant	Olfr1270	NM_146985.2	c.680C > A	p.Ser227Tyr	.	
2	87108039	G	T	HET	missense_variant	Olfr259	NM_146770.2	c.347C > A	p.Ser116Tyr	.	
3	138445390	A	AGATCCTTGCC ACTGCTGTTT GCCACACCGAT GCCTATACCC TGAGCGGAGCT GACCCCGAGG	HET	splice_donor_variant& intron_variant	Adh5	NM_007410.3	c.114_114+1insA TCCTTGCCACTG CTGTTTGCCACA CCGATGCCTATA CCCTGAGCGGA GCTGACCC CGAGGG	.	.	

(*Continued on next page*)

Table 3. *Continued*

Chrom	#Pos	ALT	REF	Zygosity	Annotation	Gene Name	Feature_ID	HGVS.c	HGVS.p	dbSNP142_ ID	Number of variants in human TNBC samples (COSMIC)
3	20242108	C	A	HET	missense_variant	Cpa3	NM_007753.2	c.64G > T	p.Asp22Tyr	.	
3	95255225	ATACC	A	HET	frameshift_variant	Prune	NM_173347.2	c.1132_1135delGGTA	p.Gly378fs	.	
3	95255231	A	AT	HET	frameshift_variant	Prune	NM_173347.2	c.1129_1130insA	p.Val377fs	.	
3	95255263	C	CAT	HET	frameshift_variant	Prune	NM_173347.2	c.1097_1098insAT	p.Lys367fs	.	
3	95255264	GCT	G	HET	frameshift_variant	Prune	NM_173347.2	c.1095_1096delAG	p.Ser365fs	.	
4	138171107	C	A	HET	missense_variant	Eif4g3	NM_172703.3	c.2693C > A	p.Ala898Asp	.	
4	118726336	C	CT	HET	frameshift_variant	Olfr1340	NM_146304.2	c.96dupT	p.Leu33fs	rs243765225	
4	44994005	G	GTCTTTCTAATT GTTACCAAA CATCTATTCTTG TCTTTCTAC TTAGGACTATT GAATTTTAG CTGGGT	HET	frameshift_variant& stop_gained	Zbtb5	NM_001163283.1	c.1377_1378insAC CCAGCTAA AATTCAATAGTC CTAAGTAG AAAGACAAGAAT AGATGTTT GGTAACAATTA GAAAGA	p.His460fs	.	
4	120947371	GATCCT	G	HET	frameshift_variant	Zfp69	NM_001005788.3	c.297_301delAGGAT	p.Ala99fs	.	
5	52538271	G	A	HET	missense_variant	Lgi2	NM_144945.2	c.1345C > T	p.Arg449Trp	.	
5	36508431	C	CTTGCTGGAAAA TGCAGAGAT TAGGAAATGTTC TAGAAATGTC CAGTTTAATAAGC TCCAGACTGGC CTCT	HET	splice_acceptor_ variant&intron_variant	Tbc1d14	NM_001113362.1	c.1510-1_1510insA GAGGCCAGTC TGGAGCTTATTAAA CTGGACATTT CTAGAACATTTCCT AATCTCTGCA TTTTCCAGCAA	.	.	
5	36507706	C	CATAACCCACAT CCGGCCGGTAA CAAGTATAAGC GCCCAAAATAC TGTGCAACATG TCATGATACGG ACCACCTTG	HET	splice_acceptor_variant& intron_variant	Tbc1d14	NM_001113362.1	c.1582-1_1582insCA AGGTGGTCC GTATCATGACATG TTGCACAGT ATTTTGGGCGCTT ATACTTGTTA CCGGCCGGATGT GGGTTAT	.	.	
5	31200672	T	TTAGTACTACCA TGTCCTGTGAT TAAA	HET	frameshift_variant&stop_ gained	Zfp513	NM_175311.4	c.361_362insTTTAA TCACAGGA CATGGTAGTACTA	p.Gln121fs	.	
6	130118998	C	CT	HOM	frameshift_variant	Klra21	NM_053151.1	c.617dupA	p.Glu207fs	.	

(*Continued on next page*)

Table 3. *Continued*

Chrom	#Pos	ALT	REF	Zygosity	Annotation	Gene Name	Feature_ID	HGVS.c	HGVS.p	dbSNP142_ ID	Number of variants in human TNBC samples (COSMIC)
6	124230362	G	GAC	HOM	frameshift_variant	Vmn2r27	NM_001104642.1	c.318_319insGT	p.Leu107fs	.	
6	37536041	G	T	HET	stop_gained	Akr1d1	NM_145364.2	c.271G > T	p.Glu91*	.	
6	116410808	C	T	HET	missense_variant	Alox5	NM_009662.2	c.1936G > A	p.Val646Ile	rs30121304	
6	124540928	G	T	HET	missense_variant	C1s1	NM_001097617.1	c.92C > A	p.Ser31Tyr	.	
6	115849644	C	T	HET	missense_variant	Mbd4	NM_010774.2	c.385G > A	p.Asp129Asn	rs30840549	
6	122881551	G	T	HET	missense_variant	Necap1	NM_026267.2	c.352G > T	p.Asp118Tyr	.	
6	121190114	G	T	HET	stop_gained	Pex26	NM_001304774.1	c.373G > T	p.Glu125*	rs242534869	
6	115560065	C	CAGG	HET	disruptive_inframe_ insertion	Tsen2	NM_199033.1	c.791_793dupAGG	p.Glu264dup	rs229576944	
6	121255361	G	T	HET	missense_variant	Usp18	NM_011909.2	c.343G > T	p.Val115Leu	rs30018341	
6	123309819	G	T	HET	missense_variant	Vmn2r19	NM_001104632.1	c.410G > T	p.Cys137Phe	.	
6	123315926	C	A	HET	missense_variant	Vmn2r19	NM_001104632.1	c.926C > A	p.Thr309Asn	rs243552529	
6	123336175	C	A	HET	missense_variant	Vmn2r19	NM_001104632.1	c.2203C > A	p.His735Asn	rs586785967	
6	123336359	G	C	HET	missense_variant	Vmn2r19	NM_001104632.1	c.2387G > C	p.Ser796Thr	rs234282974	
6	123386109	TTA	T	HET	frameshift_variant	Vmn2r20	NM_001104634.1	c.1713_1714delTA	p.Asn571fs	.	
6	123637517	A	ATAC	HET	disruptive_inframe_ insertion	Vmn2r22	NM_001104637.1	c.1112_1113insGTA	p.His371delinsGlnTyr	.	
6	123704492	A	G	HET	missense_variant	Vmn2r23	NM_001104638.1	c.358A > G	p.Ser120Gly	.	
6	124062011	T	G	HET	missense_variant	Vmn2r26	NM_019917.2	c.2544T > G	p.His848Gln	.	
7	7002941	GC	G	HOM	frameshift_variant	Aurkc	NM_001080965.1	c.945delC	p.Cys315fs	.	
7	7002943	TA	T	HOM	frameshift_variant& stop_lost	Aurkc	NM_001080965.1	c.947delA	p.Ter316fs	.	
7	10050179	G	GT	HOM	frameshift_variant	Vmn2r50	NM_001105178.1	c.366dupA	p.Gln123fs	.	
7	47464285	G	GT	HET	frameshift_variant	Mrgpra2b	NM_153101.3	c.697dupA	p.Thr233fs	.	
7	47589308	C	T	HET	missense_variant	Mrgpra3	NM_153067.2	c.869G > A	p.Gly290Asp	rs264586948	
7	18521280	C	T	HET	missense_variant	Psg25	NM_054060.1	c.1310G > A	p.Cys437Tyr	.	
7	102020492	G	GGGATTGCTGA ACATCCTCTTC AGGTCCACCTTC TCCTTGCAG TAGGGACATGTC TGCTTCTTTC CCACGATGCA	HET	splice_acceptor_ variant& intron_variant	Rnf121	NM_029211.2	c.864-1_864insT GCATCGTGGGA AAGAAGCAGAC ATGTCCCTACT GCAAGGAGAAG GTGGACCTGAA GAGGATGTTCA GCAATCC	.	.	

(*Continued on next page*)

Table 3. *Continued*

Chrom	#Pos	ALT	REF	Zygosity	Annotation	Gene Name	Feature_ID	HGVS.c	HGVS.p	dbSNP142_ID	Number of variants in human TNBC samples (COSMIC)
7	79677445	G	GAATTTAAAAC CGAGGAGGAG CTTCTGGCTTAC ATACATGAC AACTACCAAA AGGCT	HET	splice_donor_variant& intron_variant	Ticrr	NM_029835.1	c.1900_1900+1insAA TTTAAAACCGAGG AGGAGCTTCTGGC TTACATACATGA CAACTACCAAAAGGCT	.	.	
7	11756824	G	GTCTT	HET	frameshift_variant	Vmn1r73	NM_134203.1	c.568_569insTCTT	p.Gly190fs	.	
7	11756825	GACTA	G	HET	frameshift_variant	Vmn1r73	NM_134203.1	c.570_573delACTA	p.Gly190fs	.	
7	11756747	T	TGGA	HET	disruptive_inframe_ insertion	Vmn1r73	NM_134203.1	c.491_492insGGA	p.Ile164delinsMetAsp	.	
7	12152883	GTA	G	HET	frameshift_variant	Vmn1r78	NM_134208.2	c.421_422delTA	p.Tyr141fs	.	
7	12152888	T	TC	HET	frameshift_variant	Vmn1r78	NM_134208.2	c.425_426insC	p.Met142fs	.	
7	12615903	C	A	HET	missense_variant	Vmn2r54	NM_001081449.2	c.1751G > T	p.Arg584Leu	.	
7	41872539	GA	G	HET	frameshift_variant	Vmn2r58	NM_001105055.1	c.131delT	p.Phe44fs	.	
7	43189515	TCTTCG	T	HET	frameshift_variant	Zfp936	NM_001034893.1	c.403_407delCTTCG	p.Leu135fs	.	
8	27345850	T	A	HET	missense_variant	Tex24	NM_001013609.2	c.988T > A	p.Leu330Met	.	
8	26162481	C	CT	HET	frameshift_variant	Thap1	NM_199042.2	c.315_316insT	p.Ala106fs	rs236454042	
9	48945576	T	G	HET	missense_variant	Htr3b	NM_020274.4	c.601A > C	p.Ser201Arg	.	
9	120018055	AG	A	HET	frameshift_variant	Xirp1	NM_011724.3	c.1760delC	p.Pro587fs	.	
10	128269082	C	G	HET	missense_variant	Apof	NM_133997.2	c.104C > G	p.Ala35Gly	.	
10	43582730	G	GCT	HET	frameshift_variant	Cd24a	NM_009846.2	c.211_212dupCT	p.Leu72fs	.	
10	128408217	GCACCTGCAGGC ACAGATGAG ATATACTCAGAC CCTCCTCAAC ATCGTGCTGCCA GGCCTGGTCT GCCATCTTCTCT AACGCCAGG CCCAGAGACT	G	HET	splice_acceptor_variant& inframe_deletion& splice_region_variant& splice_region_variant& splice_region_variant& intron_variant	Nabp2	NM_027257.1	c.372 + 4_375delAGT CTCTGGGCCTGG CGTTAGAGAAGATG GCAGACCA GGCCTGGCAGCAC GATGTTGAG GAGGGTCTGAGTA TATCTCATC TGTGCCTGCAGGTG	p.Val125_Gln126del	.	

(*Continued on next page*)

Table 3. *Continued*

Chrom	#Pos	ALT	REF	Zygosity	Annotation	Gene Name	Feature_ID	HGVS.c	HGVS.p	dbSNP142_ID	Number of variants in human TNBC samples (COSMIC)
10	128409348	G	GCCAGCCAGCA GGCCGGACTG TGCACACCGCCG AGCCACCCGCA GGGGGAGCCAGG GGGCTGGCTC AAATCCTCTCTTT	HET	splice_acceptor_ variant&intron_variant	Nabp2	NM_027257.1	c.-23-1_-23insAAAG AGAGGATTT GAGCCAGCCCCC TGGCTCCCCC TGCGGGTGGCT CGGCGGTGTGC ACAGTCCGGCC TGCTGGCTGG	.	.	
11	101157518	GAGGTGAGGAT CTTCAACAGTGA AGCATGCTGGG GGGAAAGATCAG GCATGATTCAA TCACGTGAAACAT TCAACTCCGCAT TCATTTGGGGACA TCATATAGAGC GCATTA	G	HOM	frameshift_variant&splice_ donor_variant&splice_ region_variant&splice_ region_variant&intron_ variant	Tubg2	NM_134028.2	c.398_399 + 109del	p.Glu133fs	rs386970477	
11	5105856	C	A	HET	missense_variant	Rhbdd3	NM_001290492.1	c.1037C > A	p.Ala346Glu	.	
11	98042620	C	A	HET	splice_acceptor_ variant&intron_variant	Stac2	NM_146028.4	c.496-1G > T	.	.	
13	26769616	TC	T	HET	frameshift_variant	Hdgfl1	NM_008232.3	c.472delG	p.Glu158fs	.	
14	79213479	A	AC	HOM	frameshift_variant	Zfp957	NM_001033215.3	c.878dupG	p.Gly294fs	rs249051530	
14	47311113	C	CTCTTACCATTAA	HET	splice_donor_variant& intron_variant	Mapk1ip1l	NM_178684.5	c.717_717+1insT CTTACCATTAA	.	.	
14	50424969	G	T	HET	missense_variant	Olfr739	NM_146668.2	c.449G > T	p.Cys150Phe	.	
15	80248399	G	T	HET	missense_variant	Mief1	NM_178719.5	c.481G > T	p.Ala161Ser	.	
17	34508444	C	A	HOM	stop_gained	Btnl6	NM_030747.1	c.1111G > T	p.Glu371*	.	
17	36167489	C	CAT	HOM	frameshift_variant	Gm8909	NM_001081032.2	c.565_566insAT	p.Cys189fs	.	
17	36167491	CGG	C	HOM	frameshift_variant	Gm8909	NM_001081032.2	c.562_563delCC	p.Pro188fs	.	
17	36168196	CGGGCCGGG ACACTGC GGTGGTGAAA	C	HOM	frameshift_variant&splice_ acceptor_variant&splice_ region_variant&splice_ region_variant&intron_ variant	Gm8909	NM_001081032.2	c.65-14_75delTTTC ACCACCGCA GTGTCCCGGCCC	p.Val22fs	.	

(*Continued on next page*)

Table 3. *Continued*

Chrom	#Pos	ALT	REF	Zygosity	Annotation	Gene Name	Feature_ID	HGVS.c	HGVS.p	dbSNP142_ ID	Number of variants in human TNBC samples (COSMIC)
17	48145527	AGACT	A	HET	frameshift_variant	9830107B12Rik	NM_001177896.1	c.236_239delAGTC	p.Gln79fs	.	
17	48128531	G	C	HET	missense_variant	9830107B12Rik	NM_001177896.1	c.505C > G	p.Leu169Val	.	
17	48145662	C	A	HET	missense_variant	9830107B12Rik	NM_001177896.1	c.105G > T	p.Lys35Asn	.	
17	34469182	TC	T	HET	frameshift_variant	Btnl4	NM_030746.1	c.1620delG	p.Gly540fs	.	
17	34469188	TCTTTGTCC	T	HET	frameshift_variant	Btnl4	NM_030746.1	c.1607_1614delGG ACAAAG	p.Arg536fs	.	
17	34508222	A	AC	HET	frameshift_variant	Btnl6	NM_030747.1	c.1332_1333insG	p.Leu445fs	.	
17	34508224	G	T	HET	stop_gained	Btnl6	NM_030747.1	c.1331C > A	p.Ser444*	.	
17	34508226	AG	A	HET	frameshift_variant	Btnl6	NM_030747.1	c.1328delC	p.Thr443fs	.	
17	34508231	T	A	HET	missense_variant	Btnl6	NM_030747.1	c.1324A > T	p.Arg442Trp	.	
17	35118059	G	A	HET	stop_gained	Csnk2b	NM_001303476.1	c.304C > T	p.Gln102*	.	
17	23882480	A	AATG	HET	disruptive_inframe_ insertion	Dcpp1	NM_019910.2	c.203_204insTGA	p.Lys68delinsAsnGlu	.	
17	36081275	C	T	HET	missense_variant	H2-Bl	NM_008199.2	c.877G > A	p.Glu293Lys	.	
17	35266687	GGC	G	HET	frameshift_variant&splice_ region_variant	H2-D1	NM_010380.3	c.1046_1047delGC	p.Gly349fs	.	
17	35266693	C	CAGA	HET	disruptive_inframe_ insertion	H2-D1	NM_010380.3	c.1052_1054dupAGA	p.Gln351_Ser352insLys	.	
17	33999478	G	A	HET	stop_gained	H2-K1	NM_001001892.2	c.403C > T	p.Gln135*	.	
17	33997529	G	T	HET	missense_variant	H2-K1	NM_001001892.2	c.642C > A	p.Ser214Arg	.	
17	33997531	T	G	HET	missense_variant	H2-K1	NM_001001892.2	c.640A > C	p.Ser214Arg	.	
17	36119450	G	A	HET	missense_variant	H2-T10	NM_010395.7	c.598C > T	p.His200Tyr	.	
17	36119452	G	A	HET	missense_variant	H2-T10	NM_010395.7	c.596C > T	p.Ala199Val	.	
17	36030989	A	T	HET	stop_gained	H2-T23	NM_010398.3	c.716T > A	p.Leu239*	.	
17	25311561	G	C	HET	missense_variant	Prss28	NM_053259.2	c.714G > C	p.Lys238Asn	.	
17	19811919	C	A	HET	missense_variant	Vmn2r103	NM_001104565.1	c.1954C > A	p.Gln652Lys	.	
17	20540922	T	G	HET	missense_variant	Vmn2r109	NM_001104571.1	c.2172A > C	p.Gln724His	.	
17	23308117	T	G	HET	missense_variant	Vmn2r114	NM_001102584.1	c.1440A > C	p.Lys480Asn	.	
17	33962099	C	CACACCAG	HET	frameshift_variant	Vps52	NM_172620.3	c.1314_1315insA CACCAG	p.Asp439fs	.	
17	33961703	G	A	HET	missense_variant	Vps52	NM_172620.3	c.1216G > A	p.Val406Met	.	
17	33961725	A	G	HET	missense_variant	Vps52	NM_172620.3	c.1238A > G	p.Asp413Gly	.	

(*Continued on next page*)

Table 3. *Continued*

Chrom	#Pos	ALT	REF	Zygosity	Annotation	Gene Name	Feature_ID	HGVS.c	HGVS.p	dbSNP142_ ID	Number of variants in human TNBC samples (COSMIC)
17	33962097	T	TCTG	HET	disruptive_inframe_ insertion	Vps52	NM_172620.3	c.1312_1313insCTG	p.Tyr438delinsSerAsp	.	
17	33963235	C	T	HET	missense_variant	Vps52	NM_172620.3	c.1786C > T	p.Arg596Trp	.	
18	20086680	C	T	HET	stop_gained	Dsc1	NM_001291804.1	c.2432G > A	p.Trp811*	.	
19	7215485	C	CAGGACCCCG AGCTGCTCC CGCGCCGGCT	HET	splice_acceptor_ variant&intron_variant	Cox8a	NM_007750.2	c.115-2_115-1insA GCCGGCGC GGGAGCAGCT CGGGGTCCT	.	.	
19	11511735	C	CGT	HET	frameshift_variant	Gm8369	NM_001164202.1	c.433_434dupTG	p.Lys146fs	.	
19	6054981	GCCTGGGGAA AGATAAA CTCCAGTCACC AGTTTCCAATC ACAGGACCCCA TGCCTTCATC CCTGGAAGATT CGGGTACACA CCCAAGCCACTTA	G	HET	frameshift_variant& splice_acceptor_variant& splice_donor_variant& splice_region_variant& splice_region_variant& splice_region_variant& intron_variant	Mrpl49	NM_026246.3	c.354 + 2_355del TAAGTGGCTTGGG TGTGTACCCGAAT CTTCCAGGGAT GAAGGCATGGGGT CCTGTGATT GGAAACTGGTGA CTGGAGTTTA TCTTTCCCCAGG	p.Ala119fs	.	
X	74303936	T	C	HET	missense_variant	Atp6ap1	NM_018794.4	c.1322T > C	p.Leu441Pro	.	

The mutually exclusive coding variants with predicted higher/moderate impact (n.177 variants in n.126 genes) in MMTV-Prune-1/Wnt1 cells are listed. Among these, n.39 genes were also found mutated in the public data of human basal TNBC available on Catalog Of Somatic Mutations In Cancer (COSMIC, v91, released 07-APR-20). Chrom, chromosome; Pos, position (with the first base having position 1); ALT, alternate non-reference alleles; REF, reference base(s); Zygosity, Homo/Hetero; Annotation, annotated using Sequence Ontology terms; Multiple effects can be concatenated using "&"; Gene Name, common gene name (HGNC); Feature_ID, transcript ID (version number); HGVS.c, Variant using HGVS notation (DNA level); HGVS.p, HGVS notation (Protein level); dbSNP142_ID, dbSNP rsNo.

Table 4. Relation between Prune-1 expression and clinicopathological features of TNBC patients in the TNBC tissue cohort

	Prune expression[a] (n = 138)			
	Low	High	p value	R pearson
Age				
<40	8 (44.4%)	10 (55.6%)	0.550	0.017
>40 ≤ 60	32 (56.2%)	25 (43.8%)		
>60	30 (47.6%)	33 (52.4%)		
Histotype				
Ductal	59 (52.2%)	54 (47.8%)	0.457	0.063
Not ductal	11 (44%)	14 (56%)		
Size				
≤2 cm	31 (48.4%)	33 (51.6%)	0.860	−0.012
>2 ≤ 5	32 (52.4%)	29 (47.6%)		
>5	5 (45.4%)	6 (54.6%)		
NA	2 (100%)	0 (0%)		
LNM				
Negative	45 (54.9%)	37 (45.1%)	0.197	0.110
Positive	24 (43.6%)	31 (54.4%)		
NA	1 (100%)	0 (0%)		
Lung metastasis				
Negative	38 (57.6%)	28 (42.4%)	**0.027**[b]	0.254
Positive	2 (20%)	8 (80%)		
NA	30 (48.4%)	32 (51.6%)		
Grading				
G1-2	14 (82.3%)	3 (17.7%)	**0.005**[b]	0.237
G3	56 (46.3%)	65 (53.7%)		
Ki67				
<20%	19 (73.1%)	7 (26.9%)	**0.011**[b]	0.219
≥20%	49 (54.6%)	59 (45.4%)		
NA	2 (50%)	2 (50%)		
Disease progression				
No	37 (59.7%)	25 (40.3%)	**0.031**[b]	0.212
Yes	16 (38.1%)	26 (61.9%)		
NA	17 (50%)	17 (50%)		

The clinicopathological parameters of the patients from our TNBC cohort grouped according to their Prune-1 protein expression levels are shown (n. 138 patients). Prune-1 overexpression was found positively correlated with Ki67 proliferative index (p = 0.011; R = 0.219), high grade (p = 0.005; R = 0.237), disease progression (p = 0.031; R = 0.212), and the presence of lung metastasis (p = 0.027; R = 0.254). Any statistically correlations were found between Prune-1 levels and patients age, lymph node metastases, and tumor histotype and size. In bold the statistically significant p-values.

LMN, lymph node metastases; G1, Grade 1 or low grade (sometimes also called well differentiated); G2, Grade 2 or intermediate/moderate grade (moderately differentiated); G3, Grade 3 or high grade (poorly differentiated); NA, not available.

[a]Prune-1 protein expression is based on the intensity and percentage of expression.

[b]Statistical significant association (i.e., p < 0.05).

Furthermore, we investigated the potential relationships between Prune-1 and the tumorigenic signaling pathways that are responsible for the aggressive behavior of TNBC. For this purpose, we took into account the nuclear localization of the MAPK and NF-κB effectors, due to their previously reported expression and correlations with poor prognosis in TNBC (Kim et al., 2016; Bartholomeusz et al., 2012). Our studies showed positive significant relationships between Prune-1 and phosphorylated-p65 (phospho-[Ser311]-p65; p < 0.00001; R = 0.421) and phosphorylated-ERK1/2 (phospho-[Thr202/Tyr204]-ERK1, phospho-[Thr185/Tyr187]-ERK2; p =

Table 5. Correlation analyses between Prune-1 and tumorigenic signaling pathways (phospho-p65 and phospho-ERK 1/2 in TNBC patient cohort)

	Prune expression[a] (n = 113)			
	Low	High	p value	R pearson
Phospho-p65[b]				
Low	36 (78.3%)	10 (21.7%)	<0.00001**	0.421
High	29 (44.3%)	56 (65.7%)		
NA	5 (71.4%)	2 (28.6%)		
Phospho-ERK 1/2[c]				
Low	40 (60.6%)	26 (39.4%)	0.003**	0.277
High	17 (32.7%)	35 (67.3%)		
NA	13 (65%)	7 (35%)		

The nuclear localization of MAPK and NF-kB effectors (i.e., phosphorylated-ERK1/2 and phosphorylated-p65, respectively) were evaluated in TNBC patients (n. 113) in our tissue cohort grouped according to their Prune-1 protein expression levels. Prune-1 overexpression was found positively correlated with phosphorylated-p65 (phospho-[Ser311]-p65; $p < 0.00001$; $R = 0.421$) and phosphorylated-ERK1/2 (phospho-[Thr202/Tyr204]-ERK1, phospho-[Thr185/Tyr187]-ERK2; $p = 0.003$; $R = 0.277$). MAPK, mitogen-activated protein kinase; NF-kB, nuclear factor kappa-light-chain-enhancer of activated B cells.
A statistically significant association: i.e., **$p < 0.005$.
[a]Prune-1 protein expression is based on the intensity of expression.
[b]Phosphorylated-(Ser311)-p65.
[c]Phosphorylated-(Thr202/Tyr204)-ERK1 and phosphorylated-(Thr185/Tyr187)-ERK2.

0.003; R = 0.277), as shown in Table 5 and Figure 5D, c–f. Overall, these data highlighted the involvement of Prune-1 in TNBC progression through the MAPK signaling cascade (i.e., phospho-ERK1/2) and through the NF-κB inflammatory pathway (i.e., phospho-p65), as identified in this TNBC dataset by IHC analysis.

Following these statistical associations, we investigated additional correlations between Prune-1 expression and immune-cell infiltration. We used immunosuppressive pro-tumorigenic M2-TAMs (i.e., $CD68^+$ $CD163^+$ cells) due to their already identified prognostic role in TNBC in the tumors with higher risk of metastatic dissemination (Sousa et al., 2015; Yuan et al., 2014). These correlation analyses of our dataset showed that patients with TNBC (n = 32) overexpressing Prune-1 were also characterized by higher numbers of tumor-infiltrating TAMs (i.e., $CD68^+$ cells; Figure 5D, g–h; $p = 0.014$, $R = 0.433$; in Table 6) and with a trend to significant association with CD163+ cells ($p = 0.07$, $R = 0.32$; see Figure 5D, i–l), a marker of pro-tumorigenic M2-polarized TAMs (Spano and Zollo, 2012), and with FOXP3, a marker of Tregs ($p = 0.08$; see Figure 5D, m–n). Of interest, we did not find any strong positivity of inflammatory pathways (i.e., p65-NF-κB), p-ERK, or the presence of immune infiltrating cells (i.e., CD68, CD163, FOXP3) in the sections near tumors with high expression of Prune-1 (Figure 5D, o–t). Altogether, these results indicate that Prune-1 is a potential biomarker related to TNBC subtypes with the poorest outcomes, as characterized by higher infiltrating M2-TAMs ($CD163^+$) and Tregs ($FOXP3^+$) (Adams et al., 2017). However, to define an immunologically "cold" or "hot" TME, this analysis is also supported by CD4, CD8, and PDL1 to evaluate the TILs environment and the levels of immunosuppressive markers (Adams et al., 2017). Here, we focused mainly on TAMs within the TME of TNBC due to their prognostic value (Sousa et al., 2015; Yuan et al., 2014).

In conclusion, the clinico-immunopathological correlation studies performed on our TNBC patient cohort suggest that overexpression of Prune-1 is significantly associated with the activation of proliferative and inflammatory pathways (i.e., MAPK, NF-κB), and recruitment of immunosuppressive cells with pro-tumorigenic functions (i.e., M2-TAMs) in the TME, in those patients with TNBC with high-grade tumorigenesis progression and lung metastases. At this time, we focused on these immune cell populations (i.e., TAMs) because of their negative prognostic significance, as previously reported in TNBC patients (Adams et al., 2017).

Pharmacological inhibition of Prune-1 through AA7.1 reduces metastatic foci *in vivo* via inhibition of M2 polarization of macrophages

To further address the role of Prune-1 in M2 polarization of macrophages, we used an anti-Prune-1 molecule (AA7.1) that has been previously shown to enhance Prune-1 degradation and to impair TGF-β signaling in metastatic medulloblastoma (Ferrucci et al., 2018).

Table 6. Correlation analyses between Prune-1 and M2-polarized tumor-associated macrophages (M2-TAMs) within the TME of TNBC patients

	Prune-1 (n = 32)[a]			
	Low	High	p value	R pearson
CD68				
Low	7 (87.5%)	1 (22.5%)	0.014[b]	0.433
High	9 (37.5%)	15 (62.5%)		
CD163				
Low	5 (83.3%)	1 (16.7%)	0.070[a]	0.320
High	11 (62.3%)	15 (57.7%)		

The expression of CD68+ and CD163+ cells (i.e., M2-TAMs) in the tumor from the patients belonging to our TNBC cohort (n.32) grouped according to their Prune-1 protein expression levels are shown. The overexpression of Prune-1 was found correlated with the presence of CD68+ cells, marker of TAMs ($p = 0.014$, $R = 0.433$). A positive statistical trend between the overexpression of Prune-1 and CD163+ cells (M2-TAMs marker) was also shown ($p = 0.07$, $R = 0.32$).

[a]Prune-1 protein expression is based on the intensity of expression. Statistical trend toward significance.

[b]A statistically significant association (i.e., $p < 0.05$).

Here, the potential immunomodulatory activity exerted by AA7.1 was tested in primary murine TNBC cells. AA7.1-treated MMTV–Prune-1/Wnt1 cells showed decreased levels of Prune-1 protein (Figure 6A, 50% reduction) and mRNA (Figure 6B) levels, with a major action on degradation of h-Prune-1. Reduced levels of phospho-SMAD2 (Figure 6A) and IL-17F (Figure 6B) were also shown in the same AA7.1-treated cells. These data indicate that AA7.1 can reduce the activation of TGF-β signaling and the secretion of this inflammatory cytokine that has previously been shown to be positively modulated by Prune-1.

This immunomodulatory action of AA7.1 was then studied by evaluating changes in the expression levels of M2-associated genes in macrophages (J774A.1) grown in conditioned media from AA7.1-treated MMTV–Prune-1/Wnt1 cells (Figure 6C). Of importance, there were decreased levels of IL-10, Arg1, IL-1β, and MMP-9 in these J774A.1 macrophages grown in culture media derived from the AA7.1-treated cells compared with the vehicle control (Figure 6D). To exclude any potential carry-over of AA7.1 in the tumor-cell-conditioned medium to the macrophages, we tested for AA7.1 downregulation of Prune-1 mRNA expression in J774A.1 macrophages. These macrophages treated with AA7.1 do not show downregulation of endogenous murine Prune-1 (Figure 6E), thus indicating that the changes in the cytokine levels in the recipient J774A.1 macrophages was not due to any direct effects of AA7.1 on these immune cells, thus excluding potential carry-over effects (at least at the AA7.1 concentration used in the assay).

Of interest, there was also modulation of the extracellular protein content released from AA7.1-treated MMTV–Prune-1/Wnt1 cells. Here, there were reduced Vimentin protein levels for both the AA7.1-treated MMTV–Prune-1/Wnt1 cells and in the extracellular vesicles secreted from these treated cells (Figure 6F).

Overall here, we have shown that AA7.1 can negatively modulate the cross-talk between TNBC and macrophages, thus affecting the activation of M2-associated genes via downregulation of Prune-1, inhibition of the TGF-β pathway, reduction of IL-17F in TNBC cells, and modulation of the extracellular protein content.

Next, to investigate whether M2-polarized macrophages can affect the migration rates of TNBC cells, we performed co-culture transwell migration assays using (1) J774A.1 macrophages previously polarized using conditioned media from MMTV–Prune-1/Wnt1 cells untreated or treated with AA7.1 and (2) MMTV-Wnt1 cells (Figure 6G). Untreated macrophages were used as the negative control. This system allowed the migration rates of MMTV–Prune-1/Wnt1 cells (using only 2% FBS as chemoattractant) to be monitored in the presence of M2-polarized macrophages (Figure 6H). These data showed increased migration rates only for MMTV–Prune-1/Wnt1 cells co-cultured with J774A.1 macrophages previously grown in conditioned media from untreated MMTV–Prune-1/Wnt1 cells (Figure 6H). To this end, we show that the M2-polarized macrophages can increase the motility of the TNBC cells, thus indicating that a bidirectional communication is in place between macrophages and tumorigenic cells.

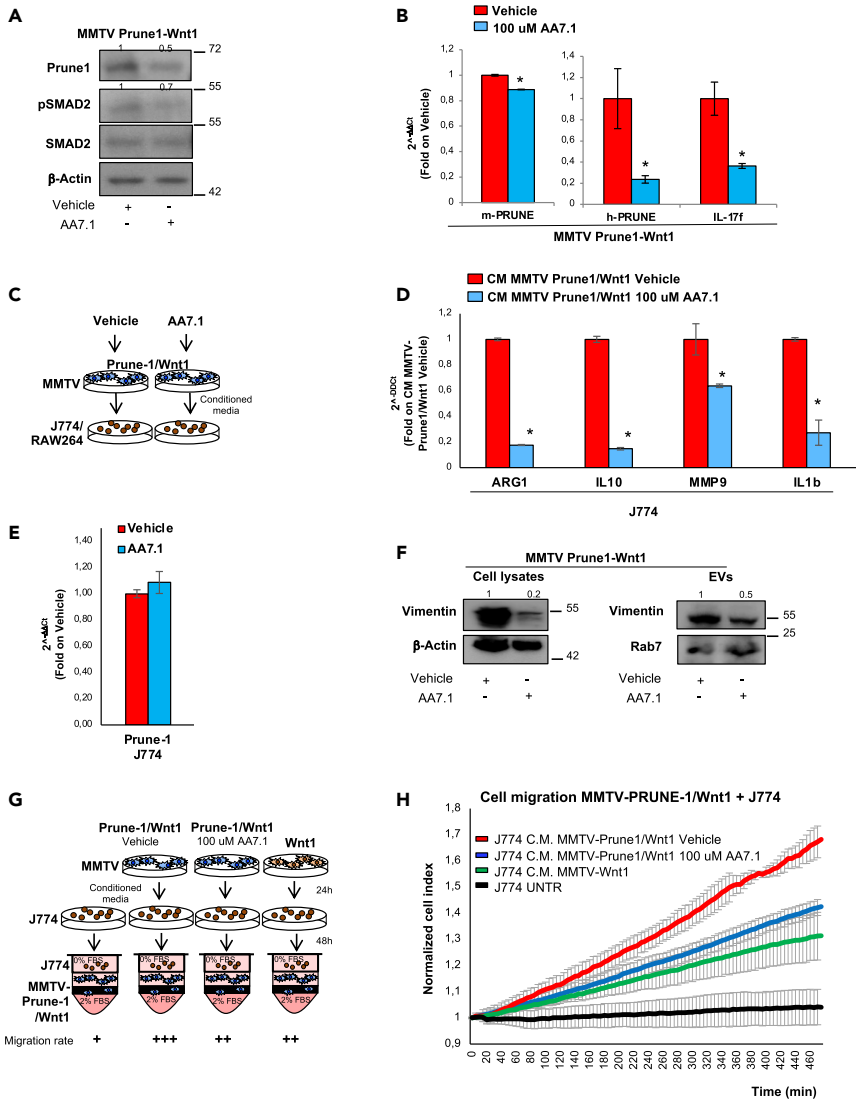

Figure 6. The AA7.1 anti-Prune-1 agent affects macrophages polarization *in vitro*

(A) Immunoblotting on total protein lysates of MMTV–Prune-1/Wnt1 cells treated with AA7.1 (100 μM, for 12 h) or PBS as the vehicle control, with the antibodies as indicated.

(B) Real-time RT-PCR of total RNA extracted from MMTV–Prune-1/Wnt1 cells treated with AA7.1 (100 μM, for 12 h) or PBS as the vehicle control, to detect human and murine Prune-1 and murine IL-17F. *, $p < 0.05$ in Student's t test compared with vehicle-treated MMTV–Prune-1/Wnt1 cells.

(C and D) Schematic representation of experimental design. J774A.1 macrophages were grown for 48 h in conditioned media collected from MMTV–Prune-1/Wnt1 cells treated with AA7.1 (100 μM, for 12 h) or PBS as the vehicle control (C). Real-time PCR analysis of some M2-associated genes, including IL-10, Arg-1, MMP-9, and IL-1β, in J774A.1 macrophages grown for 48 h in conditioned media collected from MMTV–Prune-1/Wnt1 cells treated with AA7.1 (blue) or PBS, as the vehicle control (red) (D). *$p < 0.05$ in Student's t test compared with macrophages grown in conditioned media collected from vehicle-treated MMTV–Prune-1/Wnt1 cells.

(E) Real-time RT-PCR of total RNA extracted from J774A.1 macrophages treated with AA7.1 (100 μM, for 48 h).

(F) Immunoblotting of total protein lysates or EVs of MMTV–Prune-1/Wnt1 cells treated with AA7.1 (100 μM) or PBS as the vehicle control, with the antibodies as indicated.

(G and H) Co-culture experiments to measure migration rates of MMTV–Prune-1/Wnt1 cells (using 2% FBS as chemoattractant) in the presence of J774A.1 macrophages previously grown in conditioned media collected from MMTV–Prune-1/Wnt1 cells (untreated or treated with AA7.1) and MMTV–Wnt1 cells. Untreated macrophages were used as negative control (G). Normalized Cell Index as a measure of cell migration of MMTV–Prune-1/Wnt1 cells, as generated by the xCELLigence RTCA software. Migration kinetics were monitored (every 5 min) in response to the presence of

Figure 6. *Continued*
untreated macrophages (black) or J774A.1 macrophages previously grown in conditioned media collected from vehicle-treated or AA7.1-treated MMTV–Prune-1/Wnt1 cells (red and blue, respectively) and MMTV–Wnt1 cells (green). The grading on migration rate is evaluated as the difference of Cell Index values observed at the end of the experiment. +++, 1.6; ++, 1.35; +/−, 1.04.

Furthermore, we also confirmed *in vivo* that both silencing and pharmacological inhibition (via AA7.1) of Prune-1 inhibited TNBC growth and M2-TAM polarization. For this, we used syngeneic orthotopic models with murine metastatic 4T1 TNBC cells. In the first trials, immunocompetent BALB/c mice were implanted in the mammary gland with Prune-1-silenced or EV control 4T1 clones that stably expressed the firefly luciferase gene (4T1-LUC) (Figure S12A). These syngeneic orthotopic mice were imaged weekly for tumor growth, as evaluated using bioluminescence acquisition with an imaging system (IVIS 3D Illumina; Xenogen/Caliper). At 14 and 21 days from tumor implantation, there was significant decrease in tumor growth (Figure S12B). Of importance, in the tumor tissues derived from the Sh-Prune-1-4T1 implanted mice there was a reduction of the number of infiltrating M2-TAMs (i.e., CD68+. CD163+ cells) in the TME (Figures S12C and S12D).

Similar results were obtained *in vivo* through pharmacological inhibition of Prune-1 using AA7.1. Female immunocompetent BALB/c mice were injected with 4T1-LUC cells. At 14 days from tumor implantation (i.e., once the tumors were established), the mice were grouped according to their bioluminescence values and injected intraperitoneally with 60 mg/kg AA7.1 daily or with phosphate-buffered saline (PBS) as the vehicle control (Figure S12E). Tumor growth was monitored weekly by bioluminescence acquisition. These *in-vivo* data showed significant reduction of tumor growth in the AA7.1-treated mice at 35 and 42 days from tumor implantation (Figure S12F). At the end of the experiments (i.e., 42 days from tumor implantation), the primary tumors were dissected out and embedded in paraffin for IHC analysis. These data showed significant reduction of CD163+ cells, but not CD68+ cells (Figures S12G and S12H), thus suggesting inhibition of the M2-polarization switch of macrophages in the TME.

Finally, we also investigated the AA7.1 to reduction of metastatic foci *in vivo*. For this purpose, MMTV–Prune-1/Wnt1 cells were injected (via the tail vein) into immunocompetent syngeneic (strain FVB) mice. At 14 days from cell injection, the mice were grouped according to their weight and AA7.1 (60 mg/kg/day, intraperitoneally) or PBS (as the vehicle negative control) were administered daily (Figure 7A). At 14 days from the start of the treatment (i.e., 28 days from cell injection), for *ex-vivo* targeting of tumorigenic cells, the mice were injected with a fluorescent imaging probe (XenoLight RediJect 2-DG-750; PerkinElmer) that targets cells with high metabolic activity in terms of glucose uptake (Figure 7A). Here, these *ex-vivo* data showed positive fluorescence signals in the lungs derived from all of the control mice (i.e., treated with PBS as vehicle). In contrast, tumorigenic cells were detected in the lungs using the *ex-vivo* imaging analysis following the AA7.1 treatment in only one of four mice (i.e., 25%), thus showing that AA7.1 can inhibit tumor cell homing to the lungs *in vivo* (Figure 7B). Hematoxylin/eosin staining of sections of lung tissue also confirmed the reductions in the metastatic foci for the AA7.1-treated mice compared with the controls (Figures 7C and 7D).

Altogether, these data indicate that pharmacological inhibition of Prune-1 through AA7.1 can reduce M2-polarization of macrophages and inhibit *in vivo* the TNBC cell homing to the lungs.

Discussion

Despite optimal systemic chemotherapy, metastatic TNBC remains with unmet medical needs due to a lack of targeted therapies (Rakha and Chan, 2011). Metastatic progression is the result of a complex network of communication between tumorigenic and immune cells in the TME (Spano and Zollo, 2012). TAMs, dendritic cells, T and B lymphocytes, and partially differentiated myeloid progenitors (i.e., myeloid-derived suppressor cells [MDSCs]) represent the major components of the TME in TNBC (Yu and Di, 2017), mainly due to the higher propensity of TNBC cells to generate "neoantigens" due to their genomic instability and mutational burden (Bianchini et al., 2016). Once recruited into the TME by tumor-secreted soluble mediators and exosomes, the immune cells contribute to promotion and maintenance of an immunosuppressive environment, which allows immune escape and as a consequence, enhances tumor and metastatic progression (Spano and Zollo, 2012). Due to the variegated nature of the TME in TNBC, new TNBC subtypes with prognostic significance have been defined (Adams et al., 2017). Among these newly identified

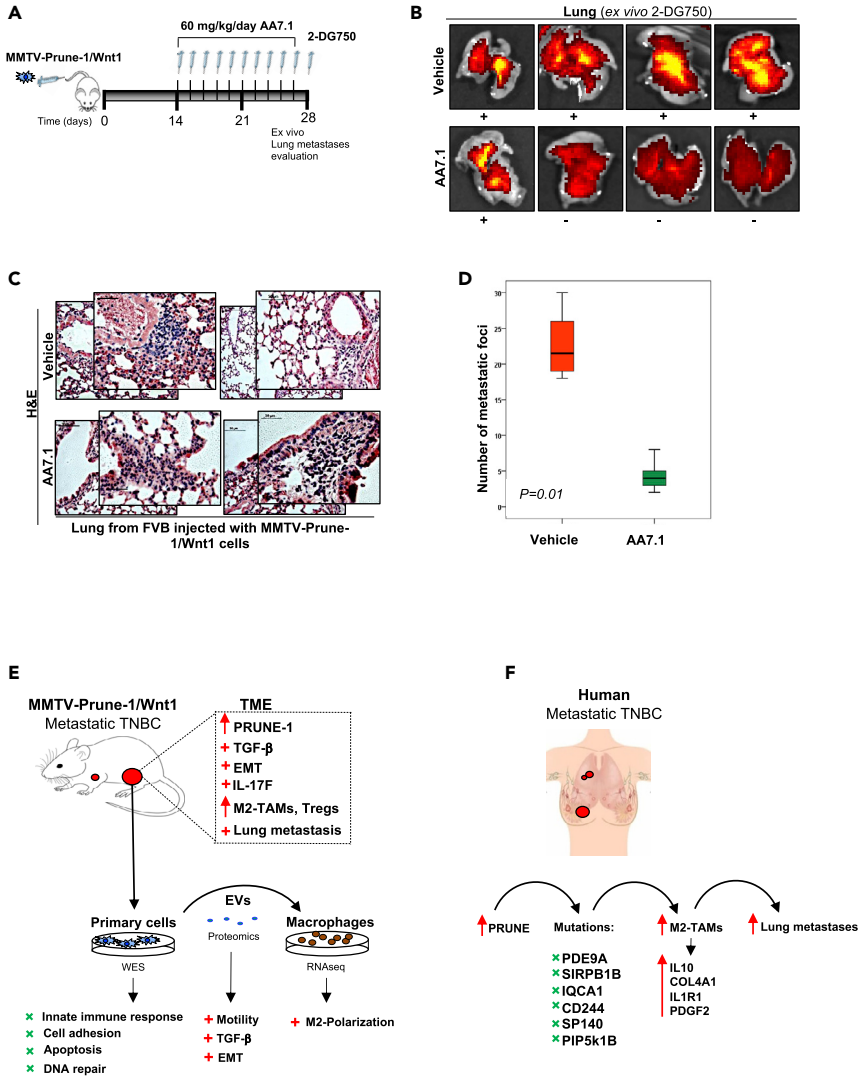

Figure 7. Hypothesized mechanisms of action of Prune-1 in the tumor microenvironment in the cross-talk between TNBC cells and macrophages

(A–D) Schematic representation of the *in-vivo* trial. MMTV–Prune-1/Wnt1 cells (1 ×10^5) were injected via the tail vein in eight immunocompetent syngeneic mice (strain FVB). After 14 days from cell injection, the mice were grouped according to their weight and AA7.1 (60 mg/kg/day, IP) or PBS (as vehicle control) was administered daily. At 14 days from treatment start (i.e., 28 days from cell injection), the mice were injected with a fluorescent imaging probe (XenoLight RediJect 2-DG-750; Perkin Elmer) for *ex-vivo* targeting of the tumorigenic cells (A). Positive fluorescence signals were detected in the lungs derived from all of the control mice (treated with PBS as vehicle) and in one of four AA7.1-treated mice (i.e., 25%) (B). Hematoxylin/eosin staining performed on sections of lung tissue from AA7.1-treated mice compared with controls. Magnification: 4x, 20x, 40x; Scale bars: 200 μm, 50 μm, 20 μm (C). Box plot (generated with the SPSS software) showing differences in the number of metastatic foci detected in the lungs from AA7.1-treated mice (green), compared with the control group (red) (D).

(E and F) The proposed mechanism of action of Prune-1 at the interplay between tumorigenic cells and TAMs in TME is shown for the murine model of metastatic TNBC (i.e., MMTV–Prune-1/Wnt1). Prune-1 acts in metastatic TNBC by promoting activation of intracellular pathways (i.e., TGF-β) and in a paracrine manner through the release of extracellular inflammatory molecules (i.e., IL-17F) and modulation of extracellular vesicle protein content (i.e., Sdcbp, Vim, Iftm3) involved in EMT and metastasis. Furthermore, mutational analyses in murine primary TNBC cells overexpressing Prune-1

Figure 7. *Continued*
(i.e., MMTV–Prune-1/Wnt1 cells) showed predicted deleterious variants in genes involved in activation of the innate immune response, apoptotic pathways, DNA repair, and cell adhesion. These gene variants were also found in patients with TNBC. In detail, in human, we identified deleterious variants for six genes that are mainly involved in the activation of the innate immune response. We also found upregulation of IL-10, COL4A1, ILR1, and PDGFB, the expression levels of which are negatively correlated with prognosis in patients with TNBC. Altogether, these actions induce recruitment of TAMs in the TNBC microenvironment and promote their polarization toward anti-inflammatory/pro-tumorigenic M2-status, thus preparing the system for lung metastasis within the premetastatic niche.

subtypes of TNBC stratified on the basis of the immune and metabolic markers in the TME, the subgroup of patients characterized by high levels of immunosuppressive markers/cells (M2-polarized-TAMs^{High}, Tregs^{High}, PDL1^{High}) in a context of high glycolytic stroma (MCT4^{High}) and low TILs environment are associated with poorest prognosis (Adams et al., 2017). Here, we focused on M2-TAMs; of importance, these cells were found in tumors that overexpressed Prune-1 (Figure 5D).

Genetically engineered mouse models are a useful resource in the study of the metastatic behavior of TNBC cells under immunocompetent conditions. However, GEMMs that resemble the features of metastatic TNBC have not been described to date (Pfefferle et al., 2013). Here, we developed a GEMM of metastatic TNBC driven by Prune-1 (MMTV–Prune-1/Wnt1) as a useful resource for preclinical studies to determine the efficacy of immunotherapeutic agents for treatment of established metastatic disease. We show that Prune-1 contributes to the generation of an immunosuppressive environment in both the primary tumor and the lung metastatic niches, through recruitment and polarization of M2-TAMs (Figure 2C).

Recently, in metastatic MB_{group3}, we identified Prune-1-driven intracellular signaling that is involved in the metastatic behavior linked to poor prognosis (Ferrucci et al., 2018). This "metastatic axis" is guided by a protein complex formed by Prune-1 and NDPK-A (NME-1). In metastatic medulloblastoma, both of these genes were overexpressed. Here, in specific TNBC-based gene expression analyses we show higher expression levels of Prune-1 and SMAD-2/4 (downstream effectors of the TGF-β cascade). For these reasons, we confirmed the activation of TGF-β *in vivo* in mammary tumors generated in the GEMM of metastatic Prune-1-driven TNBC (i.e., MMTV–Prune-1/Wnt1 cells; Figure S6A).

Furthermore, we showed increased levels of NDPK-A (NME-1) protein phosphorylated on serine residues (i.e., Ser120, Ser122, Ser125) in primary murine Prune-1-overexpressing TNBC cells (i.e., MMTV–Prune-1/Wnt1 cells; Figure S8C). Taken altogether, these data suggest that the Prune-1/NDPK-A protein complex might act as "driver" to promote metastatic dissemination also in TNBC, through enhancement of the TGF-β cascade and downregulation of PTEN. Literature data based on NDPK-A supports the concept of its role as a suppressor of metastasis in BC (Yokdang et al., 2015; Steeg, 2003). Of interest, overexpression of Prune-1 was also shown in these tumors, which were also characterized by higher NDPK-A expression levels (Forus et al., 2001). We hypothesized that Prune-1 acts through the "metastatic axis" in TNBC, as already described for MB_{group3}. An additional observation comes from the detection of extracellular NDPK-A in sera from patients with BC with metastases, and positive correlation was shown between the extracellular levels of NDPK-A and tumor growth in xenograft mice models (Yokdang et al., 2015). Of importance, extracellular Prune-1 was also detected in sera from patients with early stages of non-small-cell lung cancer (Carotenuto et al., 2014). Future efforts will be aimed at investigations into the mechanisms of actions of both of these extracellular proteins (i.e., Prune-1, NDPK-A) in metastatic TNBC, with a view to their potential prognostic value.

One additional feature is linked to a common PTEN loss observed in TNBC. This was described as its overexpression in MMTV–Wnt1 mice was reported to occur prior to tumor onset but not before metastatic behavior (Li et al., 2001). However, these findings indicated that PTEN loss and activation of Wnt signaling were not sufficient to induce metastatic spread in TNBC. These data are in agreement with PTEN downregulation in tumors that overexpress Prune-1 that was recently described for MB_{group3}. This is also of importance due to the role of PI3K/AKT activation and PTEN loss in TNBC, as previously reported (Bianchini et al., 2016) and as observed here using gene-expression data from different public BC datasets, which showed that PTEN expression levels were lower in the TNBC dataset (i.e., Brown (Burstein et al., 2015)) than in other BC datasets ($n = 1779$, $p = 7.3 \times 10^{-116}$; data not shown). Our findings show that the Prune-1-induced metastatic axis is maintained also in TNBC, and they also suggest that Prune-1 overexpression together with PTEN loss has prognostic value to identify those patients with metastatic potential in TNBC.

Transforming growth factor β has a crucial role in the TME through modulation of the polarization status of different immune cells, including TAMs (Pickup et al., 2013). Our *in-vitro* and *in-vivo* data show that Prune-1 enhances TAM recruitment and polarization toward a pro-tumorigenic M2 status, which in turn, and together with other factors, promotes STAT3 activation and increased expression levels of Arg1, MMP-9, IL-10, and IL-1β in recipient macrophages. As summarized in Figure 7E, we hypothesize here that Prune-1 acts in metastatic TNBC through activation of intracellular tumorigenic pathways (e.g., TGF-β), release of extracellular inflammatory soluble molecules (with a preferential action of IL-17F), and changes in EV protein content, from which of the importance of Vim and syntenin-1 arise, with a role in EMT and in the homing of tumorigenic cells to lung tissues (Das et al., 2016).

However, TGF-β has also been reported to modulate the activation and status of the other components of the TME (including MDSCs, lymphocytes, neutrophils, dendritic cells, cancer-associated fibroblasts) (Pickup et al., 2013). For the above reasons, we cannot exclude the possibility that Prune-1 also affects other immune-infiltrating cells and stromal components in the TME of TNBC. This issue will be addressed in future studies.

In the present study, we also provide evidence that Prune-1 in TNBC activates ERK1/2-MAPK, through increased phosphorylation of ERK1/2 and NF-κB and through increased phosphorylation of p65 and its increased nuclear localization (Figure 5D). Of importance, the question on how Prune-1 activates the ERK1/2-MAPK and NF-κB signaling pathways should be further addressed in the future. A possible mechanism might be related to Prune-1 regulation of the Wnt signaling pathway, through its interaction with GSK-3β, and to the complex network of interactions between these signaling pathways. Cross-talk with a positive-feedback loop between the Wnt and ERK pathways has been described in tumor cells (Kim et al., 2016). Moreover, the Wnt signaling pathway induces expression of S100A4, an important player in tumor progression and metastasis, which in turn positively activates the NF-κB signaling pathway (Stein et al., 2009; Boye et al., 2008). Therefore, it might act in an autocrine manner to promote NF-κB pathway activation in Prune-1-overexpressing TNBC cells.

Studies to impair TNBC have been recently reported. We have here demonstrated *in vitro* the pharmacological inhibition of Prune-1 in BC cells using a small molecule (AA7.1) (Ferrucci et al., 2018), which affects the crosstalk between tumorigenic cells and macrophages, thus reducing the expression of M2-associated genes (Figure 6D). We also show the activity of AA7.1 *in vivo*, with the demonstration of its potential to reduce M2-TAM recruitment in the TME and to inhibit lung metastatic processes (Figures 7B and 7C) via modulation of the TGF-β pathway (Figure 6A), IL17F expression levels (Figure 6B), and exosomal protein content (i.e., Vim; Figure 6F). How the expression of Prune1 in macrophages influences their direct modulation and its inhibition by AA7.1 in time-dependent and dose-dependent manners will be an issue for future studies.

Altogether we show that AA7.1 has an important immunomodulatory property. Of note, we have previously shown that AA7.1 did not induce toxicity, through evaluation of the hematological, hepatic, and renal parameters in treated mice (Ferrucci et al., 2018). Thus, future studies will be aimed at the testing of the pharmacological inhibition of Prune-1 using AA7.1, alone or in combination with current chemotherapy regimens and/or immunotherapeutics (e.g., checkpoint inhibitors) in TNBC.

Furthermore, we have shown increased levels of IL-1β in macrophages treated with conditioned media collected from Prune-1-overexpressing TNBC cells (Figures 3B and 3C). Indeed, high levels of intracellular IL-1β have been reported for macrophages polarized toward, but not at, the M2 phenotype (Pelegrin and Surprenant, 2009). Of interest, the intracellular accumulation of IL-1β in M2-polarizing macrophages is reported to be caused by extracellular ATP-derived pyrophosphates (Pelegrin and Surprenant, 2009). For the above reasons, Prune-1 enzymatic exopolyphosphatase/pyrophosphatase activities might also be involved in the mechanisms of macrophage polarization. By taking advantage of the use of specific inhibitors of Prune-1 enzymatic activities, future studies will address these hypotheses.

Moreover, and most importantly, our *in-vitro* and *in-vivo* data here also show that Prune-1 induces an immunosuppressive TME in TNBC by releasing extracellular soluble mediators (i.e., cytokines) and vesicle-containing proteins. Among the representative cytokines, IL-17F, IL-20, and IL-28 are targets of the Prune-1-activated NF-κB signaling pathways (Otkjaer et al., 2007) (Shen et al., 2006; Osterlund et al., 2007). Once

secreted, these Prune-1-induced cytokines might act on the tumor cells in an autocrine fashion or on immune cells (e.g., macrophages) in a paracrine manner within the TME. Indeed, similar to IL-17A, IL-17F activates the NF-κB and ERK1/2-MAPK signaling pathways, to promote angiogenesis and lead to upregulation of several chemokines and cytokines, thus exacerbating the inflammatory TME (Lai et al., 2011).

In the context of EV-containing proteins, among those secreted by Prune-1-overexpressing cells, we found Vim, Ifitm3, and syntenin-1 that have been reported to have roles in TNBC. Of note, Vim contributes to the aggressive phenotype and poor prognosis in TNBC (Yamashita et al., 2013). Instead, Ifitm3 was shown to be overexpressed in invasive BC, with a function related to progression and motility of TNBC cells (i.e., MDA-MB-231 cells) (Yang et al., 2013a). Most importantly, syntenin-1 is an adaptor molecule that is involved in a variety of cellular processes, including metastasis. Indeed, high expression of syntenin-1 in BC primary tumors has been significantly related to patient overall survival and progression-free survival (Yang et al., 2013b), and it is known to be negatively correlated to ER expression (Qian et al., 2013). Furthermore, syntenin-1 was shown to be overexpressed in TNBC cells with an invasive/metastatic phenotype (i.e., MDA-MB-231 cells) (Koo et al., 2002) and to have a role in promoting cell migration and invasion both *in vitro* and *in vivo*, through activation of AKT (Hwangbo et al., 2011), integrin-α1 (Yang et al., 2013a, 2013b), MAPK (Yang et al., 2013a, 2013b), and TGF-β signaling and EMT (Menezes et al., 2016), definitively promoting tumor growth and lung metastasis. Interestingly, syntenin-1 enhances the canonical TGF-β pathway (i.e., mediated by SMAD activation) and EMT, which thus leads to metastatic spread (Hwangbo et al., 2016). Lastly, the expression of syntenin-1 was shown to promote lung metastasis by influencing the inflammatory network, with the induction of inflammatory cytokines (i.e., IL-17A, IL-6) and both inflammatory and immunosuppressive cells (i.e., Th17 cells and MDSCs, respectively) in the TME of metastatic melanoma (Das et al., 2016). Overall, these EV-containing proteins represent an important finding that confirms the mechanism of communication between these TNBC cells and the immune cells within the TME.

Through WES analyses, we found mutually exclusive coding variants in the TNBC cells overexpressing Prune-1, with predicted higher/moderate impact. Among these variants, 39 gene variants were also found in the public database of human basal TNBC (COSMIC, v91) (Figure 5C). These deleterious variants are involved in activation of the innate immune response (leukocyte and macrophage activation; ANKHD1, FER1L5), cell adhesion (NEXN), apoptotic pathways (BID), and DNA repair (ERCC5) (Figure 5C). Of importance, lower expression levels of the PDE9A, Iqca1, Sirpb1b, CD244, SP140, and PIP5k1b genes was found in the BC patients with unfavorable prognosis in terms of 5-year survival analysis (dataset of Breast Invasive Carcinoma [n = 1075] from TCGA) (Figure S11). The same genes are also mutated in metastatic BC patients (dataset of metastatic BC (n = 216 (Lefebvre et al., 2016)) (Figure S11). Among these genes, CD244, Sirpb1b, and SV140 are involved in immune cell processes. CD244 has a crucial role in the activation of natural killer T cells (Mathew et al., 2009). It was defined as one of the markers of cytolytic activity in the TME of TNBC, together with the mutation status of $TP53^{mut}$ and $PIK3CA^{wt}$ (Cheng et al., 2020), thus acting as a marker for response to immunotherapy. On the other hand, Sirpb1b (or CD172B) shows strong correlations with immune system pathways that positively modulate the production of pro-inflammatory cytokines, including interleukin family cytokines, TNF-α, and GM-CSF (Huang et al., 2013), and participates in neutrophil trans-epithelial migration (Ribeiro et al., 2019). Of interest, the transcriptional factor SV140 is a master regulator that acts as a modulator of the adaptive immune response in BC. It was shown to be downregulated in BC cells, related to a lower infiltration of immune cells into tumor tissues and inversely correlated to relapse-free survival in BC of the basal subtype (Da Silveira et al., 2017). Importantly, SP140 is inversely correlated to NF-κB and regulates genes involved in cytokine production, inflammatory response, and cell-cell adhesion (Karaky et al., 2018). Then, Iqca1 was shown to be among the significantly downregulated genes in TNBC as compared with normal ductal cells, by genome-wide gene expression profiling analysis (Komatsu et al., 2013). Interestingly, a higher number of mutations in the PIP5K1B gene was found in metastatic BC as compared with both invasive and noninvasive BC (Durand et al., 2018). Regarding PDE9A, which is a regulator of cGMP signaling also in BC biology, it is less expressed in BC cells (including TNBC) compared with normal human mammary epithelial cells (Tinsley et al., 2009). Of importance, PDE9A was identified as a germline-related prognostic gene for ER-negative BC, involved in controlling cell growth and angiogenesis (Escala-Garcia et al., 2020).

Altogether, deleterious mutations in these genes through alterations to the innate immune response, enhancement of migratory properties, inhibition of apoptotic pathways, and impairment of the DNA repair system are potential routes to immune evasion mechanisms and metastasis formation in TNBC. Overall,

these data indicate that clonal selection occurred in our animal model identify mutated genes (CD 244, Sirpb1b, SV140, Iqca1, and PIP5K1B) also found in BC human cohorts.

In conclusion, these data (as summarized in Figures 7E and 7F) show that Prune-1 drives metastatic spread in TNBC through two mechanisms of action. The first is related to its induction of migration and EMT in TNBC through activation of different intracellular signaling pathways, including TGF-β. The second mechanism of action is related to its contribution to the generation of an immunosuppressive TME that is permissive to tumor growth and metastatic progression, by taking part to the communication with TAMs and inducing their recruitment and polarization toward a tumor-promoting M2 phenotype. The interplay between Prune-1 and TAMs within the TME is mediated by modulation of the release of inflammatory cytokines and extracellular vesicles driven by Prune-1. Among the cytokines, Prune-1 enhances secretion of IL-17F, IL-28, and IL-20 from TNBC cells. We also showed that EVs derived from Prune-1-overexpressing primary metastatic TNBC cells contain proteins that have roles in EMT and metastasis (e.g., syntenin-1, Vim, Ifitm3). In human, we identified deleterious variants in six genes that are mainly involved in the activation of innate immune responses. We also used RNAseq analyses to show upregulation of IL-10, COL4A1, ILR1, and PDGFB, the expression levels of which are negatively correlated with prognosis in patients with TNBC (Figure S10). Altogether, these findings support the notion of using these genes, in the near future, as potential indicators of prognosis poor outcome.

Finally, and most importantly, these data provide hope for the use of the Prune-1-targeting drug AA7.1 and any further new small molecule derivatives as immunomodulatory agents to ameliorate metastatic dissemination also via inhibition of M2-TAM polarization. These proof-of-concept studies presented here are now ready for the definition of a route for therapeutic application in TNBC.

Limitations of the study

The study provided preclinical data in a GEMM of metastatic TNBC, demonstrating the anti-tumorigenic action of AA7.1 small molecule. The predictive value of AA7.1 for therapeutic application in human TNBC patients deserves further investigations. At this time, the mutations here reported in the animal model generating lung metastasis with homologous mutated genes in human BC specimens need to be validated for prognostic use in human BC.

Resource availability

The conditions of submission and the BioMed Central Copyright and License Agreement are accepted. All the information essential to interpreting the data presented are available in the Figure legends and Supplemental Information. All resources used (antibodies, cell lines, animals, and software tools) are included in the Supplemental Information.

Lead contact

Further information and requests for resources and reagents should be directed to and will be fulfilled by the Lead Contact, Prof. Massimo Zollo (massimo.zollo@unina.it).

Materials availability

All the data and materials will be available from the Lead Contact on request with a completed Materials Transfer Agreement. Mouse lines generated in this study (transgenic mouse model MMTV–Prune-1) have been deposited to European Mutant Mouse Archive (EMMA) [code: FVB-Tg(MMTV–PRUNE)/Cnrm].

Data and code availability

The accession number for the RNAseq and WES data reported in this paper are listed below. Accession to RNAseq data:. RNAseq data: Embl/EBI (Array Express): *E-MTAB-9231*, https://www.ebi.ac.uk/arrayexpress/experiments/E-MTAB-9231/

A ccession to WES data. Embl/EBI (ENA): S PRJEB41714 (Study ID), https://www.ebi.ac.uk/ena/browser/view/PRJEB41714

MMTV-Prune-1/Wnt1:. Embl/EBI (ENA): SAMEA7851609 (Sample ID), https://www.ebi.ac.uk/ena/browser/view/ERS5598758.

MMTV-Wnt1:. Embl/EBI (ENA): SAMEA7851608 (Sample ID), https://www.ebi.ac.uk/ena/browser/view/ERS5598759

Mendeley deposition data for High Resolution: Figures 2, 5, 7, S5, S6, and S12. *Mendeley Data, V1:* (URL: https://data.mendeley.com/datasets/zdmthbkcgj/draft?a=40a706bf-5521-43d3-aa45-b322921ad243) https://doi.org/10.17632/zdmthbkcgj.1, https://doi.org/10.17632/zdmthbkcgj.1.

Methods

All methods can be found in the accompanying Transparent methods supplemental file.

Supplemental information

Supplemental Information can be found online at https://doi.org/10.1016/j.isci.2020.101938.

Acknowledgments

We thank Prof. John Collard (NCI Amsterdam, The Netherlands) for supporting the project by sharing the mouse MMTV–Wnt1 model, and we are grateful for his comments and fruitful discussions about these research findings. We thank Prof. Ettore Capoluongo (University of Naples Federico II/ CEINGE/ DAI AOU Federico II Medicina di laboratorio e Trasfusionale) for helpfull discussion related to the prognostic value of our results. The authors thank the following resources agencies for grant support: *Sviluppo di Approcci Terapeutici INnovativi per patologie neoplastiche resistenti ai trattamenti* – SATIN D.D. n. 355 del 5/06/2017 (MZ), EU-FP7-TUMIC-HEALTH-F2-2008-2016662 (MZ), the Italian Association for Cancer Research (AIRC) Grant IG #22129 (MZ), the Regione Campania L.g.R: N.5 (MZ), the European National Funds PON01-02388/1 2007-2013 (MZ), POR *Rete delle Biotecnologie in Campania Movie* (MZ), the European infrastructure for proteomics PRIME-XS-000016, the European School of Molecular Medicine for a Fellowship (VF), Fondazione Celeghin Italiana (MZ), and The European Mutant Mouse Archive (EMMA) for deposition of the transgenic mouse model MMTV–Prune-1 [code: FVB-Tg(MMTV–PRUNE)/Cnrm].

Author contributions

V.F. performed *in-vitro* co-culture experiments and EVs isolation. V.F. and L.M. performed immunoblotting analyses. F.A. and D.D.M. performed *in-vivo* trials. F.A. performed IF analyses. F.A., C.M.C., L.D., G.D.V., and A.M. performed quantitative IHC analyses. R.S. performed real-time RT-PCR assays. A.B. and G.P. analyzed RNAseq data. V.F., A.B., and G.P. analyzed WES data. D.S. monitored mice crossing. D.S. and M.C. generated cell clones and performed cytokines arrays. F.C., M.C., and M.D.B. performed TMA. J.V. and K.G. performed proteomic analyses. F.D.A. provided controls specimens. N.M. generated the MMTV–Prune-1/Wnt1 mouse. M.Z. designed the experiments and wrote the manuscript. All authors discussed the results and commented on, and approved, the manuscript.

Declaration of interests

All the authors declare no competing financial interests.

Received: June 26, 2020
Revised: October 22, 2020
Accepted: December 9, 2020
Published: January 22, 2021

References

Adams, T.A., Vail, P.J., Ruiz, A., Mollaee, M., Mccue, P.A., Knudsen, E.S., and Witkiewicz, A.K. (2017). Composite analysis of immunological and metabolic markers defines novel subtypes of triple negative breast cancer. Mod. Pathol. *31*, 288–298.

Bartholomeusz, C., Gonzalez-Angulo, A.M., Liu, P., Hayashi, N., Lluch, A., Ferrer-Lozano, J., and Hortobagyi, G.N. (2012). High ERK protein expression levels correlate with shorter survival in triple-negative breast cancer patients. Oncologist *17*, 766–774.

Bianchini, G., Balko, J.M., Mayer, I.A., Sanders, M.E., and Gianni, L. (2016). Triple-negative breast cancer: challenges and opportunities of a heterogeneous disease. Nat. Rev. Clin. Oncol. *13*, 674–690.

Boye, K., Grotterod, I., Aasheim, H.C., Hovig, E., and Maelandsmo, G.M. (2008). Activation of NF-kappaB by extracellular S100A4: analysis of signal transduction mechanisms and identification of target genes. Int. J. Cancer *123*, 1301–1310.

Burstein, M.D., Tsimelzon, A., Poage, G.M., Covington, K.R., Contreras, A., Fuqua, S.A., Savage, M.I., Osborne, C.K., Hilsenbeck, S.G., Chang, J.C., et al. (2015). Comprehensive genomic analysis identifies novel subtypes and targets of triple-negative breast cancer. Clin. Cancer Res. *21*, 1688–1698.

Callahan, R., and Smith, G.H. (2000). MMTV-induced mammary tumorigenesis: gene discovery, progression to malignancy and cellular pathways. Oncogene *19*, 992–1001.

Cancer Genome Atlas, N. (2012). Comprehensive molecular portraits of human breast tumours. Nature *490*, 61–70.

Carotenuto, M., De Antonellis, P., Liguori, L., Benvenuto, G., Magliulo, D., Alonzi, A., Turino, C., Attanasio, C., Damiani, V., Bello, A.M., et al. (2014). H-Prune through GSK-3beta interaction sustains canonical WNT/beta-catenin signaling enhancing cancer progression in NSCLC. Oncotarget *5*, 5736–5749.

Carotenuto, M., Pedone, E., Diana, D., De Antonellis, P., Dzeroski, S., Marino, N., Navas, L., Di Dato, V., Scoppettuolo, M.N., Cimmino, F., et al. (2013). Neuroblastoma tumorigenesis is regulated through the Nm23-H1/h-Prune C-terminal interaction. Sci. Rep. *3*, 1351.

Cheng, J., Ding, X., Xu, S., Zhu, B., and Jia, Q. (2020). Gene expression profiling identified TP53(Mut)PIK3CA(Wild) as a potential biomarker for patients with triple-negative breast cancer treated with immune checkpoint inhibitors. Oncol. Lett. *19*, 2817–2824.

Chow, A., Zhou, W., Liu, L., Fong, M.Y., Champer, J., Van Haute, D., Chin, A.R., Ren, X., Gugiu, B.G., Meng, Z., et al. (2014). Macrophage immunomodulation by breast cancer-derived exosomes requires Toll-like receptor 2-mediated activation of NF-kappaB. Sci. Rep. *4*, 5750.

Cox, J., Hein, M.Y., Luber, C.A., Paron, I., Nagaraj, N., and Mann, M. (2014). Accurate proteome-wide label-free quantification by delayed normalization and maximal peptide ratio extraction, termed MaxLFQ. Mol. Cell Proteomics *13*, 2513–2526.

D'Angelo, A., Garzia, L., Andre, A., Carotenuto, P., Aglio, V., Guardiola, O., Arrigoni, G., Cossu, A., Palmieri, G., Aravind, L., and Zollo, M. (2004). Prune cAMP phosphodiesterase binds nm23-H1 and promotes cancer metastasis. Cancer Cell *5*, 137–149.

Da Silveira, W.A., Palma, P.V.B., Sicchieri, R.D., Villacis, R.A.R., Mandarano, L.R.M., Oliveira, T.M.G., Antonio, H.M.R., Andrade, J.M., Muglia, V.F., Rogatto, S.R., et al. (2017). Transcription factor networks derived from breast cancer stem cells control the immune response in the basal subtype. Sci. Rep. *7*, 2851.

Dang, W., Tang, H., Cao, H., Wang, L., Zhang, X., Tian, W., Pang, X., Li, K., and Chen, T. (2015). Strategy of STAT3beta cell-specific expression in macrophages exhibits antitumor effects on mouse breast cancer. Gene Ther. *22*, 977–983.

Das, S.K., Guo, C., Pradhan, A.K., Bhoopathi, P., Talukdar, S., Shen, X.N., Emdad, L., Subler, M.A., Windle, J.J., Sarkar, D., et al. (2016). Knockout of MDA-9/Syntenin (SDCBP) expression in the microenvironment dampens tumor-supporting inflammation and inhibits melanoma metastasis. Oncotarget *7*, 46848–46861.

Decker, T., and Kovarik, P. (2000). Serine phosphorylation of STATs. Oncogene *19*, 2628–2637.

Dieci, M.V., Criscitiello, C., Goubar, A., Viale, G., Conte, P., Guarneri, V., Ficarra, G., Mathieu, M.C., Delaloge, S., Curigliano, G., and Andre, F. (2014). Prognostic value of tumor-infiltrating lymphocytes on residual disease after primary chemotherapy for triple-negative breast cancer: a retrospective multicenter study. Ann. Oncol. *25*, 611–618.

Ding, M.J., Su, K.E., Cui, G.Z., Yang, W.H., Chen, L., Yang, M., Liu, Y.Q., and Dai, D.L. (2016). Association between transforming growth factor-beta1 expression and the clinical features of triple negative breast cancer. Oncol. Lett. *11*, 4040–4044.

Drabsch, Y., and Ten Dijke, P. (2012). TGF-beta signalling and its role in cancer progression and metastasis. Cancer Metastasis Rev. *31*, 553–568.

Durand, N., Borges, S., Hall, T., Bastea, L., Doppler, H., Edenfield, B.H., Thompson, E.A., Geiger, X., and Storz, P. (2018). The phosphorylation status of PIP5K1C at serine 448 can be predictive for invasive ductal carcinoma of the breast. Oncotarget *9*, 36358–36370.

Escala-Garcia, M., Abraham, J., Andrulis, I.L., Anton-Culver, H., Arndt, V., Ashworth, A., Auer, P.L., Auvinen, P., Beckmann, M.W., Beesley, J., et al. (2020). A network analysis to identify mediators of germline-driven differences in breast cancer prognosis. Nat. Commun. *11*, 312.

Ferrucci, V., De Antonellis, P., Pennino, F.P., Asadzadeh, F., Virgilio, A., Montanaro, D., Galeone, A., Boffa, I., Pisano, I., Scognamiglio, I., et al. (2018). Metastatic group 3 medulloblastoma is driven by PRUNE1 targeting NME1-TGF-beta-OTX2-SNAIL via PTEN inhibition. Brain *141*, 1300–1319.

Forus, A., D'angelo, A., Henriksen, J., Merla, G., Maelandsmo, G.M., Florenes, V.A., Olivieri, S., Bjerkehagen, B., Meza-Zepeda, L.A., Del Vecchio Blanco, F., et al. (2001). Amplification and overexpression of PRUNE in human sarcomas and breast carcinomas-a possible mechanism for altering the nm23-H1 activity. Oncogene *20*, 6881–6890.

Fujiwara, Y., Takeya, M., and Komohara, Y. (2014). A novel strategy for inducing the antitumor effects of triterpenoid compounds: blocking the protumoral functions of tumor-associated macrophages via STAT3 inhibition. Biomed. Res. Int. *2014*, 348539.

Garzia, L., D'angelo, A., Amoresano, A., Knauer, S.K., Cirulli, C., Campanella, C., Stauber, R.H., Steegborn, C., Iolascon, A., and Zollo, M. (2008). Phosphorylation of nm23-H1 by CKI induces its complex formation with h-prune and promotes cell motility. Oncogene *27*, 1853–1864.

Giles, D.A., Moreno-Fernandez, M.E., Stankiewicz, T.E., Cappelletti, M., Huppert, S.S., Iwakura, Y., Dong, C., Shanmukhappa, S.K., and Divanovic, S. (2016). Regulation of inflammation by IL-17A and IL-17F modulates non-alcoholic fatty liver disease pathogenesis. PLoS One *11*, e0149783.

Goh, J.Y., Feng, M., Wang, W., Oguz, G., Yatim, S., Lee, P.L., Bao, Y., Lim, T.H., Wang, P., Tam, W.L., et al. (2017). Chromosome 1q21.3 amplification is a trackable biomarker and actionable target for breast cancer recurrence. Nat. Med. *23*, 1319–1330.

Hashimoto, M., Kobayashi, T., Tashiro, H., Arihiro, K., Kikuchi, A., and Ohdan, H. (2016). h-Prune is associated with poor prognosis and epithelial-mesenchymal transition in patients with colorectal liver metastases. Int. J. Cancer *139*, 812–823.

Herschkowitz, J.I., Simin, K., Weigman, V.J., Mikaelian, I., Usary, J., Hu, Z., Rasmussen, K.E., Jones, L.P., Assefnia, S., Chandrasekharan, S., et al. (2007). Identification of conserved gene expression features between murine mammary carcinoma models and human breast tumors. Genome Biol. *8*, R76.

Hoshino, A., Costa-Silva, B., Shen, T.L., Rodrigues, G., Hashimoto, A., Tesic Mark, M., Molina, H., Kohsaka, S., Di Giannatale, A., Ceder, S., et al. (2015). Tumour exosome integrins determine organotropic metastasis. Nature *527*, 329–335.

Huang, K.C., Yang, K.C., Lin, H., Tsao Tsun-Hui, T., Lee, W.K., Lee, S.A., and Kao, C.Y. (2013). Analysis of schizophrenia and hepatocellular carcinoma genetic network with corresponding modularity and pathways: novel insights to the immune system. BMC Genomics *14* (*Suppl 5*), S10.

Huang, S., Chen, Y., Podsypanina, K., and Li, Y. (2008). Comparison of expression profiles of metastatic versus primary mammary tumors in MMTV-Wnt-1 and MMTV-Neu transgenic mice. Neoplasia *10*, 118–124.

Hwangbo, C., Park, J., and Lee, J.H. (2011). mda-9/Syntenin protein positively regulates the activation of Akt protein by facilitating integrin-linked kinase adaptor function during adhesion to type I collagen. J. Biol. Chem. *286*, 33601–33612.

Hwangbo, C., Tae, N., Lee, S., Kim, O., Park, O.K., Kim, J., Kwon, S.H., and Lee, J.H. (2016). Syntenin regulates TGF-beta1-induced Smad activation and the epithelial-to-mesenchymal transition by inhibiting caveolin-mediated TGF-beta type I receptor internalization. Oncogene *35*, 389–401.

Karaky, M., Fedetz, M., Potenciano, V., Andres-Leon, E., Codina, A.E., Barrionuevo, C., Alcina, A., and Matesanz, F. (2018). SP140 regulates the expression of immune-related genes associated with multiple sclerosis and other autoimmune diseases by NF-kappaB inhibition. Hum. Mol. Genet. *27*, 4012–4023.

Kim, J.Y., Jung, H.H., Ahn, S., Bae, S., Lee, S.K., Kim, S.W., Lee, J.E., Nam, S.J., Ahn, J.S., Im, Y.H., and Park, Y.H. (2016). The relationship between nuclear factor (NF)-kappaB family gene expression and prognosis in triple-negative breast cancer (TNBC) patients receiving adjuvant doxorubicin treatment. Sci. Rep. *6*, 31804.

Kobayashi, T., Hino, S., Oue, N., Asahara, T., Zollo, M., Yasui, W., and Kikuchi, A. (2006). Glycogen synthase kinase 3 and h-prune regulate cell migration by modulating focal adhesions. Mol. Cell Biol *26*, 898–911.

Komatsu, M., Yoshimaru, T., Matsuo, T., Kiyotani, K., Miyoshi, Y., Tanahashi, T., Rokutan, K., Yamaguchi, R., Saito, A., Imoto, S., et al. (2013). Molecular features of triple negative breast cancer cells by genome-wide gene expression profiling analysis. Int. J. Oncol. *42*, 478–506.

Koo, T.H., Lee, J.J., Kim, E.M., Kim, K.W., Kim, H.D., and Lee, J.H. (2002). Syntenin is overexpressed and promotes cell migration in metastatic human breast and gastric cancer cell lines. Oncogene *21*, 4080–4088.

Lai, T., Wang, K., Hou, Q., Zhang, J., Yuan, J., Yuan, L., You, Z., and Xi, M. (2011). Interleukin 17 induces up-regulation of chemokine and cytokine expression via activation of the nuclear factor kappaB and extracellular signal-regulated kinase 1/2 pathways in gynecologic cancer cell lines. Int. J. Gynecol. Cancer *21*, 1533–1539.

Lam, J., Herant, M., Dembo, M., and Heinrich, V. (2009). Baseline mechanical characterization of J774 macrophages. Biophys. J. *96*, 248–254.

Lefebvre, C., Bachelot, T., Filleron, T., Pedrero, M., Campone, M., Soria, J.C., Massard, C., Levy, C., Arnedos, M., Lacroix-Triki, M., et al. (2016). Mutational profile of metastatic breast cancers: a retrospective analysis. PLoS Med. *13*, e1002201.

Lehmann, B.D., Bauer, J.A., Chen, X., Sanders, M.E., Chakravarthy, A.B., Shyr, Y., and Pietenpol, J.A. (2011). Identification of human triple-negative breast cancer subtypes and preclinical models for selection of targeted therapies. J. Clin. Invest *121*, 2750–2767.

Lehmann, B.D., Jovanovic, B., Chen, X., Estrada, M.V., Johnson, K.N., Shyr, Y., Moses, H.L., Sanders, M.E., and Pietenpol, J.A. (2016). Refinement of triple-negative breast cancer molecular subtypes: implications for neoadjuvant chemotherapy selection. PLoS One *11*, e0157368.

Levy, D.E., and Darnell, J.E., Jr. (2002). Stats: transcriptional control and biological impact. Nat. Rev. Mol. Cell Biol *3*, 651–662.

Li, Y., Hively, W.P., and Varmus, H.E. (2000). Use of MMTV-Wnt-1 transgenic mice for studying the genetic basis of breast cancer. Oncogene *19*, 1002–1009.

Li, Y., Podsypanina, K., Liu, X., Crane, A., Tan, L.K., Parsons, R., and Varmus, H.E. (2001). Deficiency of Pten accelerates mammary oncogenesis in MMTV-Wnt-1 transgenic mice. BMC Mol. Biol. *2*, 2.

Lin, N.U., Vanderplas, A., Hughes, M.E., Theriault, R.L., Edge, S.B., Wong, Y.N., Blayney, D.W., Niland, J.C., Winer, E.P., and Weeks, J.C. (2012). Clinicopathologic features, patterns of recurrence, and survival among women with triple-negative breast cancer in the National Comprehensive Cancer Network. Cancer *118*, 5463–5472.

Mantovani, A., Sozzani, S., Locati, M., Allavena, P., and Sica, A. (2002). Macrophage polarization: tumor-associated macrophages as a paradigm for polarized M2 mononuclear phagocytes. Trends Immunol. *23*, 549–555.

Martinez, F.O., Gordon, S., Locati, M., and Mantovani, A. (2006). Transcriptional profiling of the human monocyte-to-macrophage differentiation and polarization: new molecules and patterns of gene expression. J. Immunol. *177*, 7303–7311.

Mathew, S.O., Rao, K.K., Kim, J.R., Bambard, N.D., and Mathew, P.A. (2009). Functional role of human NK cell receptor 2B4 (CD244) isoforms. Eur. J. Immunol. *39*, 1632–1641.

Menezes, M.E., Shen, X.N., Das, S.K., Emdad, L., Sarkar, D., and Fisher, P.B. (2016). MDA-9/Syntenin (SDCBP) modulates small GTPases RhoA and Cdc42 via transforming growth factor beta1 to enhance epithelial-mesenchymal transition in breast cancer. Oncotarget *7*, 80175–80189.

Nambu, J., Kobayashi, T., Hashimoto, M., Tashiro, H., Sugino, K., Shimamoto, F., Kikuchi, A., and Ohdan, H. (2016). h-prune affects anaplastic thyroid cancer invasion and metastasis. Oncol. Rep. *35*, 3445–3452.

Neophytou, C., Boutsikos, P., and Papageorgis, P. (2018). Molecular mechanisms and emerging therapeutic targets of triple-negative breast cancer metastasis. Front Oncol. *8*, 31.

Noguchi, T., Oue, N., Wada, S., Sentani, K., Sakamoto, N., Kikuchi, A., and Yasui, W. (2009). h-Prune is an independent prognostic marker for survival in esophageal squamous cell carcinoma. Ann. Surg. Oncol. *16*, 1390–1396.

Nonaka, M., Ogihara, N., Fukumoto, A., Sakanushi, A., Kusama, K., Pawankar, R., and Yagi, T. (2009). Synergistic induction of macrophage inflammatory protein-3alpha;/CCL20 production by interleukin-17A and tumor necrosis factor-alpha; in nasal polyp fibroblasts. World Allergy Organ J. *2*, 218–223.

Orecchioni, M., Ghosheh, Y., Pramod, A.B., and Ley, K. (2019). Macrophage polarization: different gene signatures in M1(LPS+) vs. classically and M2(LPS-) vs. alternatively activated macrophages. Front Immunol. *10*, 1084.

Osterlund, P.I., Pietila, T.E., Veckman, V., Kotenko, S.V., and Julkunen, I. (2007). IFN regulatory factor family members differentially regulate the expression of type III IFN (IFN-lambda) genes. J. Immunol. *179*, 3434–3442.

Otkjaer, K., Kragballe, K., Johansen, C., Funding, A.T., Just, H., Jensen, U.B., Sorensen, L.G., Norby, P.L., Clausen, J.T., and Iversen, L. (2007). IL-20 gene expression is induced by IL-1beta through mitogen-activated protein kinase and NF-kappaB-dependent mechanisms. J. Invest Dermatol. *127*, 1326–1336.

Oue, N., Yoshida, K., Noguchi, T., Sentani, K., Kikuchi, A., and Yasui, W. (2007). Increased expression of h-prune is associated with tumor progression and poor survival in gastric cancer. Cancer Sci. *98*, 1198–1205.

Pelegrin, P., and Surprenant, A. (2009). Dynamics of macrophage polarization reveal new mechanism to inhibit IL-1beta release through pyrophosphates. EMBO J. *28*, 2114–2127.

Pfefferle, A.D., Herschkowitz, J.I., Usary, J., Harrell, J.C., Spike, B.T., Adams, J.R., Torres-Arzayus, M.I., Brown, M., Egan, S.E., Wahl, G.M., et al. (2013). Transcriptomic classification of genetically engineered mouse models of breast cancer identifies human subtype counterparts. Genome Biol. *14*, R125.

Pickup, M., Novitskiy, S., and Moses, H.L. (2013). The roles of TGFbeta in the tumour microenvironment. Nat. Rev. Cancer *13*, 788–799.

Pohl, S.G., Brook, N., Agostino, M., Arfuso, F., Kumar, A.P., and Dharmarajan, A. (2017). Wnt signaling in triple-negative breast cancer. Oncogenesis *6*, e310.

Qian, X.L., Li, Y.Q., Yu, B., Gu, F., Liu, F.F., Li, W.D., Zhang, X.M., and Fu, L. (2013). Syndecan binding protein (SDCBP) is overexpressed in estrogen receptor negative breast cancers, and is a potential promoter for tumor proliferation. PLoS One *8*, e60046.

Rakha, E.A., and Chan, S. (2011). Metastatic triple-negative breast cancer. Clin. Oncol. (R Coll. Radiol. *23*, 587–600.

Ribeiro, G.E., Leon, L.E., Perez, R., Cuiza, A., Vial, P.A., Ferres, M., Mertz, G.J., and Vial, C. (2019). Deletions in genes participating in innate immune response modify the clinical Course of Andes Orthohantavirus Infection. Viruses *11*, 680.

Santoni, M., Romagnoli, E., Saladino, T., Foghini, L., Guarino, S., Capponi, M., Giannini, M., Cognigni, P.D., Ferrara, G., and Battelli, N. (2017). Triple negative breast cancer: Key role of Tumor-Associated Macrophages in regulating the activity of anti-PD-1/PD-L1 agents. Biochim. Biophys. Acta Rev. Cancer *1869*, 78–84.

Shah, S.P., Roth, A., Goya, R., Oloumi, A., Ha, G., Zhao, Y., Turashvili, G., Ding, J., Tse, K., Haffari, G., et al. (2012). The clonal and mutational evolution spectrum of primary triple-negative breast cancers. Nature *486*, 395–399.

Shahrara, S., Pickens, S.R., Dorfleutner, A., and Pope, R.M. (2009). IL-17 induces monocyte migration in rheumatoid arthritis. J. Immunol. *182*, 3884–3891.

Shen, F., Hu, Z., Goswami, J., and Gaffen, S.L. (2006). Identification of common transcriptional regulatory elements in interleukin-17 target genes. J. Biol. Chem. *281*, 24138–24148.

Silva, G.O., He, X., Parker, J.S., Gatza, M.L., Carey, L.A., Hou, J.P., Moulder, S.L., Marcom, P.K., Ma, J., Rosen, J.M., and Perou, C.M. (2015). Cross-species DNA copy number analyses identifies multiple 1q21-q23 subtype-specific driver genes for breast cancer. Breast Cancer Res. Treat *152*, 347–356.

Sousa, S., Brion, R., Lintunen, M., Kronqvist, P., Sandholm, J., Monkkonen, J., Kellokumpu-Lehtinen, P.L., Lauttia, S., Tynninen, O., Joensuu, H., et al. (2015). Human breast cancer cells educate macrophages toward the M2 activation status. Breast Cancer Res. *17*, 101.

Spano, D., and Zollo, M. (2012). Tumor microenvironment: a main actor in the metastasis process. Clin. Exp. Metastasis *29*, 381–395.

Starnes, T., Robertson, M.J., Sledge, G., Kelich, S., Nakshatri, H., Broxmeyer, H.E., and Hromas, R. (2001). Cutting edge: IL-17F, a novel cytokine selectively expressed in activated T cells and monocytes, regulates angiogenesis and endothelial cell cytokine production. J. Immunol. *167*, 4137–4140.

Steeg, P.S. (2003). Metastasis suppressors alter the signal transduction of cancer cells. Nat. Rev. Cancer *3*, 55–63.

Stein, T., Salomonis, N., Nuyten, D.S., Van De Vijver, M.J., and Gusterson, B.A. (2009). A mouse mammary gland involution mRNA signature identifies biological pathways potentially

associated with breast cancer metastasis. J. Mammary Gland Biol. Neoplasia *14*, 99–116.

Tammenkoski, M., Koivula, K., Cusanelli, E., Zollo, M., Steegborn, C., Baykov, A.A., and Lahti, R. (2008). Human metastasis regulator protein H-prune is a short-chain exopolyphosphatase. Biochemistry *47*, 9707–9713.

Thery, C., Amigorena, S., Raposo, G., and Clayton, A. (2006). Isolation and characterization of exosomes from cell culture supernatants and biological fluids. Curr. Protoc. Cell Biol *Chapter 3*. Unit 3 22.

Thery, C., Ostrowski, M., and Segura, E. (2009). Membrane vesicles as conveyors of immune responses. Nat. Rev. Immunol. *9*, 581–593.

Thery, C., Zitvogel, L., and Amigorena, S. (2002). Exosomes: composition, biogenesis and function. Nat. Rev. Immunol. *2*, 569–579.

Tinsley, H.N., Gary, B.D., Keeton, A.B., Zhang, W., Abadi, A.H., Reynolds, R.C., and Piazza, G.A. (2009). Sulindac sulfide selectively inhibits growth and induces apoptosis of human breast tumor cells by phosphodiesterase 5 inhibition, elevation of cyclic GMP, and activation of protein kinase G. Mol. Cancer Ther. *8*, 3331–3340.

Wang, N., Liang, H., and Zen, K. (2014). Molecular mechanisms that influence the macrophage m1-m2 polarization balance. Front Immunol. *5*, 614.

Xiao, W., Zheng, S., Liu, P., Zou, Y., Xie, X., Yu, P., Tang, H., and Xie, X. (2018). Risk factors and survival outcomes in patients with breast cancer and lung metastasis: a population-based study. Cancer Med. *7*, 922–930.

Yamashita, N., Tokunaga, E., Kitao, H., Hisamatsu, Y., Taketani, K., Akiyoshi, S., Okada, S., Aishima, S., Morita, M., and Maehara, Y. (2013). Vimentin as a poor prognostic factor for triple-negative breast cancer. J. Cancer Res. Clin. Oncol. *139*, 739–746.

Yang, M., Gao, H., Chen, P., Jia, J., and Wu, S. (2013a). Knockdown of interferon-induced transmembrane protein 3 expression suppresses breast cancer cell growth and colony formation and affects the cell cycle. Oncol. Rep. *30*, 171–178.

Yang, X.O., Chang, S.H., Park, H., Nurieva, R., Shah, B., Acero, L., Wang, Y.H., Schluns, K.S., Broaddus, R.R., Zhu, Z., and Dong, C. (2008). Regulation of inflammatory responses by IL-17F. J. Exp. Med. *205*, 1063–1075.

Yang, Y., Hong, Q., Shi, P., Liu, Z., Luo, J., and Shao, Z. (2013b). Elevated expression of syntenin in breast cancer is correlated with lymph node metastasis and poor patient survival. Breast Cancer Res. *15*, R50.

Yokdang, N., Nordmeier, S., Speirs, K., Burkin, H.R., and Buxton, I.L. (2015). Blockade of extracellular NM23 or its endothelial target slows breast cancer growth and metastasis. Integr. Cancer Sci. Ther. *2*, 192–200.

Yoneda, T., Michigami, T., Yi, B., Williams, P.J., Niewolna, M., and Hiraga, T. (2000). Actions of bisphosphonate on bone metastasis in animal models of breast carcinoma. Cancer *88*, 2979–2988.

Yu, H., Kortylewski, M., and Pardoll, D. (2007). Crosstalk between cancer and immune cells: role of STAT3 in the tumour microenvironment. Nat. Rev. Immunol. *7*, 41–51.

Yu, Q.C., Verheyen, E.M., and Zeng, Y.A. (2016). Mammary development and breast cancer: a Wnt Perspective. Cancers (Basel) *8*, 65.

Yu, T., and Di, G. (2017). Role of tumor microenvironment in triple-negative breast cancer and its prognostic significance. Chin J. Cancer Res. *29*, 237–252.

Yuan, S., Zhang, S., Zhuang, Y., Zhang, H., Bai, J., and Hou, Q. (2015). Interleukin-17 Stimulates STAT3-mediated endothelial cell activation for neutrophil recruitment. Cell Physiol Biochem *36*, 2340–2356.

Yuan, Z.Y., Luo, R.Z., Peng, R.J., Wang, S.S., and Xue, C. (2014). High infiltration of tumor-associated macrophages in triple-negative breast cancer is associated with a higher risk of distant metastasis. Onco Targets Ther. *7*, 1475–1480.

Zhang, X., Tian, W., Cai, X., Wang, X., Dang, W., Tang, H., Cao, H., Wang, L., and Chen, T. (2013). Hydrazinocurcumin Encapsuled nanoparticles "re-educate" tumor-associated macrophages and exhibit anti-tumor effects on breast cancer following STAT3 suppression. PLoS One *8*, e65896.

Zhou, Z., Hamming, O.J., Ank, N., Paludan, S.R., Nielsen, A.L., and Hartmann, R. (2007). Type III interferon (IFN) induces a type I IFN-like response in a restricted subset of cells through signaling pathways involving both the Jak-STAT pathway and the mitogen-activated protein kinases. J. Virol. *81*, 7749–7758.

Zollo, M., Andre, A., Cossu, A., Sini, M.C., D'angelo, A., Marino, N., Budroni, M., Tanda, F., Arrigoni, G., and Palmieri, G. (2005). Overexpression of h-prune in breast cancer is correlated with advanced disease status. Clin. Cancer Res. *11*, 199–205.

iScience, Volume *24*

Supplemental Information

Prune-1 drives polarization of tumor-associated macrophages (TAMs) within the lung metastatic niche in triple-negative breast cancer

Veronica Ferrucci, Fatemeh Asadzadeh, Francesca Collina, Roberto Siciliano, Angelo Boccia, Laura Marrone, Daniela Spano, Marianeve Carotenuto, Cristina Maria Chiarolla, Daniela De Martino, Gennaro De Vita, Alessandra Macrì, Luisa Dassi, Jonathan Vandenbussche, Natascia Marino, Monica Cantile, Giovanni Paolella, Francesco D'Andrea, Maurizio di Bonito, Kris Gevaert, and Massimo Zollo

Supplemental Information

Prune-1 drives polarization of tumor-associated macrophages (TAMs) within the lung metastatic niche in triple-negative breast cancer

Veronica Ferrucci,[1,2,3] Fatemeh Asadzadeh,[1,2,#] Francesca Collina,[4,#] Roberto Siciliano,[1] Angelo Boccia,[1] Laura Marrone,[1,2] Daniela Spano,[1] Marianeve Carotenuto,[2] Cristina Maria Chiarolla,[1] Daniela De Martino, [2] Gennaro De Vita, [2] Alessandra Macrì,[1] Luisa Dassi,[1] Jonathan Vandenbussche,[5] Natascia Marino,[1,6] Cantile Monica,[4] Giovanni Paolella,[1] Francesco D'Andrea,[7] Maurizio di Bonito,[4] Kris Gevaert,[5] and Massimo Zollo[1,2,3,8,9 *]

[1] CEINGE, Biotecnologie Avanzate, Naples, 80145, Italy

[2] Dipartimento di Medicina Molecolare e Biotecnologie Mediche (DMMBM), 'Federico II' University of Naples, Naples, 80134, Italy

[3] European School of Molecular Medicine (SEMM), University of Milan, Milan, Italy

[4] Pathology Unit, Istituto Nazionale Tumori-IRCS- Fondazione G.Pascale, Naples, 80131, Italy

[5] VIB-UGent Centre for Medical Biotechnology, Ghent, 9052, Belgium

[6] Department of Medicine, Indiana University-Purdue University Indianapolis, Indianapolis, 46202, USA

[7] Dipartimento di Sanità pubblica – AOU, Università degli Studi di Napoli Federico II, Naples, 80131, Italy

[8] DAI Medicina di Laboratorio e Trasfusionale, AOU Federico II, Naples, 80131, Italy

[9] Lead Contact

[#] These authors contributed equally to this study

[*] Correspondence: massimo.zollo@unina.it (M.Z.)

Supplemental Information

Supplemental Figures and legends

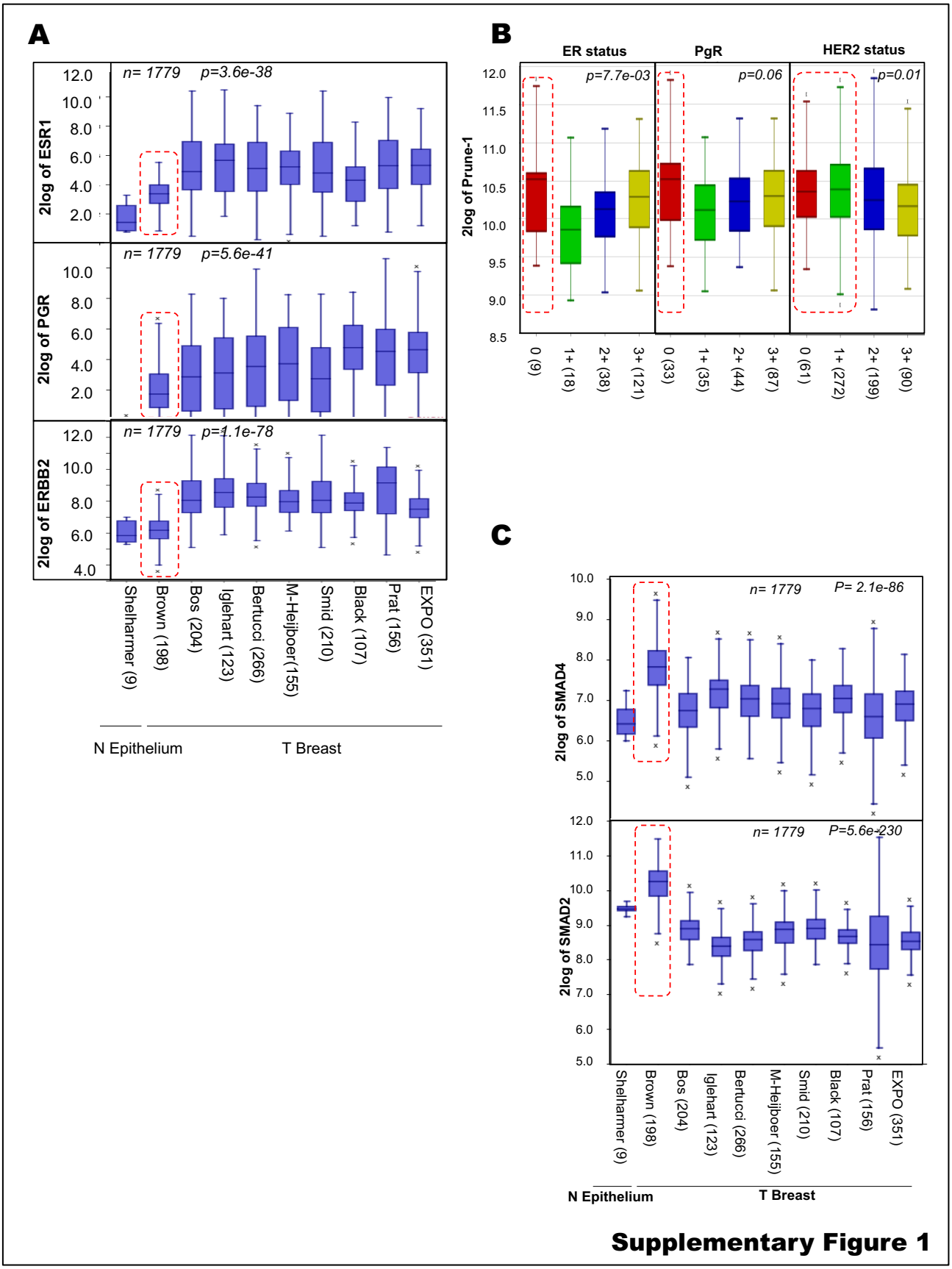

Supplementary Figure 1

Figure S1. Related to Figure 1A. Prune-1 mRNA levels are negatively correlated to ER, PgR and HER2 status.

(A) RNA log2 expression analysis of ER (*i.e.,* ESR1), PgR, and HER2 (*i.e.,* ERBB2) levels of primary BC samples across different publically available datasets, compared with normal epithelium (N Epithelium; Shelharmer dataset only). Data from 10 independent public-domain breast cancer gene-expression datasets confirm lower ER, PgR, and HER2 expression levels in TNBC samples (*i.e.,* Brown; red dashed line) (n = 1779; P = $3.0e^{-169}$). ER, estrogen receptor; PgR, progesterone receptor; HERBB2 or HER2, human epidermal growth factor receptor 2. **(B)** RNA log2 expression of Prune-1 across primary BC samples grouped according to their ER, PgR, and HER2 status (stratified from 0 to 3+ score, as evaluated by IHC) in the publically available dataset of the Tumor Breast Invasive Carcinoma, with gene expression data acquired from The Cancer Genome Atlas (n = 1097). Higher Prune-1 expression levels are seen for BC samples with negative scores for both ER and PgR, and in those with scores ranging from 0 to 1+ for HER2 status (red dashed lines). ER, estrogen receptor; PgR, progesterone receptor; HER2, human epidermal growth factor receptor 2. **(C)** Overexpression of SMAD2 and SMAD4 in TNBC. RNA log2 expression analysis of SMAD2 (top) and SMAD4 (bottom) levels for primary BC samples across the different publically available datasets (T Breast), compared with normal epithelium (N Epithelium). Data from 10 independent public-domain breast cancer gene-expression datasets are shown. There was overexpression of both SMAD2 and SMAD4 in TNBC samples (*i.e.,* Brown [Burstein et al., 2015] n = 1779; SMAD2: P = 5.6e-230; SMAD4: P = 2.1e-86.

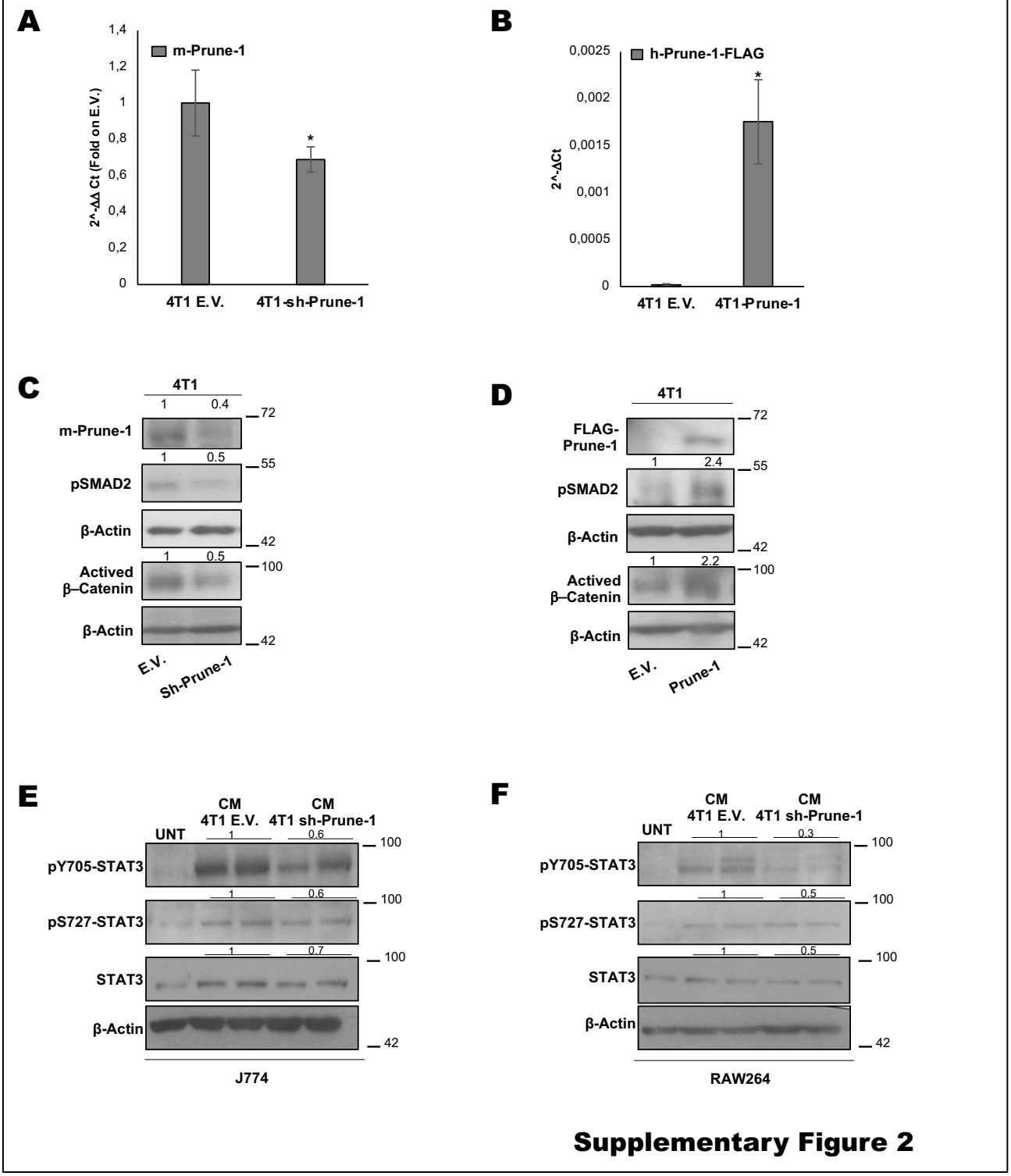

Supplementary Figure 2

Supplementary Figure S2. Related to Figure 1B-E. Prune-1 at the interplay of communication between murine TNBC cells (4T1) and macrophages.

(A) Real-time PCR analysis of murine Prune-1 (m-Prune-1) in 4T1 down-regulated clones. The down-regulation levels of m-Prune-1 is shown as fold (0.6) on E.V. 4T1 clones. Error bars indicate standard deviation (SD) of the mean of three independent cell clones. *, P<0.05 in Student's t-test compared to Empty Vector control clones. **(B)** Mean relative expression (ΔCt) of human Prune-1 (h-Prune-1) from three independent stable 4T1 overexpressing cell clones measured using real-time PCR analysis; Empty vector (E.V.) 4T1 clones were used as negative controls. Data are represented as mean +/- SD. *, P<0.05 in Student's t-test compared to Empty Vector control clones. **(C, D)** Immunoblotting for Prune-1–silenced **(C)** and Prune-1–overexpressing **(D)** 4T1 stable clones. Empty vector (E.V.) 4T1 clones were used as the negative control. Down-regulation and up-regulation of phospho-Ser467-SMAD2 and activated β-catenin, respectively, are seen in Prune-1–silenced cells (0.5-fold) **(C)** and Prune-1–overexpressing cells (phospho-Ser467-SMAD2: 2.4-fold; activated β-catenin: 2.2-fold) **(D)**, respectively. Densitometer analyses are also shown. β-Actin levels were used as the loading control. **(E, F)** Immunoblotting for the indicated proteins in J774 **(E)** and Raw264 **(F)** macrophages grown for 30 min in conditioned media from Prune-1–silenced and control 4T1 clones are shown. Empty vector (E.V.) 4T1 clones and untreated (UNT) macrophages were used as the negative controls. β-Actin levels were used as the loading control.

All experiments were performed in triplicate. All data are expressed as the mean ± standard deviation. *, P < 0.05 in Student's t-test.

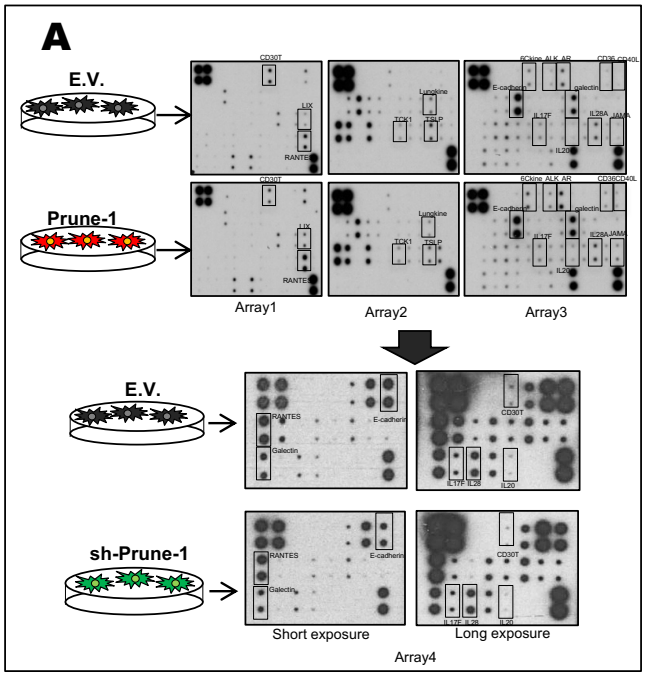

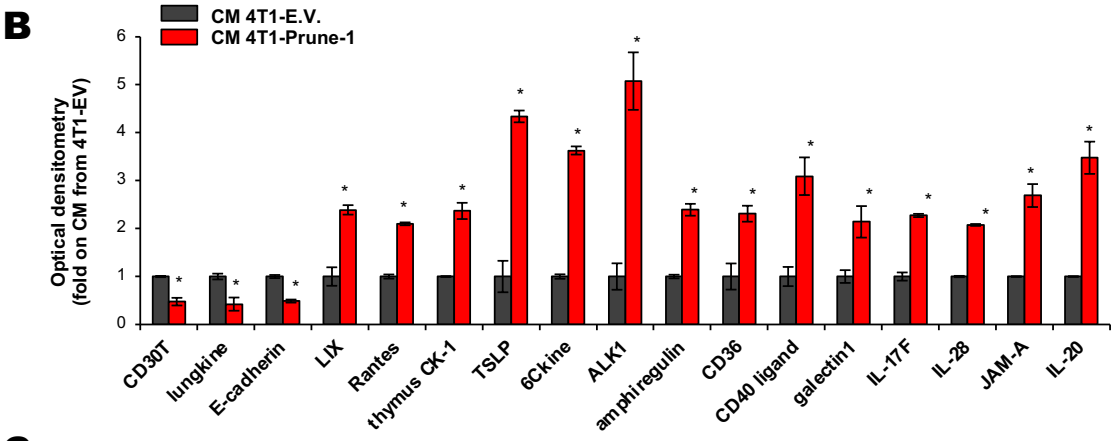

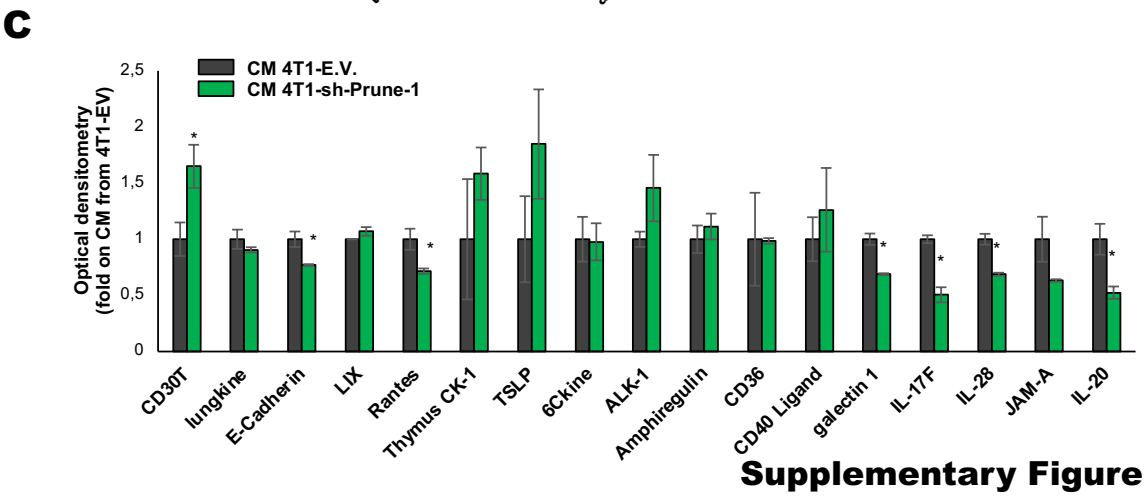

Supplementary Figure 3

Supplementary Figure S3. Related to Figure 1F. Secretion of inflammatory cytokines from TNBC cells (4T1) are modulated by Prune-1.

(A) Upper panel: Mouse cytokine antibody arrays incubated with pooled conditioned media (CM) from Prune-1–overexpressing and empty vector (E.V.) 4T1 cell clones. **Bottom panel:** Mouse cytokine antibody array was performed to determine expression levels of 17 cytokines (as previously found significantly up-regulated and down-regulated by Prune-1) in conditioned media (CM) from Prune-1–silenced 4T1 cell clones. **(B, C)** Fold-induction of cytokines in the conditioned media from 4T1-overexpressing **(B)** or 4T1-silenced **(C)** cell clones on empty vector clones. All experiments were performed in triplicate. All data are expressed as the mean ± standard deviation. *, $P<0.05$ in Student's t-test compared to cytokines levels in conditioned media of 4T1 Empty Vector control clones.

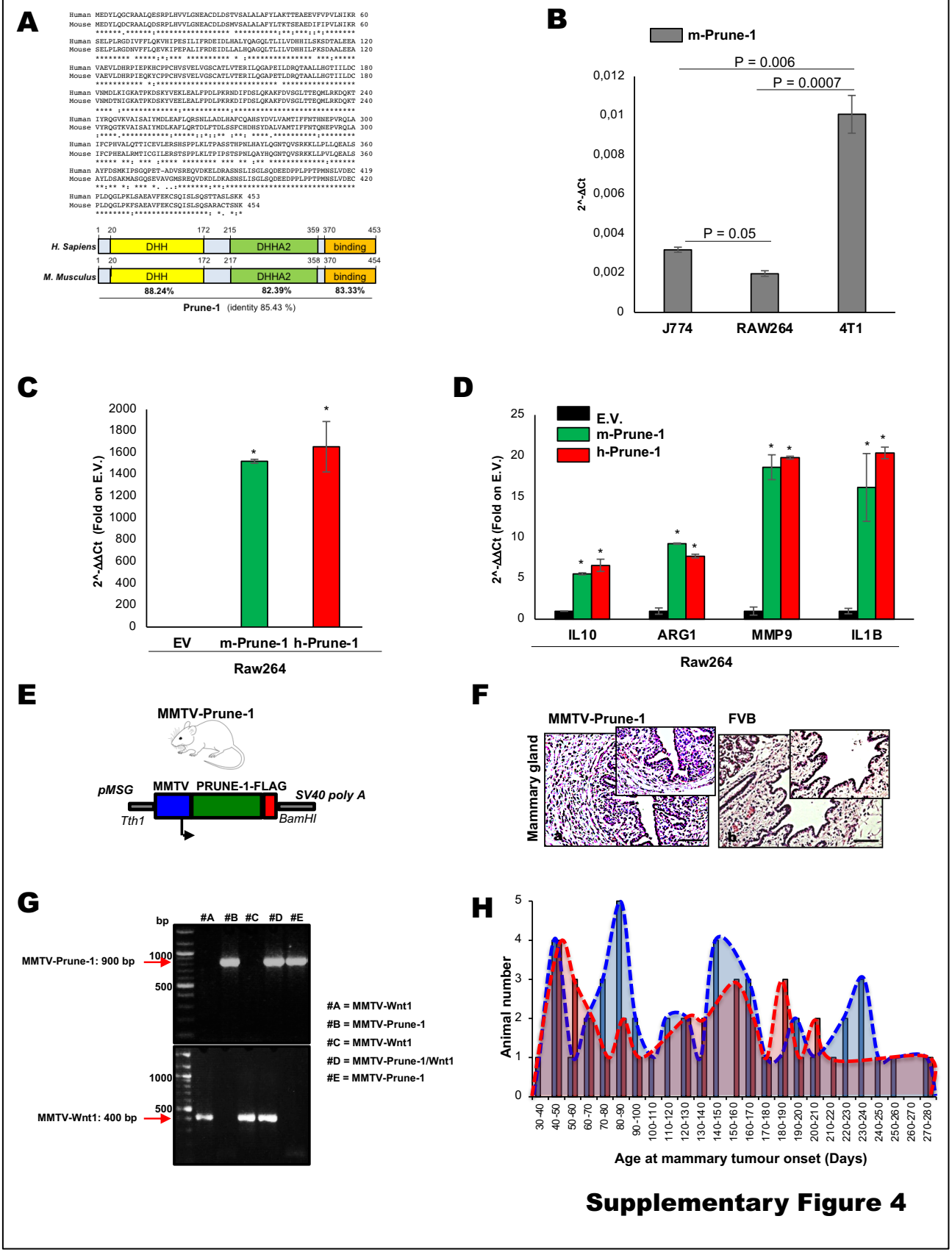

Supplementary Figure 4

Supplementary Figure S4. Related to Figure 2A-B. A genetically engineered mouse model overexpressing Prune-1 in mammary gland.

(A) Sequence homology analyses between human (h) and murine (m) Prune-1 protein sequences show significant similarity (overall aa: 85.43% identity; DHH and DHHA2 enzymatic domains: 88.24% and 82.39% identity, respectively; NME1 binding domain: 83.33% identity. These sequence alignments were realized using the ClustalX 2.1 software. **(B)** Real-time PCR analysis showing relative expression (ΔCt) of endogenous murine Prune-1 (m-Prune-1) in J774A.1, Raw264 and 4T1 cells. **(C, D)** Real-time PCR analysis of Raw264 transiently transfected for 48 h with human (h) or murine (m) Prune-1 cDNA plasmid constructs, showing the fold-expression of m-Prune and h-Prune-1 **(C)**, and the inflammatory cytokines **(D)**, as compared to the empty-vector-transfected cells. Data are means ± standard deviation. *, P<0.05 in Student's t-test compared to empty-vector-transfected cells. **(E, F)** Schematic diagram of plasmid pMSG-MMTV-LTR-Prune-1-FLAG used for the generation of the MMTV–Prune-1 transgenic mouse model. The pMSG vector (Pharmacia Biotech Sevrage, Uppsala, Sweden) contains the Mouse mammary tumor virus (MMTV) long terminal repeat upstream of a polylinker. The human Prune-1 cDNA, containing the complete protein coding region with the FLAG tag fused in-frame at the carboxyl-terminus terminal was cloned into polylinker sites of pMSG in sense orientation relative to the MMTV long terminal repeat and the downstream SV-40 early promoter. The resultant construct was designated pMSG-MMTV-Prune-1-FLAG **(E)**. Representative hematoxylin-eosin sections of normal mammary gland from wild-type female FVB mice (80 days) **(a)** compared with mammary hyperplasia developed from female MMTV–Prune-1 transgenic mice (80 days). **(b) (F)** Magnification, 40×. Scale bar: 20 μm. **(G)** PCR-based analysis for genotyping of the mice. Top: genomic tail DNA samples from mice were amplified using specific primers against transgenes MMTV–Prune-1 (900 bp) or MMTV–Wnt1 (500 bp). **(H)** Age-standardised mammary tumor incidence rate in female virgin MMTV–Prune-1/Wnt1 and MMTV–Wnt1 mice. Prune-1 expression in mammary glands of MMTV–Prune-1/Wnt1 mice (n = 31) does not alter breast tumor onset compared to MMTV–Wnt1 mice (n = 44). Mice were monitored from birth up to breast tumor onset, at up to 280 days.

All experiments were performed in triplicate. All data are expressed as the mean ± standard deviation. *, P < 0.05 in Student's t-test.

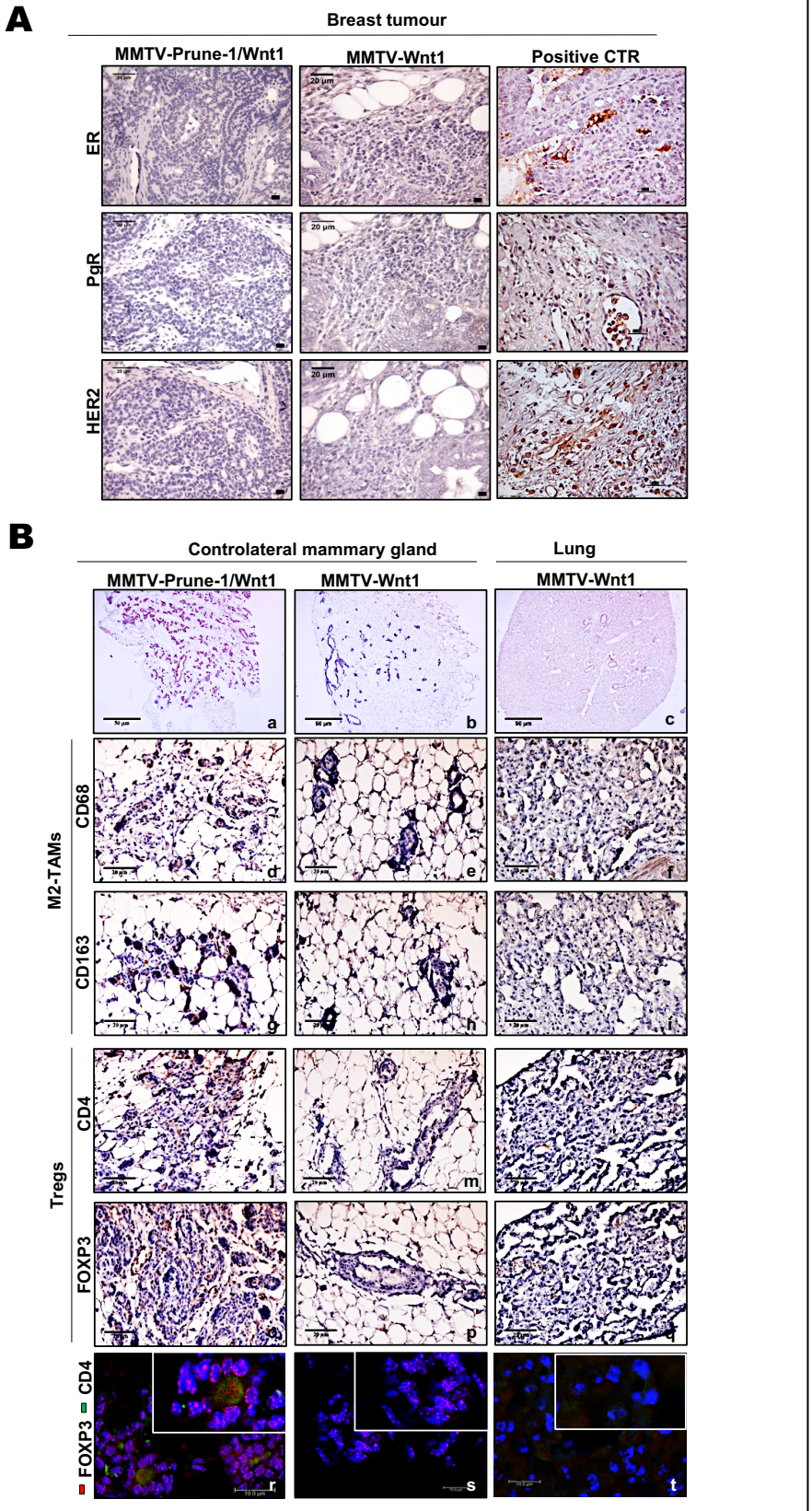

Supplementary Figure 5

Supplementary Figure S5. Related to Figure 2C. A genetically engineered mouse model of metastatic TNBC overexpressing Prune-1 in mammary gland.

(A) Representative immunohistochemistry (IHC) staining on sections of mammary tumors developed from double transgenic MMTV–Prune-1/Wnt1 and MMTV–Wnt1 mice for antibodies as indicated (*i.e.,* ER, PgR, HER2). Undetectable levels of both ER and PgR (*i.e.,* ER^{-}, PgR^{-}, $HER2^{-}$) are shown, compared to the positive control on the right. Magnification, 40×; Scale bar: 20 μm. **(B)** Representative hematoxylin-eosin staining **(a-c)**, IHC **(d-q)** and immunofluorescence (IF; **r-t**) performed on sections of contralateral mammary gland of MMTV–Prune-1/Wnt1 and MMTV–Wnt1 mice and lung from MMTV–Wnt1 mice using antibodies against the following: CD68 **(d-f)** and CD163 **(g-i)**, as markers for M2-TAMs; CD4 **(l-n)**, as a marker for T cells; and FOXP3 **(o-q)**, as a marker for Tregs. Double indirect IF was performed to detect Tregs (*i.e.,* CD4+ FOXP3+, **r-t**). CD4: green; FOXP3: red; DAPI: blue. Acquisitions were performed using a quantitative pathology workstation (Mantra) with image analysis software (Inform). Magnification, 5x, 40×. Scale bar: 50 μm, hematoxylin-eosin; 20 μm, IHC; 10 μm, IF.

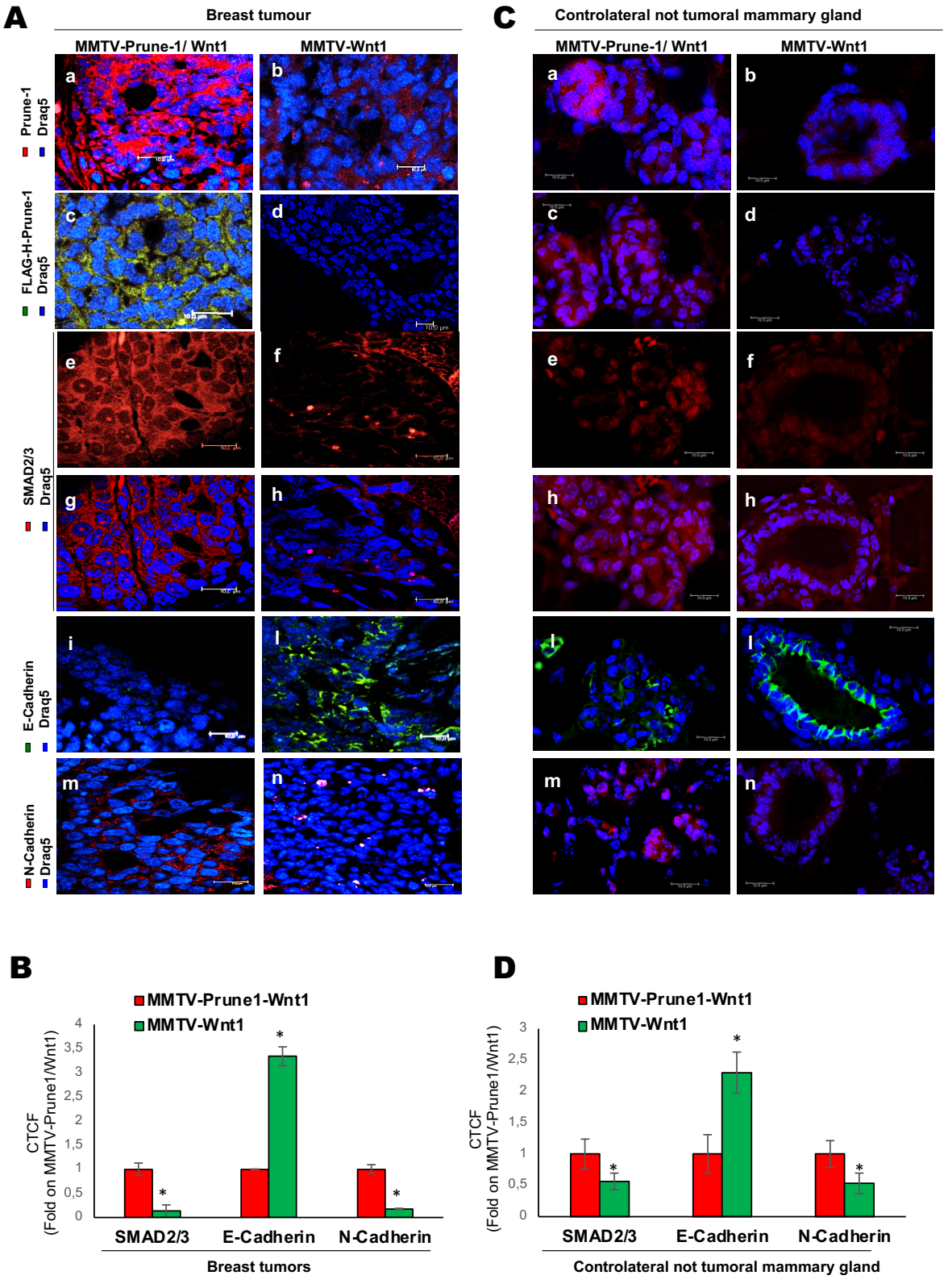

Supplementary Figure 6

Supplementary Figure S6. Related to Figure 2C. Prune-1 enhances TGF-β pathway and EMT process in mammary tumorigenesis of a genetically engineered mouse model of metastatic TNBC.

(A-D) Representative immunofluorescence staining for antibodies, as indicated in mammary tumors **(A)** and contralateral nontumoral mammary gland **(C)** from MMTV–Prune-1/Wnt1 and MMTV–Wnt1 mice. Endogenous Prune-1 (**a-b**), FLAG-tagged-human-Prune-1 (**c-d**), SMAD2-3 (**e-h**), E-cadherin (**i-l**) and N-cadherin (**m-n**). Draq5 was used for nuclear staining (blue). Scale bar: 10 μm. The intensity of the staining for each antibody was measured in each cell, normalized compared to MMTV–Prune-1/Wnt1, and expressed as fold-increase/ decrease **(B, D)**. More than 100 cells were counted. CTCF, corrected total cell fluorescence. Data are means ± standard deviation. *, $P<0.05$ in Student's t-test compared to MMTV-Prune-1/Wnt1.

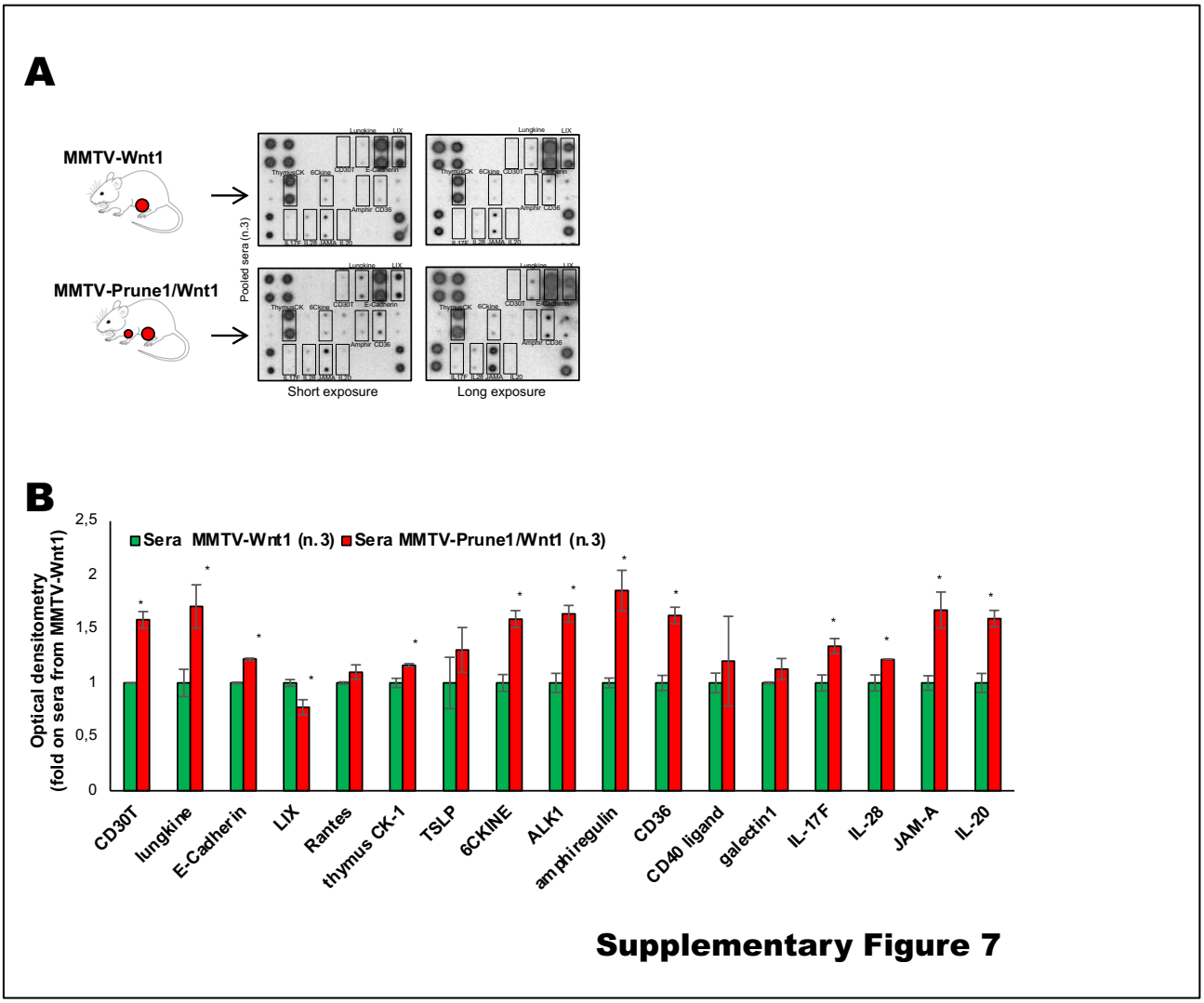

Supplementary Figure S7. Related to Figure 2D. Secretion of inflammatory cytokines in sera of a GEMM of metastatic TNBC overexpressing Prune-1.

(A) Mouse cytokine antibody array was performed to determine expression levels of 17 cytokines (shown previously significantly up-regulated and down-regulated by Prune-1) in sera collected and pooled from MMTV–Prune-1/Wnt1 (n=3) and MMTV–Wnt1 (n=3) mice. **(B)** Fold-induction of cytokines in the conditioned media from sera collected and pooled from MMTV–Prune-1/Wnt1 (n=3) and MMTV–Wnt1 (n=3) mice. Data are means ± standard deviation. *, P<0.05 in Student's t-test compared to sera from MMTV-Wnt1 mice.

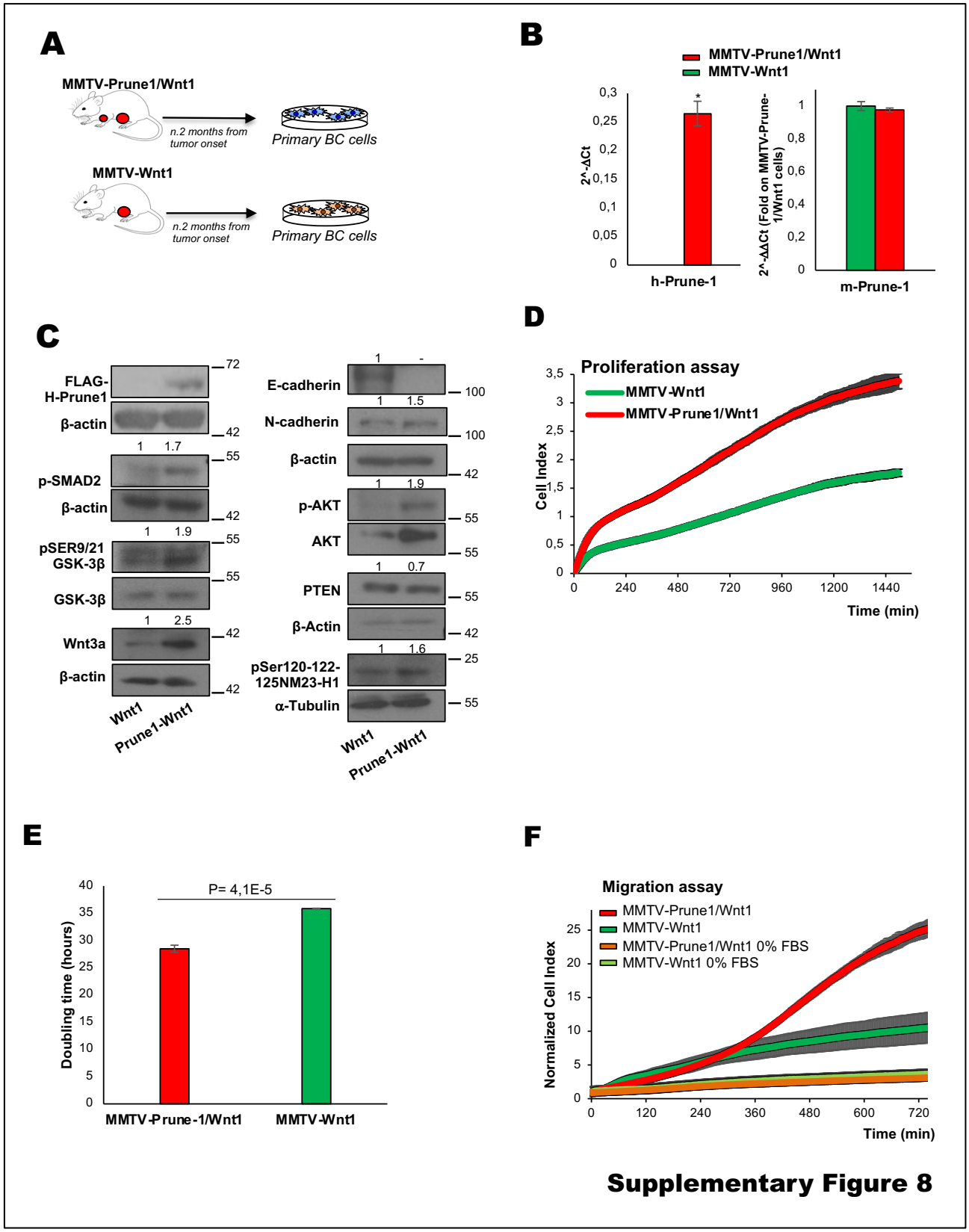

Supplementary Figure 8

Supplementary Figure S8. Related to Figure 3A. Prune-1 enhances migratory properties in primary cells obtained from GEMM of metastatic TNBC.

(A) Schematic diagram showing primary cells obtained from the tumors generated from MMTV–Prune-1/Wnt1 and MMTV–Wnt1 mice at 2 months from tumor onset. **(B)** Real-time PCR analysis showing the expression levels of transgene human and endogenous murine Prune-1 (*i.e.,* h-Prune-1, m-Prune-1) in primary cells obtained from MMTV–Prune-1/Wnt1 and MMTV–Wnt1 tumors. *, $P<0.05$ in Student's t-test compared to MMTV–Wnt1. **(C)** Representative immunoblotting for antibodies as indicated from MMTV–Prune-1/Wnt1 and MMTV–Wnt1 cells. **(D)** Cell Index as a measure of cell proliferation of MMTV–Prune-1/Wnt1 (red) and MMTV–Wnt1 (green) cells (xCELLigence RTCA software). Data are means ±standard deviation of triplicate samples. **(E)** Doubling time of MMTV–Prune-1/Wnt1 (28.4 h, red) and MMTV–Wnt1 (35.8 h, green) cells grown up to 120 h (xCELLigence RTCA software). Data are means ±standard deviation of triplicate samples. **(F)** Cell Index as a measure of cell migration of MMTV–Prune-1/Wnt1 (red) and MMTV–Wnt1 (green) cells (xCELLigence RTCA software). Migration kinetics were monitored in response to 10% fetal bovine serum (FBS; red, green) and to 0% FBS (brown, light green) as negative controls. MMTV–Prune-1/Wnt1 cells (red) show increased migration in response to the 10% FBS gradient, compared with MMTV–Wnt1 cells (green). Cell migration driven by 0% FBS gradient was used as the negative control (MMTV–Prune-1/Wnt1 cells, orange; MMTV–Wnt1 cells, light green). Data are means ±standard deviation of triplicate samples.

All experiments were performed in triplicate. All data are expressed as the mean ± standard deviation. *, $P < 0.05$.

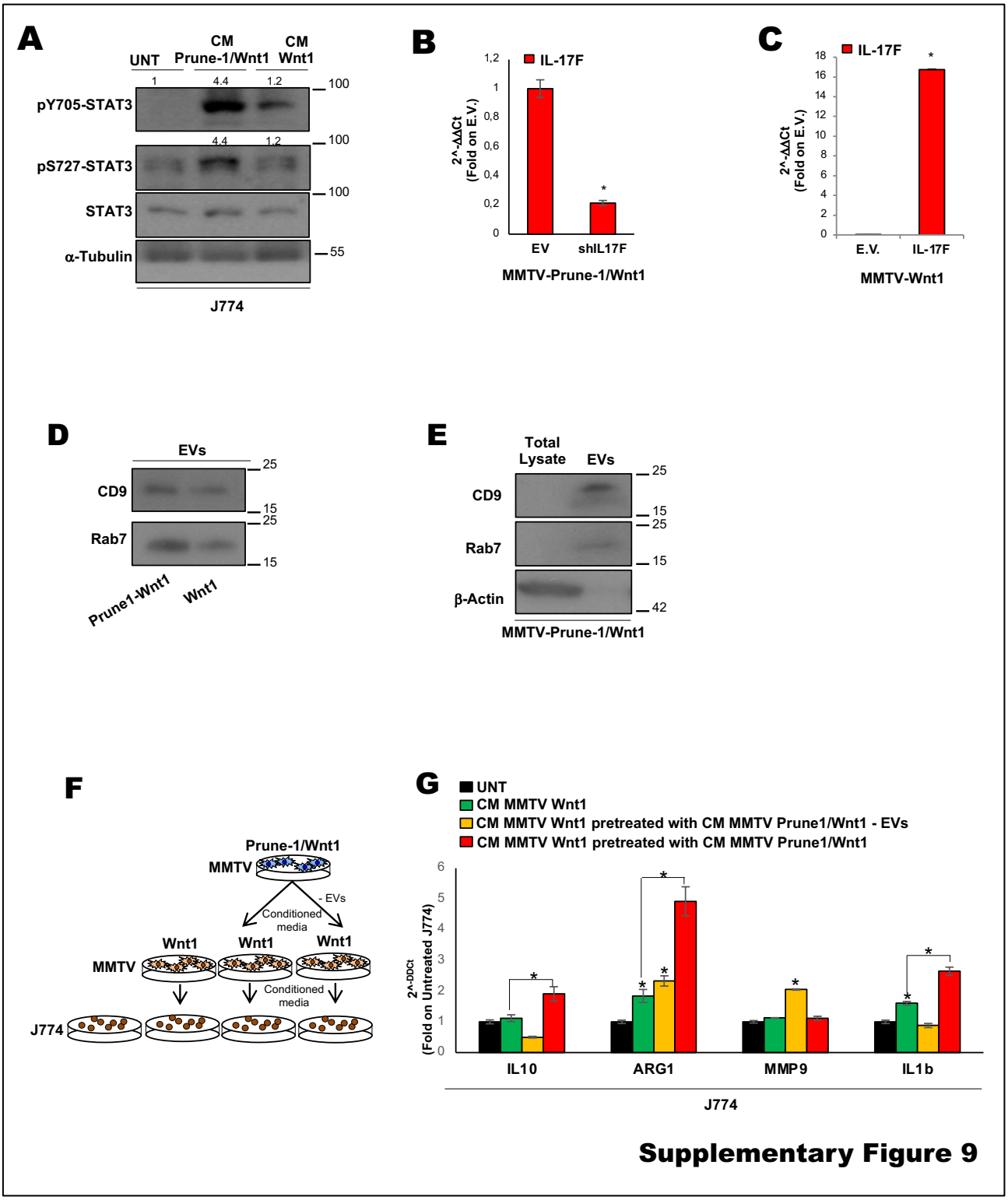

Supplementary Figure 9

Supplementary Figure S9. Related to Figures 3-4. Prune-1 induces macrophage polarization toward M2 phenotype via IL-17F and extracellular vesicles.

(A) Immunoblotting for the indicated proteins in J774 macrophages starved for 6 h and then stimulated for 30 min in conditioned media collected from MMTV–Prune-1/Wnt1 and MMTV–Wnt1 cells. Densitometer analyses for the proteins are shown. α-Tubulin was used as the loading control. **(B)** Real-time PCR analysis of murine IL-17F in MMTV–Prune-1/Wnt1 cells transfected with sh-IL-17F or empty vector (E.V.) control. *, P<0.05 in Student's t-test compared to empty vector transfected cells. **(C)** Real-time PCR analysis of murine IL-17F in MMTV–Wnt1 cells transfected with murine IL-17F or EV control. *, P<0.05 in Student's t-test compared to empty vector transfected cells. **(D)** Immunoblotting for the indicated proteins in extracellular vesicles (EVs) isolated from media culture supernatant of MMTV–Prune-1/Wnt1 or MMTV–Wnt1 cells. **(E)** Immunoblotting for the indicated proteins in total lysate or in EVs isolated from the conditioned media collected from MMTV–Prune-1/Wnt1 cells. **(F, G)** Schematic representation of experimental design. J774 macrophages were grown for 48 h in conditioned media collected (after 24 h) from MMTV–Wnt1 cells that had been previously grown for 24 h in the conditioned media collected from MMTV–Prune-1-Wnt cells depleted or not in EVs. J774 macrophages were untreated or grown in conditioned media collected (after 24 h) from MMTV–Wnt1 cells, and used as negative and positive controls, respectively **(F)**. Real-time PCR analysis of some M2-associated genes, including IL-10, Arg-1, MMP-9, and IL-1β, in J774 macrophages grown for 48 h in conditioned media collected (after 24 h) from MMTV–Wnt1 cells that had been previously grown for 24 h in conditioned media collected from MMTV–Prune-1-Wnt cells depleted (yellow) or not (red) in EVs. **(G)**. J774 macrophages untreated (black) or grown in conditioned media from MMTV–Wnt1 cells (green) were used as negative and positive controls, respectively. *, P<0.05 in Student's t-test compared to untreated macrophages, or, where indicated, compared to macrophages grown in conditioned media from MMTV-Wnt1 cells.

All experiments were performed in triplicate. All data are expressed as the mean ± standard deviation. *, P < 0.05, in Student's t-test

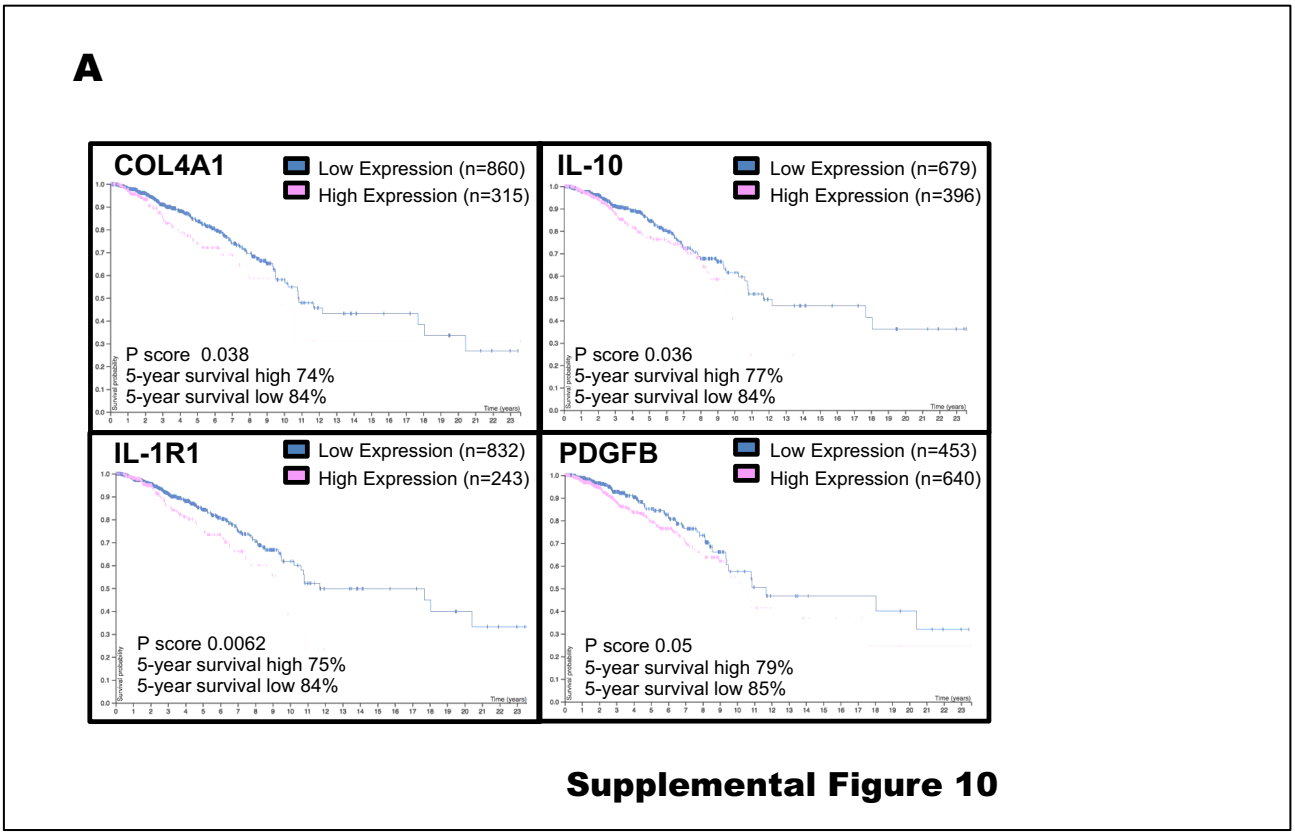

Supplementary Figure S10. Related to Figure 5B. "Core genes" identified in macrophages positively correlated with poor prognosis in BC.

(A) Analyses of survival data obtained from the publically available dataset of Breast Invasive Carcinoma (n=1075) from The Cancer Genome Atlas (TCGA). Of interest, we found that high expression of the IL-10, COL4A1, ILR1, and PDGFB genes was associated with decreased 5-year survival in patients with TNBC.

A

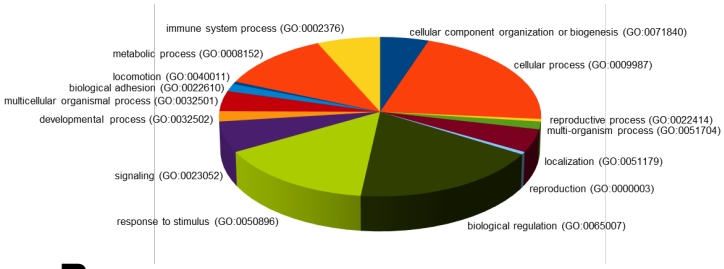

B

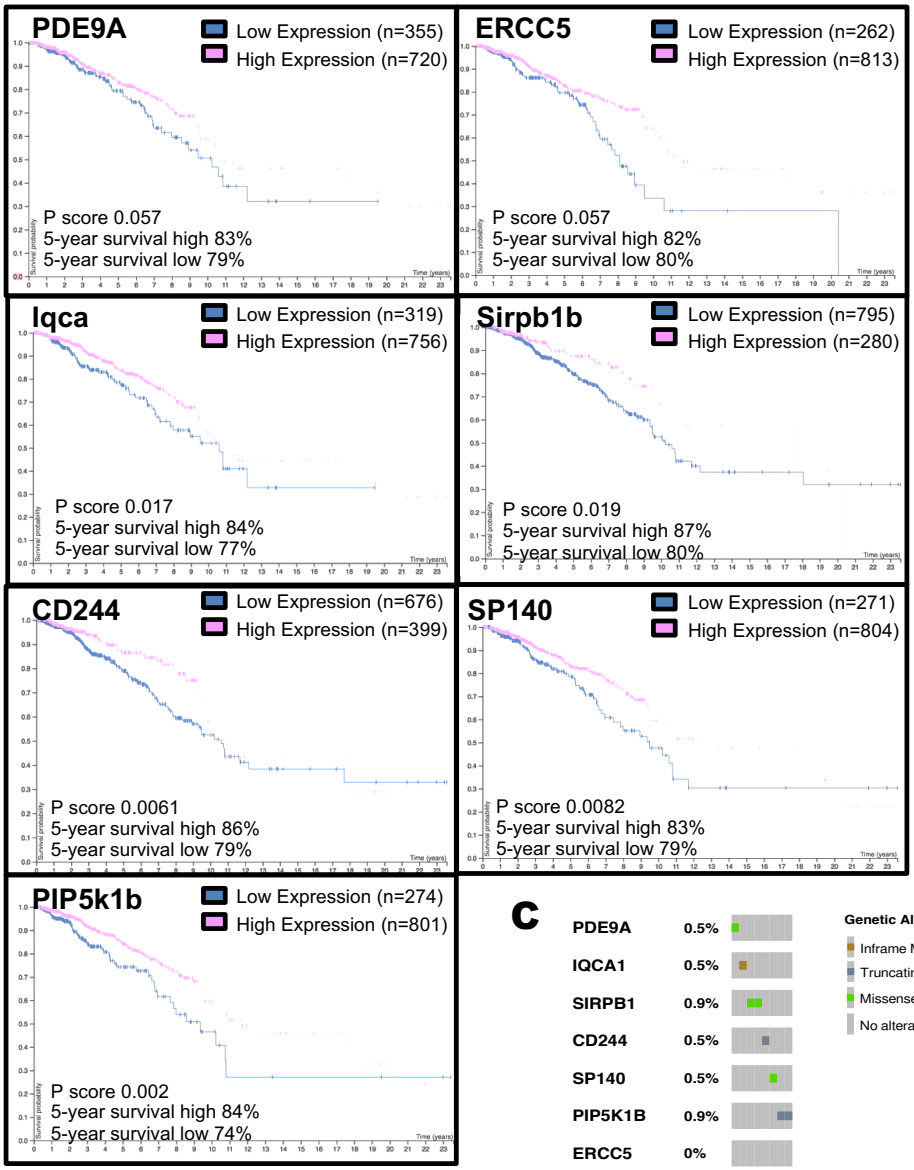

C

Supplementary Figure 11

Supplementary Figure S11. Related to Figure 5C. Mutation spectra in primary murine TNBC cells that overexpressed Prune-1.

(A) Pie chart illustrating Gene Ontology (GO) analysis of deleterious variants mutually exclusively found in MMTV–Prune-1/Wnt1 cells (as compared to MMTV–Wnt1 cells). **(B)** Analyses of survival data obtained from the publically available dataset of Breast Invasive Carcinoma (n=1075) from The Cancer Genome Atlas (TCGA). Of interest, we found that low expression of the PDE9A, ERCC5, Iqca, Sirpb1b, CD244, SP140, and PIP5k1b genes was associated with decreased 5-year survival in patients with TNBC. **(C)** Frequency of genetic alterations in the PDE9A, ERCC5, Iqca, Sirpb1b, CD244, SP140, and PIP5k1b genes in the publically available dataset of metastatic BC (n=216). Altogether, these show genetic alterations with a frequency of 3.7% (Cbioportal for cancer genomics; https://www.cbioportal.org)

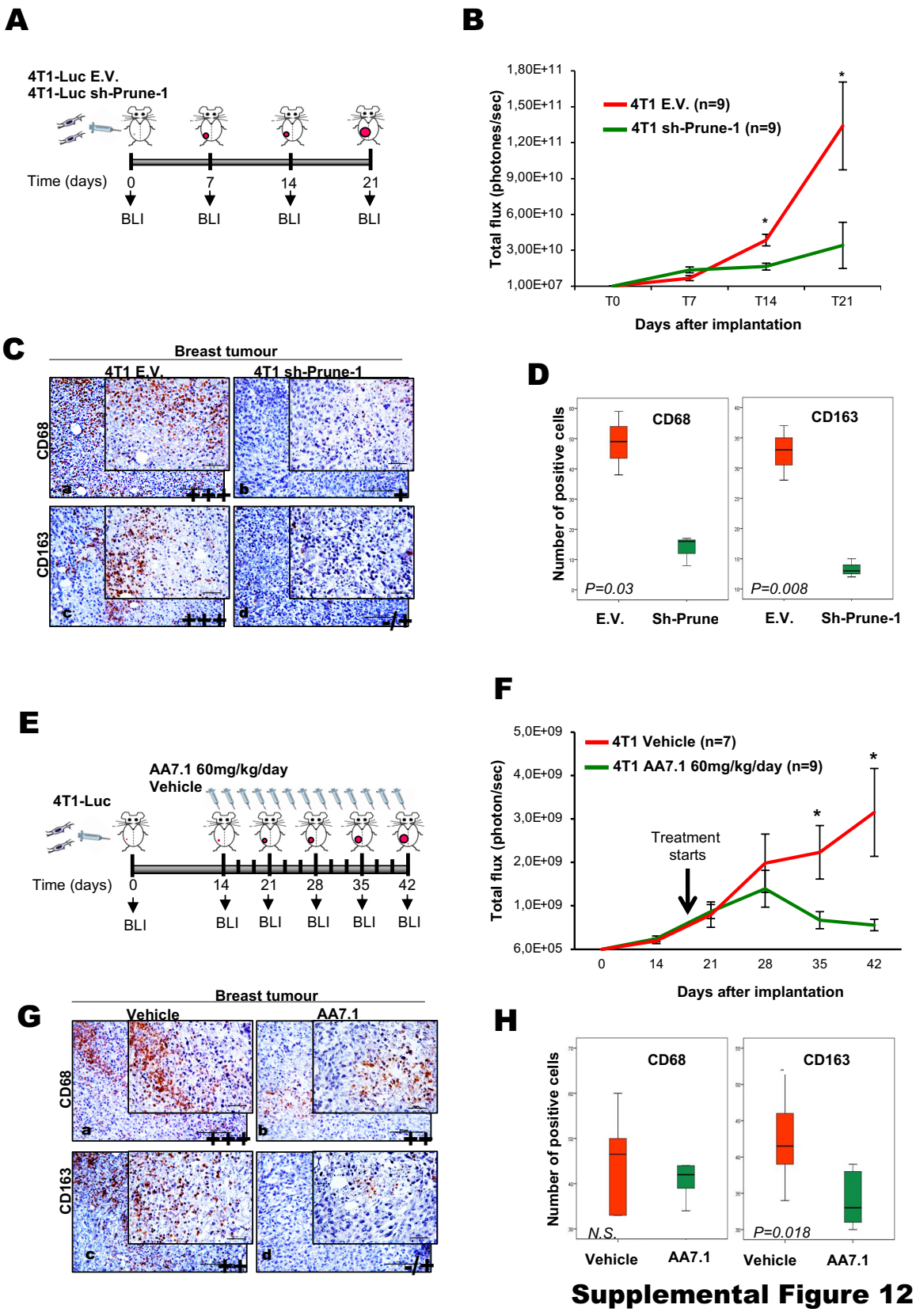

Supplemental Figure 12

Supplementary Figure S12. Related to Figures 6-7. Silencing or pharmacological inhibition of Prune-1 reduces TNBC growth *in vivo*.

(A-D) Prune-1 down-regulation impairs *in-vivo* primary tumor growth of TNBC by inhibition of TAM recruitment and polarization toward an M2-phenotype. **(A)** Representative orthotopic xenograft procedure using Prune-1–silenced 4T1 cells stably expressing the firefly luciferase gene (4T1-LUC cells) and the empty vector (E.V.) as the control, and then implanted into the mammary fat pads of 18 immunocompetent BalbC mice (nine mice per group). The mice were imaged every 7 days using *in-vivo* bioluminescent imaging (IVIS Spectrum) to monitor tumor growth from time of implantation (T0) to 21 days (T21) after tumor implantation. **(B)** Tumor growth (quantified photon emission; photon/s) from the region of interest of mice orthotopically injected with 4T1-LUC stable clones. Differences in total fluxes from the two groups of mice at 14 and 21 days from tumor implantation show impairment of tumor growth *in vivo* in mice implanted with Prune-1–silenced 4T1-LUC cell clones. *, $P<0.05$ in Student's t-test compared to mice orthotopically injected with 4T1-LUC stable clones**. (C)** Representative immunohistochemistry of paraffin-embedded tumors generated by implanting 4T1-LUC cells into mammary fat pads of BalbC mice, using the indicated antibodies. Magnification, 20×, 40×. Scale bars: 20 μm, 10 μm. **(D)** Box plot (SPSS software) showing cells positive for CD68 and CD163 expression within primary tumors from mice implanted with Prune-1–silenced (4T1–Sh-Prune-1) and empty vector (E.V.) 4T1 cell clones. Infiltrating M2-TAMs ($CD68^+$ $CD163^+$ cells) were evaluated using three different tumors from each group of mice. CD68: $P = 0.03$; CD163: $P = 0.008$. **(E-H)** Pharmacological inhibition of Prune-1 affects *in-vivo* primary tumor growth in TNBC through impairment of M2-TAM polarization in the TME. **(E)** Representative orthotopic xenografts using 4T1 cells stably expressing the firefly luciferase gene (4T1-LUC cells), and then implanted into the mammary fat pads of 16 immunocompetent BalbC mice. After tumors were established (14 days after implantation), the mice received intraperitoneal administration of AA7.1 60 mg/kg daily or PBS (vehicle control). Tumorigenesis was followed *in vivo* using bioluminescent imaging (IVIS Spectrum), from time of implantation (T0) to 42 days (T42) after implantation. **(F)** Tumor growth according to quantified photon emission (photon/s) from the region of interest of mice orthotopically injected with 4T1-LUC stable clones. The differences in total flux from the two groups of mice after 21 and 28 days from treatment (T35, T42 from tumor implantation, respectively) showed significant impairment of tumor growth *in vivo* in mice treated with AA7.1. *, $P<0.05$ in Student's t-test compared to vehicle-treated mice as controls. **(G)** Representative immunohistochemistry of paraffin-embedded tumors generated by implantation of 4T1-LUC cells into mammary fat pads of BalbC mice, using indicated antibodies. Magnification, 20×, 40×. Scale bars: 20 μm, 10 μm. **(H)** Box plot (SPSS software) showing cells positive for CD68 and CD163 expression within primary tumors

from mice implanted with 4T1-LUC cells treated with AA7.1 or PBS, as vehicle control. Infiltrating M2-polarized TAMs ($CD68^+$ $CD163^+$ cells) evaluated using three different tumors from each group of mice. CD68: P = 0.9; CD163: P = 0.018.

Table S1. Related to Figure 1A and Figure S1C. Gene expression correlation analyses between Prune-1, SMAD2 and SMAD4 in Breast Cancer samples stratified according to their Estrogens/Progesteron receptor status. PgR, Progesteron receptor; ER, Estrogen receptor; HER2, Human epidermal growth factor 2. The data were obtained from "R2-Genomic and Visualization Platform" using "Tumor Breast Invasive Carcinoma" dataset containing gene expression data acquired from publicly accessible Cancer Genome Atlas (TCGA) breast cancer cohort (n=1097 breast cancer samples logged in TCGA).

PgR, ER, HER2 status	Variable 1	Variable 2	r-value	p-value
PgR negative (n=344)	PRUNE-1	SMAD2	0.35	$2.3e^{-11}$
		SMAD4	0.328	$4.6e^{-10}$
ER negative (n=238)	PRUNE-1	SMAD2	0.35	$2.8e^{-08}$
		SMAD4	0.308	$1.3e^{-06}$
HER2 negative (n=563)	PRUNE-1	SMAD2	0.209	$5.3e^{-07}$
		SMAD4	0.193	$4.1e^{-06}$

Table S2: Related to Figure 2B. Incidence of lung metastases in MMTV-Prune1/Wnt1 and MMTV-Wnt1 mice. MMTV–Wnt1 mice did not develop lung metastasis at 2 months from tumor onset, while MMTV–Prune-1/Wnt1 mice showed macro-metastasis in the lungs at 97% penetrance.

Genotype	Genetic background	ID	Tumour growth timing	Lung metastases
MMTV-Wnt1	FVB	432	2 months	NO
MMTV-Wnt1	FVB	446	2 months	NO
MMTV-Wnt1	FVB	Z1-C21	2 months	NO
MMTV-Wnt1	FVB	573	2 months	NO
MMTV-Wnt1	FVB	502	2 months	NO
MMTV-Wnt1	FVB	Z1-C226	2 months	NO
MMTV-Wnt1	FVB	43	2 months	NO
MMTV-Wnt1	FVB	19	2 months	NO
MMTV-Prune1/Wnt1	FVB	409	2 months	**YES**
MMTV-Prune1/Wnt1	FVB	389	2 months	NO
MMTV-Prune1/Wnt1	FVB	444	2 months	**YES**
MMTV-Prune1/Wnt1	FVB	428	1 month 20 days	**YES**
MMTV-Prune1/Wnt1	FVB	521	2 months	NO
MMTV-Prune1/Wnt1	FVB	476	2 months	**YES**
MMTV-Prune1/Wnt1	FVB	493	2 months	**YES**
MMTV-Prune1/Wnt1	FVB	Z1-C231	3 months	**YES**
MMTV-Prune1/Wnt1	FVB	772	2 months	**YES**
MMTV-Prune1/Wnt1	FVB	821	2 months	**YES**
MMTV-Prune1/Wnt1	FVB	Z1-802	2 months	**YES**

Table S3: Related to Figure 3B-C. M2-associated genes found up-regulated in J774A.1 and/ or Raw264 grown in conditioned media collected from MMTV-Prune-1/Wnt1 cells, as compared to untreated macrophages.

Gene symbol	Protein function (GO)
AF251705	CMRF35-like molecule; Acts as an activating receptor in mast cells and macrophages
Abtb2	Ankyrin repeat and BTB/POZ domain-containing protein 2; May be involved in the initiation of hepatocyte growth
Ahr	Aryl hydrocarbon receptor; Ligand-activated transcriptional activator. Binds to the XRE promoter region of genes it activates. Activates the expression of multiple phase I and II xenobiotic chemical metabolizing enzyme genes (such as the CYP1A1 gene). Mediates biochemical and toxic effects of halogenated aromatic hydrocarbons. Involved in cell-cycle regulation. Likely to play an important role in the development and maturation of many tissues. Regulates the circadian clock by inhibiting the basal and circadian expression of the core circadian component PER1.
Aqp9	Aquaporin-9; Forms a channel with a broad specificity. Mediates passage of a wide variety of non-charged solutes including carbamides, polyols, purines, and pyrimidines in a phloretin- and mercury-sensitive manner, whereas amino acids, cyclic sugars, Na(+), K(+), Cl(-), and deprotonated monocarboxylates are excluded.
Arg1	Arginase-1; Key element of the urea cycle converting L-arginine to urea and L-ornithine, which is further metabolized into metabolites proline and polyamides that drive collagen synthesis and bioenergetic pathways critical for cell proliferation, respectively; the urea cycle takes place primarily in the liver and, to a lesser extent, in the kidneys.
Arl4c	ADP-ribosylation factor-like protein 4C; Small GTP-binding protein which cycles between an inactive GDP-bound and an active GTP-bound form, and the rate of cycling is regulated by guanine nucleotide exchange factors (GEF) and GTPase-activating proteins (GAP). GTP-binding protein that does not act as an allosteric activator of the cholera toxin catalytic subunit. May be involved in transport between a perinuclear compartment and the plasma membrane, apparently linked to the ABCA1-mediated cholesterol secretion pathway.
Bhlhe40	Class E basic helix-loop-helix protein 40; Transcriptional repressor involved in the regulation of the circadian rhythm by negatively regulating the activity of the clock genes and clock-controlled genes. Acts as the negative limb of a novel autoregulatory feedback loop (DEC loop) which differs from the one formed by the PER and CRY transcriptional repressors (PER/CRY loop). Both these loops are interlocked as it represses the expression of PER1/2 and in turn is repressed by PER1/2 and CRY1/2.
Ccl12	C-C motif chemokine 12; Chemotactic factor that attracts eosinophils, monocytes, and lymphocytes but not neutrophils. Potent monocyte active chemokine that signals through CCR2. Involved in allergic inflammation and the host response to pathogens and may play a pivotal role during early stages of allergic lung inflammation; Belongs to the intercrine beta (chemokine CC) family
Ccl22	C-C motif chemokine 22; Chemotactic for activated T-lymphocytes. May play an important role in the collaboration of dendritic cells and B- lymphocytes with T-cells in immune responses
Ccl6	C-C motif chemokine 6; CCL6(22-95) and CCL6(23-95) are potent chemoattractants; Belongs to the intercrine beta (chemokine CC) family
Ccl7	C-C motif chemokine 7; Chemotactic factor that attracts monocytes and eosinophils, but not neutrophils. Augments monocyte anti-tumor activity
Cd36	Platelet glycoprotein 4; Multifunctional glycoprotein that acts as receptor for a broad range of ligands. Ligands can be of proteinaceous nature like thrombospondin, fibronectin, collagen or amyloid-beta as well as of lipidic nature such as oxidized low-density lipoprotein (oxLDL), anionic phospholipids, long-chain fatty acids and bacterial diacylated lipopeptides. They are generally multivalent and can therefore engage multiple receptors simultaneously, the resulting formation of CD36 clusters initiates signal transduction and internalization of receptor-ligand complexes.
Cish	Cytokine-inducible SH2-containing protein; SOCS family proteins form part of a classical negative feedback system that regulates cytokine signal transduction. CIS is involved in the negative regulation of cytokines that signal through the JAK-STAT5 pathway such as erythropoietin, prolactin and interleukin 3 (IL3) receptor. Inhibits STAT5 trans-activation by suppressing its tyrosine phosphorylation.
Edn1	Endothelin-1; Endothelins are endothelium-derived vasoconstrictor peptides; Belongs to the endothelin/sarafotoxin family.
Egr1	Early growth response protein 1; Transcriptional regulator. Recognizes and binds to the DNA sequence 5'-GCG(T/G)GGGCG-3'(EGR-site) in the promoter region of target genes. Binds double-stranded target DNA, irrespective of the cytosine methylation status (By similarity). Regulates the transcription of numerous target genes, and thereby plays an important role in regulating the response to growth factors, DNA damage, and ischemia. Plays a role in the regulation of cell survival, proliferation and cell death. Activates expression of p53/TP53 and TGFB1.
Egr2	E3 SUMO-protein ligase EGR2; Sequence-specific DNA-binding transcription factor. Binds to two specific DNA sites located in the promoter region of HOXA4. Binds to the promoter region of ERBB2. May play a role in the regulation of hindbrain segmentation, might act in combination with the Hox network to specify odd and even rhombomeres, and might participate in the control of the expression of some of the homeobox containing genes; Belongs to the EGR C2H2-type zinc-finger protein family.
Emp1	Epithelial membrane protein 1
Emp2	Epithelial membrane protein 2; Functions as a key regulator of cell membrane composition by regulating proteins surface expression. Also, plays a role in regulation of processes including cell migration, cell proliferation, cell contraction and cell adhesion. Negatively regulates caveolae formation by reducing CAV1 expression and CAV1 amount by increasing lysosomal degradation. Facilitates surface trafficking and the formation of lipid rafts bearing GPI-anchor proteins. Regulates surface expression of MHC1 and ICAM1 proteins increasing susceptibility to T-cell mediated cytotoxicity.
F2rl2	Proteinase-activated receptor 3; High affinity receptor for activated thrombin coupled to G proteins that stimulate phosphoinositide hydrolysis. May play a role in platelets activation; Belongs to the G-protein coupled receptor 1 family.

Fabp4	Fatty acid-binding protein, adipocyte; Lipid transport protein in adipocytes. Binds both long chain fatty acids and retinoic acid. Delivers long-chain fatty acids and retinoic acid to their cognate receptors in the nucleus; Belongs to the calycin superfamily. Fatty-acid binding protein (FABP) family.
Fam198b	Protein FAM198B; Family with sequence similarity 198, member B; Belongs to the FAM198 family.
Flrt3	Leucine-rich repeat transmembrane protein FLRT3; Functions in cell-cell adhesion, cell migration and axon guidance, exerting an attractive or repulsive role depending on its interaction partners. Plays a role in the spatial organization of brain neurons. Plays a role in vascular development in the retina. Plays a role in cell-cell adhesion via its interaction with ADGRL3 and probably also other latrophilins that are expressed at the surface of adjacent cells. Interaction with the intracellular domain of ROBO1 mediates axon attraction towards cells expressing NTN1.
Frmd6	FERM domain containing 6.
Gnb4	Guanine nucleotide-binding protein subunit beta-4; Guanine nucleotide-binding proteins (G proteins) are involved as a modulator or transducer in various transmembrane signaling systems. The beta and gamma chains are required for the GTPase activity, for replacement of GDP by GTP, and for G protein- effector interaction
H2-Eb1	Histocompatibility 2, class II antigen E beta; Belongs to the MHC class II family.
Hbegf	Proheparin-binding EGF-like growth factor; Growth factor that mediates its effects via EGFR, ERBB2 and ERBB4. Required for normal cardiac valve formation and normal heart function. Promotes smooth muscle cell proliferation. May be involved in macrophage-mediated cellular proliferation. It is mitogenic for fibroblasts, but not endothelial cells. It is able to bind EGF receptor/EGFR with higher affinity than EGF itself and is a far more potent mitogen for smooth muscle cells than EGF. Also acts as a diphtheria toxin receptor
Il10	Interleukin-10; Inhibits the synthesis of a number of cytokines, including IFN-gamma, IL-2, IL-3, TNF and GM-CSF produced by activated macrophages and by helper T-cells.
Il1b	Interleukin-1 beta; Potent proinflammatory cytokine. Initially discovered as the major endogenous pyrogen, induces prostaglandin synthesis, neutrophil influx and activation, T-cell activation and cytokine production, B-cell activation and antibody production, and fibroblast proliferation and collagen production; Belongs to the IL-1 family.
Lyzl4	Lysozyme-like protein 4; May be involved in fertilization. Has no detectable bacteriolytic in vitro. Has no lysozyme activity in vitro.
Mmp12	Macrophage metalloelastase; May be involved in tissue injury and remodeling. Has significant elastolytic activity. Can accept large and small amino acids at the P1' site, but has a preference for leucine. Aromatic or hydrophobic residues are preferred at the P1 site, with small hydrophobic residues (preferably alanine) occupying P3.
Mmp9	Matrix metalloproteinase-9; Could play a role in bone osteoclastic resorption. Cleaves type IV and type V collagen into large C-terminal three quarter fragments and shorter N-terminal one quarter fragments.
Myc	Myc proto-oncogene protein; Transcription factor that binds DNA in a non-specific manner, yet also specifically recognizes the core sequence 5'- CAC[GA]TG-3'. Activates the transcription of growth-related genes. Binds to the VEGFA promoter, promoting VEGFA production and subsequent sprouting angiogenesis.
Myrf	Myelin regulatory factor; Myelin regulatory factor: Constitutes a precursor of the transcription factor. Mediates the autocatalytic cleavage that releases the Myelin regulatory factor, N-terminal component that specifically activates transcription of central nervous system (CNS) myelin genes; Belongs to the MRF family.
Olr1	Oxidized low-density lipoprotein receptor 1; Receptor that mediates the recognition, internalization and degradation of oxidatively modified low density lipoprotein (oxLDL) by vascular endothelial cells. OxLDL is a marker of atherosclerosis that induces vascular endothelial cell activation and dysfunction, resulting in pro-inflammatory responses, pro- oxidative conditions and apoptosis. Its association with oxLDL induces the activation of NF-kappa-B through an increased production of intracellular reactive oxygen and a variety of pro- atherogenic cellular responses.
Padi2	Protein-arginine deiminase type-2; Catalyzes the deimination of arginine residues of proteins; Belongs to the protein arginine deiminase family.
Plbd1	Phospholipase B-like 1; Exhibits weak phospholipase activity, acting on various phospholipids, including phosphatidylcholine, phosphatidylinositol, phosphatidylethanolamine and lysophospholipids. However, in view of the small size of the putative binding pocket, it has been proposed that it may act rather as an amidase or a peptidase (By similarity)
Ppbp	Chemokine (C-X-C motif) ligand 7, isoform CRA_b; Pro-platelet basic protein.
Ptgs1	Prostaglandin G/H synthase 1; Converts arachidonate to prostaglandin H2 (PGH2), a committed step in prostanoid synthesis. Involved in the constitutive production of prostanoids in particular in the stomach and platelets. In gastric epithelial cells, it is a key step in the generation of prostaglandins, such as prostaglandin E2 (PGE2), which plays an important role in cytoprotection. In platelets, it is involved in the generation of thromboxane A2 (TXA2), which promotes platelet activation and aggregation, vasoconstriction and proliferation of vascular smooth muscle cells.
Socs2	Suppressor of cytokine signaling 2; SOCS family proteins form part of a classical negative feedback system that regulates cytokine signal transduction. SOCS2 appears to be a negative regulator in the growth hormone/IGF1 signaling pathway. Probable substrate recognition component of a SCF-like ECS (Elongin BC-CUL2/5-SOCS-box protein) E3 ubiquitin ligase complex which mediates the ubiquitination and subsequent proteasomal degradation of target proteins.
Syn1	Synapsin-1; Neuronal phosphoprotein that coats synaptic vesicles, binds to the cytoskeleton, and is believed to function in the regulation of neurotransmitter release. Regulation of neurotransmitter release. The complex formed with NOS1 and CAPON proteins is necessary for specific nitric-oxide functions at a presynaptic level.
Trib1	Tribbles homolog 1; Adapter protein involved in protein degradation by interacting with RFWD2/COP1 ubiquitin ligase. Promotes CEBPA degradation and inhibits its function. Controls macrophage, eosinophil and neutrophil differentiation via the COP1-binding domain. Regulates myeloid cell differentiation by altering the expression of CEBPA in a COP1- dependent manner. Interacts with MAPK kinases and regulates activation of MAP kinases, but has no kinase activity (By similarity); Belongs to the protein kinase superfamily. CAMK Ser/Thr protein kinase family.

Supplemental Information

TRANSPARENT METHODS

Cell proliferation, migration, co-culture transwell assays and doubling time using Cell Index technology

MMTV–Prune-1/Wnt1 and MMTV–Wnt1 cells were harvested, washed with PBS, resuspended to 2 $\times 10^5$ cells/mL in high-glucose Dulbecco's modified Eagle's medium (Euroclone) without fetal bovine serum (FBS), and aliquoted into single wells of plates (xCELLigence CIM plate 16; #05665817001; Acea Biosciences). Cell migration was driven by a 10% FBS gradient, with 0% FBS used as the negative control. Measurements were taken at 2-min intervals, as impedance changes across the electrodes at the bottoms of the wells, for 12 h.

The effects of conditioned media from Prune-1–overexpressing, Prune-1–silenced, and empty-vector 4T1 cell clones were investigated on macrophage (J774A.1, Raw264.7) migration using a real-time XCelligence System Analysis instrument (ACEA Biosciences). Briefly, 1 $\times 10^6$ 4T1 cells of each clone were resuspended in 10 mL complete RPMI 1640 medium and plated into 10-cm-diameter plates. After 24 h, the conditioned media were collected and put into the lower chambers as the chemoattractant in the cell motility assays. Here, 2.5 $\times 10^4$ macrophages were seeded into the upper chambers, in complete RPMI 1640 medium. Three replicates were used for each experimental point. The Cell Index was automatically determined every 2 min, for 12 h. For each experimental point, the mean ±standard deviation of the Cell Index was calculated. Two independent sets of experiments were performed.

The co-culture transwell migration assay with MMTV–Prune-1/Wnt1 cells and J774A.1 macrophages were performed using a real-time XCelligence System Analysis instrument (ACEA Biosciences). Briefly, J774A.1 macrophages were starved for 6 h, then grown for 48 h in conditioned media collected from vehicle- or AA7.1-treated MMTV–Prune-1/Wnt1 cells, or from MMTV–Wnt1 cells. Then, MMTV–Prune-1/Wnt1 cells (2.5 $\times 10^5$) were harvested, washed with PBS, resuspended in high-glucose Dulbecco's modified Eagle's medium (Euroclone) without FBS and aliquoted into single wells of plates (xCELLigence CIM plate 16; #05665817001; Acea Biosciences). Macrophages (1 $\times 10^5$ cells) were plated into single plates of "RTCA E-Plate Inserts" at the top of the microplates. Untreated macrophages were used as negative controls. Cell migration was driven by a 2% FBS gradient. Measurements were taken at 5-min intervals, as impedance changes across the electrodes at the bottoms of the wells, for 8 h.

For cell proliferation assays, MMTV–Prune-1/Wnt1 and MMTV–Wnt1 cells were harvested, washed with PBS, resuspended in high-glucose Dulbecco's modified Eagle's medium (Euroclone)

with 10% FBS and aliquoted (1×10^4 cells) into single wells of plates (xCELLigence E-plate 16; Acea Biosciences). Cell proliferation was recorded at 2-min intervals, as impedance changes across the electrodes at the bottoms of the wells, for up to 24 h.

For doubling time measurements, MMTV–Prune-1/Wnt1 and MMTV–Wnt1 cells were harvested, washed with PBS, resuspended (5×10^3 cells) in high-glucose Dulbecco's modified Eagle's medium (Euroclone) with 10% FBS, and seeded into single wells of plates (xCELLigence E-plate 16; Acea Biosciences). Cell proliferation was recorded at 2-min intervals, as impedance changes across the electrodes at the bottoms of the wells, for up to 120 h. The doubling time was calculated using the RTCA software, from the logarithmic phase of the growth curves as a readout of cell proliferation and behavior that integrates changes in cell number, attachment, and morphology.

Coculture experiments

The effects of conditioned media from Prune-1–silenced, empty-vector 4T1 cell clones, and MMTV–Prune-1/Wnt1 and MMTV–Wnt1 cells were analyzed for activation of J774A.1 macrophages. Briefly 1×10^6 4T1 cells of each clone were resuspended in 10 mL complete RPMI 1640 or DMEM medium, plated into 10-cm-diameter plates, and grown at 37 °C for 24 h. Then the conditioned media were collected. One day before culture in the conditioned media, J774A.1 and Raw264.7 macrophages were plated into 10-cm-diameter plates. At the time of the culturing in conditioned media, macrophages were at 50% confluence, and after 6 h of starvation in serum-free medium, the macrophages were grown in conditioned media for 30 min (for Western blotting) or 48 h (for real-time PCR). Each experimental point was carried out in duplicate. After the culturing in the conditioned media, the macrophages were washed with PBS, collected, and used for protein and/or RNA extraction.

Cytokine antibody array

The conditioned media from three different Prune-1–overexpressing, Prune-1–silenced, and empty-vector 4T1 cell clones were pooled. In the same manner, the sera from three different MMTV–Prune-1/Wnt1 and MMTV–Wnt1 cells were also collected and pooled. The relative levels of cytokines in the pooled conditioned media and murine sera were measured (RayBio Mouse Cytokine Antibody Array C, series 2000; Prodotti Gianni), according to the manufacturer protocol. Densitometric analysis was carried out using the Quantity One software (BioRad). Expression levels were normalized to the levels of the positive control spots (contained within the membrane). For each cytokine, the mean ±standard error was determined.

In-vivo mouse experiments

Mouse experiments were approved by the Institutional Animal Care and Ethical Committee of CEINGE 'Federico II' University of Naples (Protocol 29, September 30, 2012; *Dipartimento Sanità Pubblica Veterinaria* D.L. 116/92). The transgenic mouse model MMTV–Prune-1 (Strain ID: EM:09937; code: FVB-Tg(MMTV-PRUNE)/Cnrm) has been archived to The European Mutant Mouse Archive (EMMA).

Extracellular vesicles isolation

Extracellular vesicles were purified from media culture supernatants of MMTV–Prune-1/Wnt1 and MMTV–Wnt1 cells through methodology previously described (Thery et al., 2006), with modifications. Briefly, MMTV–Prune-1/Wnt1 and MMTV–Wnt1 cells were grown in 'exosomes-depleted medium' (obtained via overnight centrifugation at 100,000 ×g) until they reached 80% confluence. After 48 h, the conditioned medium was collected by centrifugation at 300× *g* for 10 min. The supernatant was then pre-cleared to remove cells, dead cells, and cellular debris by centrigufation at 2,000× *g* for 20 min. The extracellular vesicles were then obtained via ultracentrifugation at 100,000× *g* for 70 min. After washing with PBS, the extracellular vesicles were further purified (ExoQuick Exosome Precipitation Solution; Cat.#EXOQ5A-1; System Biosciences) by incubation for 12 h and centrifugation at 1,500× *g* for 60 min.

Mutation analyses

Whole exome sequencing was performed on tumorigenic cells obtained from primary tumors developed in MMTV–Prune-1-Wnt1 and MMTV–Wnt1 mice. The samples were prepared according to the preparation guidelines for the SureSelect Target Enrichment kits (SureSelect Mouse Capture kits; Agilent). The libraries were sequenced with an Illumina HiSeq sequencer platform. The mapping reference was *mm10* from UCSC (original GRCm38 from NCBI, December 2011), and the annotation database dbSNP version 142.

For the MMTV–Prune-1-Wnt1 sample, for the post-alignment statistics, the initial mappable reads (*i.e.,* number of mapped reads to mouse genome) was 74,311,106, the non-redundant reads (*i.e.,* number of de-duplicate reads from Picard tools version picard-tools-1.118) 68,415,279, the on-target reads (*i.e.,* number of reads mapped to target regions) 45,504,404, the on-target yield (*i.e.,* the sum of the bases in the final alignment to the target regions) 5,298,453,340 bp and the mean depth of target regions (*i.e.,* {on-target yield} / {Target regions}) 107.3 X.

For the MMTV–Wnt1 sample, for the post-alignment statistics, the initial mappable reads was 81,372,126, the non-redundant reads 74,412,189, the on-target reads 50,202,591, the on-target yield 5,880,337,790 bp, and the mean depth of target regions 119.1 X.

The mutually exclusive variants of the MMTV–Prune-1-Wnt1 sample were selected by using the *Ablebitis* tool. These mutations were filtered by excluding: (i) the synonymous, (ii) the noncoding exon variants, (iii) those mapping within intronic and the intergenic regions, (iv) the in-frame deletions and insertions, (v) the upstream or downstream gene variants, and (vi) the 3' and 5' UTR region. Then the variants annotated with putative impact/ deleteriousness as 'low' were excluded. Only the 'coding' variants (that had passed all filters) with a putative impact/ deleteriousness as 'high, modifier or moderate' were analysed through Ensembl Variant Effect Predictor to determine the effects of the selected variants on the protein sequence. Finally, the variants predicted as 'tolerated' by Sorting Intolerant From Tolerant, version 5.2.2, (GRCh38) were also excluded.

Survival data analyses

The analyses of the survival data were obtained from the publicity available dataset of Breast Invasive Carcinoma (n=1075) from TCGA. In detail, the patients were classified into two expression groups (based on the 'fragments per kilobase million' value of each gene), and the correlation between expression levels and patient survival was examined. The survival outcomes of the two groups were compared by log-rank tests.

RNAseq analyses

Library construction and sequencing: Total RNA was isolated from cells using Trizol reagent (Invitrogen), according to the manufacturer protocol. cDNA libraries were prepared using the TruSeq Stranded mRNA LT Sample Prep kits (Illumina), according to the manufacturer guidelines, TruSeq Stranded mRNA Sample Preparation Guide, Part # 15031047 Rev. E. In brief, after being purified from total RNA, the mRNA was randomly fragmented and reverse transcribed into cDNA. Adapters were ligated onto both ends of the cDNA fragments to amplify them using PCR. After amplification, the fragments with insert size between 200 bp and 400 bp were selected for paired-end sequencing. The sequencing process was performed on an Illumina NovaSeq 6000 instrument, using the NovaSeq 6000 S4 Reagent kits, and according to the TruSeq Stranded mRNA Sample Preparation Guide, Part # 15031047 Rev. E.

Expression profiling: The quality of reads was determined by using FastQC[1] version 0.11.7. Trimmomatic[2] version 0.38 was used to filter out low-quality reads by performing the following

trimming tasks: cutting of adapter sequences, cutting of bases off the ends of reads if below a quality score of 3, cutting of windows of four bases if the average quality fell below a quality score of 15, and, finally, dropping reads shorter than 36 bp. HISAT2 version 2.1.0[3], a spliced alignment program, was used to align the trimmed reads to the reference genome (Mouse GRCm38/mm10). The expression levels of known genes were determined using StringTie version 1.3.4d[4], with the mm10 reference annotation as the assembly guide. Raw read counts where normalized using the median ratio normalization method[5], and the resulting normalized count tables were fed to GFOLD version 1.1.4[6], to perform gene expression analysis, setting the significant cut-off for fold-change to the default 0.01. Accession to RNAseq data: http://www.ebi.ac.uk/arrayexpress/experiments/E-MTAB-9231.

Gene-set enrichment analysis: Gene-set enrichment analysis was performed using GSEA Pre-ranked version 4.0.3[7,8]. As input, we used the list of *gfold* values calculated by GFOLD, which can be considered as a sort of reliable log2 fold-change, ranked by *gfold* value, and the list of gene-sets from the Molecular Signatures Database[7,9] (MSigDB version 7.0) belonging to the collection of canonical pathways (CPs) of the Curated Gene Sets (C2). To avoid unrankable values in the input list, genes with *gfold*=0, which GFOLD classifies as nondifferentially expressed, were removed from the list before running GSEA. The number of permutations to assess the statistical significance of the enrichment score, done by gene set, was set to 1000. To identify a subset of 'core genes' potentially responsible for most of the features associated with different phenotypes, we compared the lists of genes from the leading edge of enriched gene-sets coming from each CP sub-collection (Biocarta, Kegg, Pid, Reactome, Naba), and selected those shared by at least four out of five of these sub-collections.

Cell culture

The triple-negative murine 4T1 Dual LN P3 (referred to as 4T1; ATCC: #CRL-2539) breast-cancer cell line was grown in RPMI 1640 medium (Euroclone) supplemented with 10% (v/v) fetal bovine serum (FBS; Invitrogen), 2 mM L-glutamine (Invitrogen), and 1% (v/v) antibiotics (10000 U/mL penicillin, 10 mg/mL streptomycin [Invitrogen]) (Pen/Strep). J774A.1 murine macrophages (referred to as J774 cells; ATCC: #TIB-67) were grown in high-glucose Dulbecco's modified Eagle's medium (DMEM; Euroclone) supplemented with 10% (v/v) FBS, 2 mM L-glutamine, and 1% (v/v) antibiotics (Pen/Strep). RAW-264.7 murine macrophages (referred to as RAW-264 cells; ATCC: #TIB-71) were grown in high-glucose DMEM supplemented with 10% (v/v) FBS, 4 mM L-glutamine, and 1% (v/v)

antibiotics (Pen/Strep). The cells were grown at 37 °C in a humidified atmosphere of 95% air, 5% CO_2 (v/v).

Primary murine TNBC cells from tumors generated by MMTV–Prune-1/Wnt1 and MMTV–Wnt1 mice were obtained (2 months from tumor onset). MMTV–Prune-1/Wnt1 and MMTV–Wnt1 mice were grown in high-glucose DMEM (Euroclone) supplemented with 20% (v/v) FBS, 2 mM L-glutamine, 1% non-essential amino acid solution (M7145; Sigma-Aldrich/Merck) and 1% (v/v) antibiotics (Pen/Strep).

Generation of 4T1 stable clones and transient transfection in MMTV-Prune-1/Wnt1 cells

A construct encoding a fusion protein containing three Flag epitopes (Flag sequence: DYKDDDDK) upstream the Prune-1 protein was generated in the pcDNA3.1 Hygro vector (H-Prune-1-3X-Flag-Hygro plasmid). This construct was transfected to 4T1 cells to generate clones overexpressing the Flag-h-Prune-1 fusion protein (referred to as Prune-1–overexpressing 4T1 clones). The pcDNA3.1 Hygro vector was also transfected to generate control clones.

To generate 4T1 clones in which mouse prune endogenous expression was down-regulated (referred to as Prune-1–silenced 4T1 clones), the cells were transfected with a plasmid containing sh-Prune (Open Biosystems). Similarly, control clones were generated by transfecting the 4T1 cells with the empty vector plasmid.

One day before transfection, the 4T1 cells were plated in 60-mm dishes. At the time of transfection, the cell confluence was 50%, and the cells were transfected with 2.4 μg each vector, using TransIT-LT1 Transfection Reagent (#MIR2300; Mirus Bio LLC), according to the manufacturer instructions. Forty-eight hours after transfection, the cells were cultured under the selection pressure of 250 μg/mL hygromycin B (Invitrogen) for the pcDNA3.1 Hygro constructs. After the selection, about 20 clones for each transfected construct were picked and the expression levels of human and mouse prune proteins were evaluated.

For transient transfection, the day before transfection, the MMTV-Prune-1/Wnt1 cells were plated in 60-mm dishes. At the time of transfection, the cell confluence was 50%, and the cells were transfected with 1 μg IL-17shRNA Pllasmid (m) #sc-146204-SH, using TransIT-LT1 Transfection Reagent (#MIR2300; Mirus Bio LLC), according to the manufacturer instructions. After 24 hours, 1 $\times 10^6$ MMTV-Prune-1/Wnt1 transfected cells were resuspended in 10 mL complete DMEM medium, plated into 10-cm-diameter plates, and grown at 37 °C for 24 h. Then the conditioned media were collected.

Genotyping

Mice had their tail docked (0.25 inches) for DNA analysis from 8-10 days of age. Tail samples were digested with 100 mM Tris-HCl, pH 8.8, 5 mM EDTA, pH 8.0, 0.2% SDS, 200 mM NaCl and 100 μg/mL proteinase K at 55 °C overnight. Samples were then vortexed and centrifuged for 5 min (14,000 rpm, at room temperature) to pellet debris. PCR analyses for MMTV–Prune-1 and MMTV–Wnt1 detection were performed using PCR (GeneAmp System 9700; Applied Biosystem) under the following conditions: 94 °C for 5 min; 94 °C for 30 s, 55 °C for 45 s, 72 °C for 1 min (×45 cycles); 72 °C for 10 min.

Oligonucleotide sequences for MMTV-Prune-1: Forward, GTGAGACAAGTGGTTTCCTGA; Reverse, GCTCGATGGGTCGATGGTCT.

Oligonucleotide sequences for MMTV-Wnt1 (Liu et al., 2008): Forward, GGACTTGCTTCTCTTCTCATAGCC; Reverse, CCACACAGGCATAGAGTGTCTGC.

Immunoblotting

The cells were washed in cold phosphate-buffered saline (PBS) and lysed in cell lysis buffer (20 mM sodium phosphate, pH 7.4, 150 mM NaCl, 10% [v/v] glycerol, 1% [w/v] nadeoxycholate, 1% [v/v] Triton X-100) supplemented with protease inhibitors (Roche, Basel, Switzerland). Cell lysates were cleared by centrifugation at 16,200× *g* for 10 min at room temperature, and the supernatants were removed and assayed for protein concentrations (Protein Assay Dye Reagent; Bio-Rad). Cell lysates (50 μg protein lysate) were separated on SDS-PAGE gels of different percentages, depending on the molecular weights of the proteins of interest. The proteins were then electrophoretically transferred to PVDF membranes (Millipore). After 1 h in blocking solution with 5% (w/v) dry milk fat in PBS, or 5% (w/v) bovine serum albumin (Sigma-Aldrich) in Tris-buffered saline (both of which contained 0.02% [v/v] Tween-20), the membranes were incubated with the primary antibody overnight at 4 °C, and then with the secondary antibodies for 1 h at room temperature. Primary and secondary mouse or rabbit horseradish-peroxidase-conjugated antibodies (NC 27606; ImmunoReagents, Inc) were diluted in 5% (w/v) bovine serum albumin in TBS-Tween or in 5% (w/v) milk fat in PBS-Tween, according to the manufacturer instructions. The protein bands were visualized with a chemiluminescence detection system (Pierce-Thermo Fisher Scientific Inc., IL, USA). Western blotting was performed in triplicate. The densitometry analysis was carried out using the ImageJ software program. The peak areas of the bands were measured on the densitometry plots, and the percentages were calculated. Then, the density areas of the peaks were normalized with those of the loading controls, and the ratios for the corresponding controls (*e.g.*, empty vector) are presented as fold-changes.

Immunohistochemistry of paraffin-embedded tissues

Paraffin sections (thickness, 3 μm) of the tumor specimens were deparaffinized (Bioclear, 06-1782D; Bio-Optica) for 30 min, rehydrated in 100%, 90%, then 70% ethanol, and washed with PBS and then PBS containing 0.02% Triton-X 100 (215680010; Acros Organics). After incubation in pre-warmed target retrieval solution (S170084; Dako) at 97 °C for 45 min, the sections were washed with PBS and placed in a solution of absolute methanol and 0.3% hydrogen peroxide for 15 min. The tissue sections were then blocked with Antibody Diluent Background Reducing (S302281; Dako) for 1 h at room temperature, and then incubated with the primary antibodies overnight at 4 °C in a humidified chamber. Tissue sections were washed in PBS and incubated with labeled streptavidin biotin LSAB mouse and rabbit reagents (K0672; Dako). Detection was with the Liquid DAB Substrate Chromogen System (K3468, Dako). All of the slides were counterstained with Gill's hematoxylin (Bio-Optica). The slides were then washed, dehydrated with 70%, 90%, and then 100% ethanol, and mounted with cover slips using Eukitt (09-00250; Bio-Optica). Micrographs were taken with a high-definition digital microscope camera (ICC50 HD; Leica) or with Mantra Quantitative Pathology Workstation, using the 40× objective. The quantification was performed by using inForm image analysis software.

The detection of macro-metastases in lungs derived from MMTV–Prune-1/Wnt1 and MMTV–Wnt1 cells was performed following staining with Bouin's fixative (25% of 37% formaldehyde solution, 70% picric acid, 5% acetic acid) for 24 h.

Immunofluorescence of paraffin-embedded tissue sections

Paraffin sections of the tumor specimens (thickness, 3 μm) were deparaffinised and rehydrated by immersing the slides in Xylene Substitute (A5597; Sigma), as three washes for 5 min each, then serially in 100%, 95%, 70%, 50%, and 30% ethanol (two washes for 10 min, for each), and deionised water (two washes, for 5 min each). The washes were then followed by PBS, PBS containing 0.02% Triton-X 100 (215680010; Acros Organics), and PBS (two washes for 5 min, for each). For antigen retrieval, the slides were immersed in boiling 10 mM sodium citrate buffer (pH 6.0) using a microwave oven, and then maintained at sub-boiling temperature for 10 min. The slides were left to cool at room temperature for 30 min. The sections were then washed by immersion in distilled water for 5 min. To block endogenous peroxidase activity, the tissue sections were placed in a solution with 3.0% hydrogen peroxide in methanol for 15 min. Then, to decrease the nonspecific background fluorescence, the tissues were digested by treating them with a solution containing 0.2% trypsin (T2600000; Sigma-Aldrich) and 0.001% $CaCl_2$ for 10 min at 37 °C, in a humidified chamber. The slides were then washed in PBS, PBS containing 0.02% Triton-X 100 (215680010; Acros Organics), and PBS (two washes for 5 min, for each). The tissue sections were blocked with 6% bovine serum

albumin (A9418; Sigma), 5% fetal bovine serum (ECS0180L; Euroclone), and 20 mM $MgCl_2$ in PBS containing 0.02% Triton-X 100, for 1 h at room temperature, and incubated overnight with the primary antibodies at 4 °C in a humidified chamber. Tissue sections were washed in PBS and PBS containing 0.02% Triton-X100, and incubated with anti-mouse Alexa Fluor 488 (ab150113; Abcam), anti-rabbit Alexafluor 488 (150077; Abcam) and antirabbit Alexa Fluor 546 (#A10040; ThermoFisher), as the secondary antibodies. DNA was stained with DRAQ5 (#62254; ThermoFisher). The slides were then washed, dehydrated with 70%, 90%, and 100% ethanol, and mounted with cover slips using 50% glycerol (G5150; Sigma-Aldrich). Confocal microscopy was carried out using Mantra Quantitative Pathology Workstation, using the 40× objective or a laser scanning confocal microscope Leica TCS SP5, using the 63× oil immersion objective. The quantification was performed by using inForm image analysis software.

Antibodies used

The following antibodies were used in this study: anti-Flag (1:5000; Sigma-Aldrich); anti-FLAG (1:200; TA100023; Origene); anti-phospho-p44/42 MAPK (ERK1/2) (Thr 202/Tyr 204) (1:500; Cell Signaling Technology); anti-ERK1/2 (1:500; Santa Cruz Biotechnology); anti-phospho-NF-κB p65 (Ser 311) (1:200; Santa Cruz Biotechnology); anti-NF-κB p65 (1:3000; Abcam); anti-STAT3 (1:5000; Abcam); anti-phospho-STAT3 (Tyr 705) (1:1000; Abcam); anti-phospho-STAT3 (Ser 727) (1:1000; Abcam); anti-Prune-1 (1:500; Abcam); anti-phospho-Ser467-Smad2 (1:1000; Cell Signaling); anti-PTEN (1:1000; 9552, Cell Signaling); anti-phospho-Ser473-Akt (1:500; Cell Signaling); anti-N-cadherin (1:1000; Cell Signaling) anti-E-cadherin (1:500; Transduction Laboratories:); anti-GSK (1:500, Transduction Laboratories); anti-Ser9/21-GSK (1:200; Cell Signaling); anti-FAK (1:1000; Abcam); anti-phospho-Y397-FAK (Abcam); anti-CD68 (1:200; Abcam); anti-CD163 (1:200; SantaCruz); anti-activated β-catenin (1:500; Millipore); anti- β-catenin (1:2000; Transduction Laboratories); anti-Wnt3a (1:500; Abcam); anti-cyclin D1 (1:5000; Abcam); and anti-Her2 (1:200; Cell Signaling); Anti-Vimentin (1:200; ab137321; Abcam) The following in-house antibodies were produced: rabbit polyclonal anti-Prune-1 (C45; 1:500; (Ferrucci et al., 2018)); rabbit polyclonal anti-phospho-NME1 (pS120-pS122-pS125; 1:500; (Garzia et al., 2008). These antibodies were detected using horseradish peroxidase–conjugated anti-mouse (1:5000; Amersham) and anti-rabbit (1:3000; Amersham). An anti-β-actin (1:5000; Sigma-Aldrich) and anti-α-tubulin (1:3000; Abcam) antibodies were used as controls for equal loading.

Quantitative real-time polymerase chain reaction (RT-PCR)

Total RNA was isolated from cells using Trizol reagent (Invitrogen), according to the manufacturer protocol. cDNA was synthesized using random hexamers with iScript cDNA synthesis kits (Bio-Rad), according to the manufacturer protocols. After digestion with DNAse RNAse-free, 2 μg total RNA in 20 μL was used in each reaction. qRT-PCR was performed using the SYBR Green PCR Master Mix (Applied Biosystems) and a sequence detection system (model 7900HT, Applied Biosystems), according to the manufacturer protocols. The primers were designed with the Primer Express 2.1 program (Applied Biosystems). All qRT-PCRs were performed in duplicate, with 50 ng ss-cDNA used in each 10-μL reaction. β-Actin mRNA was used to normalize mRNA concentrations. For statistical analysis of gene expression data, the relative expression $2^{-\Delta Ct}$ ±standard deviation and the mean fold change = $2^{-(\text{average } \Delta\Delta Ct)}$ ±standard deviation were calculated using mean differences in ΔCt between the genes and the internal control. The ΔCt was calculated using the differences in the mean Ct between the genes and the internal control.

Generation of *MMTV*–Prune-1-Flag construct

The pMSG vector (Pharmacia Biotech Sevrage, Uppsala, Sweden) contains the mouse Mammary tumor virus long terminal repeat (MMTV-LTR) upstream of a polylinker. The human Prune-1 cDNA containing the complete protein coding region with the FLAG tag fused in-frame at the carboxyl-terminus was cloned into polylinker sites of pMSG in a sense orientation relative to the MMTV-LTR, and downstream of the SV-40 early promoter. The resultant construct was designated pMSG-MMTV–Prune-1-FLAG.

To generate MMTV–Prune-1, transgenic animals in an FVB background were used, with pronuclear injections of the fertilized oocytes, and embryo transfer to the pseudopregnant females. Male MMTV–Wnt1 mice (FVB) were crossed with MMTV–Prune-1 (FVB) to generate the double transgenic MMTV–Prune-1/Wnt1 mouse model.

Tail vein injection of MMTV–Prune-1/Wnt1 cells in FVB mice

MMTV–Prune-1/Wnt1 cells (1×10^5) were injected (via tail vein) in immunocompetent syngenic (strain FVB) mice (n=8). At 14 days from cell injection, the mice were grouped according to their weight and AA7.1 (60 mg/kg/day, IP) or PBS (as vehicle negative control) were administered daily. At 14 days from treatment start (*i.e.,* n.28 days from TNBC cell injection), the mice were injected with a fluorescent imaging probe (XenoLight RediJect 2-DG-750; Perkin Elmer) that targets cells with high metabolic activity in terms of glucose uptake, for *ex-vivo* targeting of tumorigenic cells.

Orthotopic syngenic mice models of 4T1 cells in BalbC mice

Five-week-old female immunocompetent BalbC mice were anesthetized with ketamine/ xylazine (87.5 mg/kg, 12.5 mg/kg, respectively). They were then implanted in the VIII right-side mammary gland with 2.5 $\times 10^5$ 4T1 cells of Prune-1–silenced, extracellular vesicle clones, or 4T1-LUC cells (stably expressing the firefly luciferase gene through lentiviral particles; RediFect Red-Fluc-Puromycin; CLS960002; Perkin Elmer, Waltham, MA, USA)). The mice were imaged weekly and tumor growth was evaluated by bioluminescence acquisition using an imaging system (IVIS 3D Illumina; Xenogen/ Caliper), as described by Asadzedeh et al. (79). Briefly, for the acquisitions, the mice were anesthetized by inhalational of isofluorane, and D-luciferin (15 mg/mL stock; 122799; PerkinElmer) was injected intraperitoneally (100 µL per 10 g body weight). To quantify the bioluminescent imaging (BLI), the integrated fluxes of photons (ph/s) within each area of interest were determined using the Living Images Software Package 3.2 (Xenogen-Perkin Elmer).

For treatment with AA7.1 *in-vivo*, starting 14 days from tumor implantation (i.e., once tumors were established), the mice were grouped according to their bioluminescence values and injected intraperitoneally with AA7.1 60 mg/kg daily, or with PBS as the vehicle control. Tumor growth was monitored every 7 days by BLI aquisition, with means ±standard error of the photon integrated fluxes calculated for each experimental point. At the end of the experiments, the primary tumors were dissected out and embedded in paraffin for immunohistochemistry (IHC) analysis.

Proteomic analysis performed on extracellular vesicles

The extracellular vesicles (EVs) isolated from culture media from MMTV–Prune-1/Wnt1 and MMTV–Wnt1 cells (following methodology described previously (Thery et al., 2006)) were prepared for mass spectrometry as follows. The EVs were lysed by addition of 0.4% sodium dodecyl sulfate (SDS). After a brief period of incubation, the samples were diluted to drop the SDS concentration to 0.1% SDS. To purify the samples, we used the short SDS-PAGE method (to remove the disturbing components from the proteins upon subsequent protein staining). Briefly, we ran only in the stacking part of the polyacrylamide gel. Once the SDS-PAGE run was finished, the proteins were visualised by Coomassie blue and cut out of the gel to perform in-gel digestion. These samples were analysed using a mass spectrometer (LTQ-Orbitrap VELOS), with a 60-min gradient run. The data obtained by the mass spectrometry were presented to the Swiss-Prot '*Mus musculus*' database. To identify MS/MS spectra and further proteins, we used the Mascot database search engine. The identification was carried out with confidence settings of 99%. The threshold score itself was set by the 99% confidence interval setting, the size of the database, tolerances set to the measured masses to the precursor and the fragments. After the database search the results were stored in the ms_lims system (Helsens et al., 2010).

Statistical analysis

Data representative of three independent experiments were analyzed using unpaired two-tailed t-tests (Student's t-tests). For all of the Figures, error bars represent standard deviation (SD) of the mean, and $p \leq 0.05$ was considered significant.

***In-vivo* human experiments**

Patients and specimens: From 2003 to 2010, 138 patients who underwent a mastectomy, quadrantectomy or metastectomy at the 'Giovanni Pascale' National Cancer Institute of Naples, Italy, were enrolled into this study. In our institution, the proportion of tumors classified as TNBC is 15% to 19% of the total number of breast cancer surgeries. All cases of TNBC and nonTNBC samples were reviewed according to WHO classification criteria, using standard tissue sections and appropriate IHC slides. Medical records for all of the cases of TNBC and nonTNBC samples were reviewed for clinical information, including histologic parameters that were determined from the hematoxylin-eosin stained slides. The following clinical and pathological parameters were evaluated for each tumor included in the study: patient age at initial diagnosis, tumor size, histologic subtype, grade, nodal status, tumor recurrence or distant metastasis. In addition, all of the specimens were characterized for all routine diagnostic immunophenotypic parameters.

Tissue microarray building: The 138 patients were used for tissue microarray building, using the most representative areas from each single case. All of the tumors and controls were reviewed by two experienced pathologists (MDB/GB). Discrepancies between two pathologists from the same case were resolved in a joint analysis of the cases.

IHC analysis: IHC staining was carried out on slides from formalin-fixed, paraffin embedded tissues, corresponding to the TNBC tissue microarrays, to evaluate the expression of Prune-1, ER, PgR, c-Erb B2, Ki67, pERK, NF-κB-p65-Ser311, CD68, and CD163 markers. Slides were incubated with antibodies against routinely diagnostic markers: mouse anti-human ERα (1:35; DAKO), mouse anti-human PR (1:50; DAKO), rabbit anti-c-Erb B2 (1:300; DAKO), and mouse anti-human Ki67 (1:75; DAKO), and with primary antibodies listed as follow: rabbit anti-prune (1:200; made in home) (Ferrucci et al., 2018), rabbit anti- ERK1/2 (phospho Thr202/Tyr204) (1:500 dilution; Cell Signaling), rabbit anti-NFkB p65 (phospho S311) (1:400; Abcam), mouse anti-CD68 (prediluited, Ventana, Roche), mouse anti-CD163 (1:75; Novocastra). The negative controls omitted the primary antibody. Detection was achieved with a Liquid DAB + Substrate Chromogen System (Dako).

Sections were counterstained with hematoxylin and mounted. Results were interpreted using light microscopy.

Evaluation of IHC: Antigen expression was evaluated independently by two pathologists using light microscopy. Observers were unaware of the clinical outcome. For each sample, at least five fields (inside the tumor and in the area showing tumor invasion; 400×400) and >500 cells were analyzed. Using a semiquantitative scoring system microscopically, and referring to each antigen scoring method in other studies, an observer evaluated the intensity, extent, and subcellular distribution of Prune-1, ER, PgR, c-Erb B2, Ki67, ERK 1/2 (phospho Thr202/Tyr204), NF-kB p65 Ser311, CD68, and CD163 markers. The cut-off used to distinguish 'positive' from 'negative' cases was ≥1% ER/PR positive tumor cells. IHC analyses of c-erbB-2 expression described the intensity and staining pattern of the tumor cells. Only membrane staining intensity and pattern were evaluated using the 0 to 3+ score, as illustrated in the HercepTest kit scoring guidelines. The FDA-recognized test, the Herceptest (DAKO), describes four categories: no staining, or weak staining in <10% of the tumor cells (0); weak staining in part of the membrane in >10% of the tumor cells (1+); complete staining of the membrane with weak or moderate intensity in >10% of the neoplastic cells (2+); and strong staining in >10% (3+). Scores of 0 or 1+ were considered negative for *HER-2/neu* -expression, 2+ was uncertain, and 3+ was positive. Cases 2 + undergo FISH analysis (Collina et al., 2016).

The proliferative index Ki67 was defined as the proportion (%) of immunoreactive tumor cells out of the total number of cells. The proportion of positive cells per case was scored according to two different groups: group 1: ≤20% (low proliferative activity); group 2: >20% (high proliferative activity).

There are no standardized criteria for Prune-1, ERK (phospho Thr202/Tyr204), NF-κB p65 (phospho Ser311), CD68, and CD163 marker staining evaluation, so the median of the percentage positivity for each marker was used as the cut-off. We schematized the score evaluation as follows: for cytoplasmic prune staining, we used a combo score considering both intensity of reaction (high (3)/ moderate (2)/ low (1)/ absent (0)) and cell percentage positivity (0=negative/ 1=>1%<30%/ 2=>30<60/ 3=>60%) and considered high expression cases when the combo value was >5; also for nuclear phospo-p65 (Ser311), we used a combo score considering both an intensity score (based on a four-point system: high (3)/ moderate (2)/ low (1)/ absent (0) staining) and cell percentage positivity (0=negative/ 1=<50%/ 2=≥50%), and considered high expression cases when the combo value was >2 (median value); for nuclear phospho-ERK we considered cell percentage positivity as low when it was ≤20%, high when >20%.

To characterize microenvironment markers, we selected 32 cases in our casuistry (16 high and 16 low for Prune expression) and we performed the analysis on whole sections. We used these following scores: for cytoplasmic CD68, as low when it was <30%, high when ≥30%, for cytoplasmic CD163, as low when it was <30%, high when ≥30%.

Statistical analysis: Student's *t*-tests and Pearson χ^2 tests were used to determine whether a relationship existed between the categorical variables included in the study. The level of significance was defined as $P < 0.05$. All of the statistical analyses were carried out using the Statistical Package for Social Science v. 20 software (SPSS Inc., Chicago, IL, USA).

Supplemental References

Collina, F., Cerrone, M., Peluso, V., Laurentiis, M. D., Caputo, R., Cecio, R. D., Liguori, G., Botti, G., Cantile, M. and Bonito, M. D. (2016). Downregulation of androgen receptor is strongly associated with diabetes in triple negative breast cancer patients. *Am J Transl Res,* 8**,** 3530-9.

Ferrucci, V., De Antonellis, P., Pennino, F. P., Asadzadeh, F., Virgilio, A., Montanaro, D., Galeone, A., Boffa, I., Pisano, I., Scognamiglio, I., et al. (2018). Metastatic group 3 medulloblastoma is driven by PRUNE1 targeting NME1-TGF-beta-OTX2-SNAIL via PTEN inhibition. *Brain,* 141**,** 1300-1319.

Garzia, L., D'angelo, A., Amoresano, A., Knauer, S. K., Cirulli, C., Campanella, C., Stauber, R. H., Steegborn, C., Iolascon, A. and Zollo, M. (2008). Phosphorylation of nm23-H1 by CKI induces its complex formation with h-prune and promotes cell motility. *Oncogene,* 27**,** 1853-64.

Helsens, K., Colaert, N., Barsnes, H., Muth, T., Flikka, K., Staes, A., Timmerman, E., Wortelkamp, S., Sickmann, A., Vandekerckhove, J., et al. (2010). ms_lims, a simple yet powerful open source laboratory information management system for MS-driven proteomics. *Proteomics,* 10**,** 1261-4.

Liu, B., Yu, H. M., Huang, J. and Hsu, W. (2008). Co-opted JNK/SAPK signaling in Wnt/beta-catenin-induced tumorigenesis. *Neoplasia,* 10**,** 1004-13.

Thery, C., Amigorena, S., Raposo, G. and Clayton, A. (2006). Isolation and characterization of exosomes from cell culture supernatants and biological fluids. *Curr Protoc Cell Biol,* Chapter 3**,** Unit 3 22.